

Fall 2005

A FE-FD hybrid scheme for solving parabolic two-step micro heat transport equations in irregularly shaped three dimensional double-layered thin films exposed to ultrashort-pulse lasers

Brian R. Barron
Louisiana Tech University

Follow this and additional works at: <https://digitalcommons.latech.edu/dissertations>



Part of the [Materials Science and Engineering Commons](#), and the [Mechanical Engineering Commons](#)

Recommended Citation

Barron, Brian R., "" (2005). *Dissertation*. 582.
<https://digitalcommons.latech.edu/dissertations/582>

This Dissertation is brought to you for free and open access by the Graduate School at Louisiana Tech Digital Commons. It has been accepted for inclusion in Doctoral Dissertations by an authorized administrator of Louisiana Tech Digital Commons. For more information, please contact digitalcommons@latech.edu.

NOTE TO USERS

This reproduction is the best copy available.

UMI[®]

A FE-FD HYBRID SCHEME FOR SOLVING PARABOLIC TWO-STEP MICRO
HEAT TRANSPORT EQUATIONS IN IRREGULARLY SHAPED THREE
DIMENSIONAL DOUBLE-LAYERED THIN FILMS
EXPOSED TO ULTRASHORT-PULSE LASERS

by

Brian R. Barron, B.S., M.Div, M.S.

A Dissertation Presented in Partial Fulfillment
of the Requirements for the Degree
Doctor of Philosophy

COLLEGE OF ENGINEERING AND SCIENCE
LOUISIANA TECH UNIVERSITY

November 2005

UMI Number: 3192316

INFORMATION TO USERS

The quality of this reproduction is dependent upon the quality of the copy submitted. Broken or indistinct print, colored or poor quality illustrations and photographs, print bleed-through, substandard margins, and improper alignment can adversely affect reproduction.

In the unlikely event that the author did not send a complete manuscript and there are missing pages, these will be noted. Also, if unauthorized copyright material had to be removed, a note will indicate the deletion.

UMI[®]

UMI Microform 3192316

Copyright 2006 by ProQuest Information and Learning Company.

All rights reserved. This microform edition is protected against unauthorized copying under Title 17, United States Code.

ProQuest Information and Learning Company
300 North Zeeb Road
P.O. Box 1346
Ann Arbor, MI 48106-1346

LOUISIANA TECH UNIVERSITY

THE GRADUATE SCHOOL

September 22, 2005

Date

We hereby recommend that the dissertation prepared under our supervision
by Brian Barron

entitled A FE-FD Hybrid Scheme for Solving Parabolic Two-Step Micro Heat Transport

Equations in Irregularly Shaped Three Dimensional Double-Layered Thin Films Exposed to

Ultrashort-Pulse Lasers

be accepted in partial fulfillment of the requirements for the Degree of
Doctor of Philosophy

Whizhly Dui

Supervisor of Dissertation Research

Richard J. Greechie
Head of Department

Computational Analysis & Modeling
Department

Recommendation concurred in:

Adri Parron

Ra Ra

Raja Kumar

Richard J. Greechie

Advisory Committee

Approved:

Bala Ramachandran
Director of Graduate Studies

Approved:

Terry McConathy
Dean of the Graduate School

Stan Nappa
Dean of the College

GS Form 13
(5/03)

ABSTRACT

Multi-layer thin films are important components in many micro-electronic devices. These films are often used when a single film layer is insufficient to meet devices specifications. The continued reduction in component size has the side effect of increasing the thermal stress on these films and consequently the devices they comprise. Understanding the transfer of heat-energy at the micro-scale is important for thermal processing using a pulse-laser. Often, micro-voids may be found in processed devices. This is due to thermal expansion. Such defects may cause an amplification of neighboring defects resulting in severe damage and consequently the failure of the device. Thus a complete understanding of thermal dissipation and defects is necessary to avoid damage and to increase the efficiency of thermal processing.

A hybrid finite element - finite difference (FE-FD) method has been developed for solving three dimensional parabolic two-step heat transport in irregular double-layered thin film exposed to ultrashort pulsed lasers. This scheme first discretizes the thin film system along the xy -plane by a finite element method. Then the z -direction is discretized via a weighted finite difference scheme. The two are combined into a numerical scheme which is then coded into a computer simulation. It is shown that the scheme is unconditionally stable with respect to the initial condition and the heat source. Three distinct numerical examples are studied. The first being a $0.05 \mu\text{m}$ gold thin film disk, with 1 mm diameter, atop a same-dimensioned chromium padding layer. This disk is exposed to an ultra-fast laser burst and the thermal properties are demonstrated.

Secondly, the same thin-film disk array is exposed to a double burst laser pulse and the thermal properties examined. Finally the ultrashort laser is moved in a complete circle about the center of the double-layered thin disk and the thermal properties are examined.

The outcome of this study provides an efficient and reliable numerical method for solving micro-scale heat transport equations, and gives a better understanding of the nature of heat transport in such a system. Also, the hybridization procedure offers a new way to examine three dimensional heat transport systems – one that utilizes the strengths of both the finite element and the finite difference methodologies. The research results have a significant impact on the development of short-pulse laser applications in structural monitoring of thin metal films, laser patterning of such films and laser synthesis and processing of thin film deposition.

APPROVAL FOR SCHOLARLY DISSEMINATION

The author grants to the Prescott Memorial Library of Louisiana Tech University the right to reproduce, by appropriate methods, upon request, any or all portions of this Dissertation. It is understood that "proper request" consists of the agreement, on the part of the requesting party, that said reproduction is for his personal use and that subsequent reproduction will not occur without written approval of the author of this Dissertation. Further, any portions of the Dissertation used in books, papers, and other works must be appropriately referenced to this Dissertation.

Finally, the author of this Dissertation reserves the right to publish freely, in the literature, at any time, any or all portions of this Dissertation.

Author 

Date 09/22/2005

TABLE OF CONTENTS

LIST OF TABLES	viii
LIST OF FIGURES	ix
NOMENCLATURE	xi
ACKNOWLEDGEMENTS	xv
DEDICATION	xvi
CHAPTER ONE	1
1.1 Overview	1
1.2 Objective of Research	3
1.3 Organization of the Dissertation	4
CHAPTER TWO	5
2.1 General Heat Transfer Model	5
2.2 Microscale Heat Transfer	7
2.2.1 Differences with Macroscale Heat Transfer	7
2.2.2 Wave Nature of Microscale Heat Transfer	8
2.3 Dual Phase Lagging Behavior	9
2.3.1 Phase Lag	9
2.3.2 Model Formulation	10
2.4 Previous Work	17
CHAPTER THREE	21
3.1 Problem Description	21
3.2 General Procedure	23
3.2.1 Approach Described	23
3.2.2 Reasoning Behind Hybrid Approach	24

CHAPTER FOUR	27
4.1 Finite Element Method	27
4.1.1 Modified Galerkin Weighted Residual Approach	27
4.1.2 Formulation	27
4.1.3 Establishing a Triangular Mesh	30
4.2 Modified Weighted Average Finite Difference Scheme	32
4.2.1 Finite Difference Method Outline	32
4.2.2 Notation	32
4.3 Combined Hybrid Scheme	33
4.3.1 Formulation	33
4.3.2 Implementation of Scheme	34
4.4 Stability of Model	38
4.5 Algorithm for Solution	51
4.5.1 Computational Algorithms	51
4.5.2 Mathematica as a Programming Language	52
CHAPTER FIVE	57
5.1 Description	57
5.2 Case One – Base Case	58
5.3 Case Two – Double Pulse Heat Source	67
5.4 Case Three – Moving Heat Source	70
CHAPTER SIX	78
6.1 Conclusions	78
6.2 Future Work	79
APPENDIX A Positive Eigenvalues	80
APPENDIX B Source Code	82
REFERENCES	100

LIST OF TABLES

Table 2.1	Phonon-electron coupling factor (G), for some noble and transition metals [Tzou 1996]	15
Table 5.1	Known parameters for the system	57

LIST OF FIGURES

Figure 2.1	An example element in three dimensions	5
Figure 2.2	Primary scattering mechanisms of free electrons within a metal	9
Figure 2.3	Interrelationship between laser heating models [Qui 1993a]	13
Figure 2.4	Normalized temperature change (reflectivity change) in gold film predicted by dual-phase-lag model [Tzou 1996]	17
Figure 3.1	Graphical representation of modeled example	21
Figure 3.2	Plot of laser heat source	23
Figure 4.1	Triangular mesh for x-y plane	31
Figure 5.1	Schematic representation for case one	58
Figure 5.2	Normalized electron temperature change on surface	59
Figure 5.3	Normalized lattice temperature change on surface	61
Figure 5.4	Electron temperature profile (z-direction)	62
Figure 5.5	Lattice temperature profile (z-direction)	63
Figure 5.6	Electron temperature distribution in the x-z plane	64
Figure 5.7	Lattice temperature distribution in the x-z plane	65
Figure 5.8	Electron and lattice temperature distribution in the x-y plane (0.25 ps) ...	66
Figure 5.9	Normalized electron temperature change on surface (double pulse)	67
Figure 5.10	Normalized lattice temperature change on surface (double pulse)	68
Figure 5.11	Electron temperature distribution (double pulse)	69
Figure 5.12	Lattice temperature distribution (double pulse)	70

Figure 5.13	Graphical representation of pulsed laser on thin film surface	71
Figure 5.14	Normalized electron temperature distribution center surface of disk (moving source)	72
Figure 5.15	Normalized lattice temperature distribution center surface of disk (moving source)	73
Figure 5.16	Contour electron temperature distributions for moving source case	74
Figure 5.17	Electron and lattice temperature distribution in the x-y plane (0.25 ps) ..	75
Figure 5.18	Electron and lattice temperature distribution in the x-y plane (0.75 ps) ..	76
Figure 5.19	Electron and lattice temperature distribution in the x-y plane (1.75 ps) ..	77

NOMENCLATURE

A	coefficient for numerical scheme
B	coefficient for numerical scheme
c	specific heat per unit mass, $J/kg\cdot K$
c	constant
$C_{(e,l)}$	volumetric heat capacity of electron gas (e) and metal lattice (l), $J/m^3\cdot K$
C_p	volumetric heat capacity, $J/m^3\cdot K$
C_T	thermal wave speed, m/s
dm	element mass, kg
E	energy stored in element, J
G	electron phonon coupling factor, $W/m^3\cdot K$
h	Planck's constant, $J\cdot s$
J	laser influence, J/m^2
k	Boltzmann constant, J/K
K	conductance matrix in FEM
M	capacitance matrix in FEM
m_e	electron mass, kg
N	number of elemental nodal points
\bar{n}	outward pointing normal vector
n_a	atomic number density per unit volume, m^{-3}
n_e	number density per unit volume, m^{-3}

ps	picosecond
Q	heat flux, w
R	reflectivity
$R(x,y,z,t)$	residual function
r_z	change in time divided by change in direction squared, $\frac{\Delta t}{\Delta z^2}$
S	source term, W/m^3
t	physical time, s
T	temperature function, K
T_0	initial temperature, K
t_p	laser pulse duration, fs
u	generalized expression for the actual solution to PDE system
U	generalized expression for estimation of PDE system solution
V	generalized expression for estimation of PDE system solution
v_s	speed of sound, m/s
w	weight function
W	work function, J

Greek Symbols

δ_z^2	central difference-in-space operator
∇	delta operator (first order derivative)
δ_{ij}	Kronecker delta
∇^2	Laplace operator (second order derivative)
Δt	time increment

Δz	z-axis space increment
Ω	area of triangular element, m^2
α	thermal diffusivity, m^2/s
α_p	generalized coordinates
δ	laser penetration depth, nm
ε	difference values between proposed solutions to system of equations
ϕ_p	eigen vector
γ	specific heat coefficient, J/m^3-K^2
φ	basis and weighting function designation
κ	thermal conductivity, $W/m-K$
λ_p	eigen value
ρ	density, kg/m^3
τ	relaxation time, s

Subscripts and Superscripts

0	initial value at $t = 0$
Au	gold
Cr	chromium
D	Debye Temperature, K
E	energy norm
e	electron
k	index along z-plane
L	final value in system
l	lattice

ACKNOWLEDGEMENTS

What flows after these words marks a moment in time. After these words we find completion – completion of a task. Before these words reside years of pursuit. It is therefore impossible to quantify the quality of influence over these years in these short paragraphs. Who to include? Where to begin? I begin by thanking my dissertation committee. Their input has made this a better document. To that end, Dr. Weizhong Dai has tirelessly listened, guided and prodded me through the journey of research. Without his immense patience and help, the work which follows would not exist. Thank you.

I must also acknowledge that I would not have entered the journey of research if it had not been for family and friends. My brothers Steve and Randy (and their spouses Beth and Kim), my sister Donna (and Matt, her husband) and my mother, Shirley and father, Randall Barron have nurtured and sustained me through quite perilous times. Lucky and Helen Raley, my in-laws, have always treated me as one of their own. My Kansas City family, Randy, Polly, Jennifer, Cameron, Katie and Spencer Carney; along with Audrey Phelps have made this a supportive and happy time for me. I could not have written these words without their profound influence.

My own family – Kitty, Zachary, Cameron and Katie, have had to endure some frustrating times and moments when their priorities had to match mine. I am grateful for their love and support.

DEDICATION

To Kitty, who has stuck with me, listened patiently, faked interest and always loved me. I love you very much.

Also to my father, Dr. Randall F. Barron. What an honor it is to quote you in this work! You have been a resource for me far beyond the pages of this text. As I think about entering the realm of professional research I am struck by the old axiom, “You often become just like your parents.” Well, let me be the first to say that I could do a whole lot worse than “growing into Dad!”

CHAPTER ONE

INTRODUCTION

1.1 Overview

Multi-layer thin films are important components in many micro-electronic device. These films are often used when a single film layer is insufficient to meet devices specifications. The continued reduction in component size has the side effect of increasing the thermal stress on these films and consequently the devices they comprise. Thus the transportation of heat energy through thin films is of vital importance in micro-technological applications.

Understanding the transfer of heat-energy at the micro-scale is important for the thermal processing using a pulse-laser [Qui 1993a]. Often, microvoids may be found in processed devices. This is due to thermal expansion. Such defects may cause an amplification of neighboring defects resulting in severe damage and, consequently, the failure of the desired device. Thus a complete understanding of thermal dissipation and defects is necessary to avoid damage and to increase the efficiency of thermal processing.

Micro-scale heat transfer differs from macro-scale heat transfer in some important ways. On the micro-scale, energy transport is governed by phonon-electron interaction in metallic films. Macroscopic energy transport relies upon a heat diffusion model based on Fourier's law. This law loses accuracy on a micro-scale because of its emphasis on averaged behavior over many grains. Research has resulted in an energy equation which

captures both the classical heat equation and thermal waves in the same framework [Qui 1993a], [Tzou 1996]. When the heating time from the pulse-laser is greater than the relaxation time of the metallic film, the energy transfer formulation takes the form of a parabolic two-phase partial differential equation system [Qui 1993a]. It is expressed

$$C_e \frac{\partial T_e}{\partial t} = \kappa \nabla^2 T_e - G(T_e - T_l) + S \quad (1.1)$$

$$C_l \frac{\partial T_l}{\partial t} = G(T_e - T_l) \quad (1.2)$$

where T_e is electron temperature and T_l is lattice temperature; κ is the thermal conductivity; C_e and C_l are the volumetric electron heat capacity and the volumetric lattice heat capacity respectively; G is the electron-lattice coupling factor and S is the strength of the laser heating source. The details of which are discussed in chapter two.

The standard notation ∇^2 is the Laplace operator.

In classical (macro scale) heat transfer, the electron and lattice temperatures are assumed to be equal. Thus this system reduces to the classical model when such an assumption is made. However, for sub-picosecond pulses and sub-microscale, the laser energy is absorbed primarily by free electrons confined within the thin material layer. This energy is then transferred to the lattice resulting in a lag between the excitement of the electrons and the transfer of energy to the lattice. As the duration of the laser pulse is short, the source of heat is turned off before thermal equilibrium between electrons and lattice is reached. This necessitates a two step model for describing energy transfer in such a situation. Equations (1.1) and (1.2) and their consideration over classical energy transfer models have been discussed in [Tzou 1996].

1.2 Objective of Research

The objective of this research is to develop a hybrid scheme for solving the parabolic two-phase heat equation in an irregular shaped double layer thin film. The finite element methodology is implemented as well as the finite difference methodology. The benefits of both methods are utilized while minimizing their draw backs by hybridizing them.

To achieve this objective, the following development is pursued:

1. Develop a finite element scheme for an irregularly shaped geometry in the x-y dimensions which will generate the matrix coefficients for the hybridized method.
2. Develop a finite difference scheme for the z-axis, (depth plane) and time level for the hybridized method. This scheme has at least a second order accuracy in time and space.
3. Combine these two methodologies to formulate the hybridized method.
4. Analyze stability and accuracy for the hybridized method.
5. Apply the hybridized method to the investigation of temperature rise of a gold/chromium layered disk system subjected to short-pulse laser irradiation on the surface.

The outcome of this study will provide an efficient and reliable numerical method for solving micro-scale heat transport equations, and give a better understanding of the nature of heat transport in such a system. Also, the hybridization procedure offers a new way to examine three dimensional heat transport systems – one that utilizes the strengths of both the finite element and the finite difference methodologies. The research results

have a significant impact on the development of short-pulse laser applications in structural monitoring of thin metal films, laser patterning of such films and laser synthesis and processing of thin film deposition.

1.3 Organization of the Dissertation

The dissertation is organized in the following manner. Chapter Two introduces the process of micro-scale heat transfer by phonon-electron interaction model, the dual-phase-lagging behavior, and a review of previous research. Chapter Three introduces the proposed model for solving the dual-phase heat equation in three dimensions. A hybrid method is described which combines the benefits of the finite element scheme for an irregularly shaped planar surface and the finite difference scheme to describe the depth and time dimensions. To show the applicability for this scheme, we examine a specific case in Chapter Four. Temperature change and distribution in a two layered disk (gold-chromium), subjected to pulse laser irradiation is modeled. The stability and accuracy of this scheme is examined. Chapter Five examines the modeled results for three distinct cases. Finally, conclusions are drawn and possible future study is examined in Chapter Six.

CHAPTER TWO

BACKGROUND AND PREVIOUS WORK

2.1 General Heat Transfer Model

The heat transfer model attempts to predict the energy transfer which may take place between and within materials as a result of a temperature difference. Heat transfer “supplements the first and second principles of thermodynamics by providing additional rules which may be used to establish energy-transfer rates” [Holman 1997, pg. 1]. Classically, there are three basic heat transfer situations – conduction, convection and radiation [Holman 1997]. When a temperature gradient exists, there is an energy transfer from the high-temperature region to the low-temperature region. This reality describes the conduction type of heat transfer.

If we consider an element in a Cartesian coordinate system as described in Figure 2.1, we can illustrate a general (macro-scale) heat transfer model.

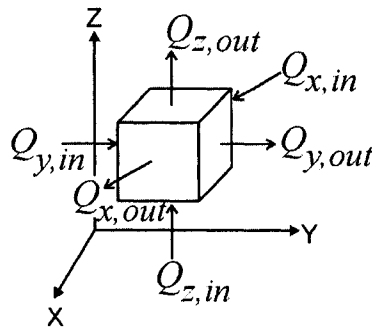


Figure 2.1 An example element in three dimensions

The First Law of Thermodynamics, also known as the Energy Conservation Principle, may be understood as follows [Holman 1997]

$$\dot{Q}_{net} - \dot{W}_{net} = \Delta E \quad (2.1)$$

where \dot{Q}_{net} represents the net energy transfer as heat in the system, \dot{W}_{net} represents the net energy transfer as work and ΔE represents the change in energy stored within the element.

The heat transfer into the element, along one spatial direction, may be determined from the Fourier rate equation for conduction. It is represented

$$\dot{Q}_{x,in} = -\kappa dA_x \frac{\partial T}{\partial x} = -\kappa dydz \frac{\partial T}{\partial x}. \quad (2.2)$$

The quantity κ is the thermal conductivity of the material, T is the temperature at a particular location and time t . This above example is along the x-direction. However similar procedures can be followed for the y- and z-directions.

The heat conducted out of the element, again in one direction, may be written

$$\dot{Q}_{x,out} = \dot{Q}_{x,in} + \frac{\partial \dot{Q}_x}{\partial x} dx = \dot{Q}_{x,in} - \frac{\partial}{\partial x} \left(\kappa \frac{\partial T}{\partial x} \right) dx dy dz \quad (2.3)$$

Combining (2.2) and (2.3) yields the net heat transfer rate

$$\dot{Q}_{x,net} = \dot{Q}_{x,in} - \dot{Q}_{x,out} = \frac{\partial}{\partial x} \left(\kappa \frac{\partial T}{\partial x} \right) dx dy dz \quad (2.4)$$

The work transfer rate may be written in the general form in terms of the rate of energy dissipation per unit volume, S . It is also considered the “source” term. The net work transfer rate for the element is

$$\dot{W}_{net} = -S dx dy dz \quad (2.5)$$

Also, the rate of change of energy stored in the element is

$$\Delta E = dm c \frac{\partial T}{\partial t} = (\rho dx dy dz) c \frac{\partial T}{\partial t} = \rho c \frac{\partial T}{\partial t} dx dy dz = C_p \frac{\partial T}{\partial t} dx dy dz \quad (2.6)$$

The quantity dm is the element mass, ρ is the density of the material and c is the specific heat per unit mass. C_p is the product of ρ and c and represents the specific heat per unit volume.

Making substitutions from Equations (2.4), (2.5) and (2.6), including the y- and z- directions, we obtain

$$\frac{\partial}{\partial x} \left(\kappa \frac{\partial T}{\partial x} \right) + \frac{\partial}{\partial y} \left(\kappa \frac{\partial T}{\partial y} \right) + \frac{\partial}{\partial z} \left(\kappa \frac{\partial T}{\partial z} \right) + S = C_p \frac{\partial T}{\partial t} \quad (2.7)$$

We may define the Laplacian operator applied to the variable u as

$$\nabla^2 u = \frac{\partial^2 u}{\partial x^2} + \frac{\partial^2 u}{\partial y^2} + \frac{\partial^2 u}{\partial z^2} \quad (2.8)$$

Applying the Laplacian operator to the notation of equation (2.7) yields the general formulation for the heat transfer equation

$$C_p \frac{\partial T}{\partial t} = \nabla (\kappa \nabla T) + S \quad (2.9)$$

If we consider the thermal conductivity, κ , as constant, we obtain

$$C_p \frac{\partial T}{\partial t} = \kappa \nabla^2 T + S \quad (2.10)$$

2.2 Microscale Heat Transfer

2.2.1 Differences with Macroscale Heat Transfer

While the conventional, (macroscale) model is widely used to understand the transfer of heat energy, it is often not physically realistic. Equation (2.10) is a parabolic equation. As a result, any temperature disturbance will propagate at an infinite speed. This is physically unrealizable [Herwig 2000].

Because Fourier's law does not predict finite wave speeds, the law does not accurately approximate the heat transfer in certain cases. The assumption of

instantaneous energy transmission fails during a short duration of initial transient, or when the thermal propagation speed is not high, such as in low temperatures [Barron 1985]. In other words, Fourier's law breaks down at temperatures near absolute zero or when the observation time is extremely small during a transient. For these cases, the wave nature of thermal transport becomes dominant, rendering Fourier's law incomplete as an approximation for these cases [Glass 1985]. Specific to this work, Fourier's law does not accurately predict the transient temperature during microscale ($<10^{-12}$ s) laser heating of thin metal films ($<10^{-6}$ m) [Qui 1993c].

2.2.2 Wave Nature of Microscale Heat Transfer

In solids that are not good electrical conductors, the principal mode of conduction heat transfer is that of vibrational energy transfer from one atom to its neighbors. Atoms in solids are constantly vibrating at very high frequencies and with relatively small amplitudes. The atomic vibrations of adjacent atoms are coupled through atomic bonding. These vibrations are coordinated in such a way that traveling lattice waves are produced, which propagate through the lattice at the speed of sound. A single quantum of vibrational energy is called a *phonon*.

However, in metals, the free electron mechanism of heat transport is much more efficient than the phonon mechanism, because phonons are more easily scattered than free electrons and because electrons have higher velocities. Figure 2.2 illustrates the different mechanisms by which electrons can be scattered. All of these mechanisms are important in the study of microscale heat transfer [Smith 2004].

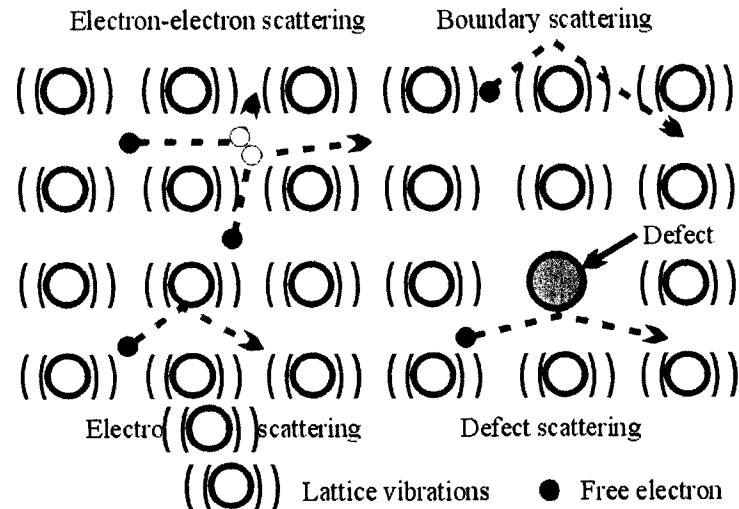


Figure 2.2 Primary scattering mechanisms of free electrons within a metal

The mean free path of an electron in a bulk material is typically on the order of 10 to 30 nm, where electron lattice scattering is dominant. However, when the film thickness is on the order of the mean free path, boundary scattering becomes important [Tzou 1996]. Thin films are manufactured using a number of methods and a wide variety of conditions. The manufacturing method and environmental conditions during manufacture can have serious influence on the microstructure of the film, which in turn influences defect and grain boundary scattering. Also, when heated by ultrashort pulses, the electron system becomes so hot that electron-electron scattering can become significant. Thus, microscale heat transfer requires consideration of the microscopic energy carriers and the full range of possible scattering mechanisms.

2.3 Dual Phase Lagging Behavior

2.3.1 Phase Lag

Qui and others have proposed a *phase lag* model to explain the wave-like propagation of heat on a microscale. This model expresses two primary phases for heat

conduction. The first involves the deposition of energy on electrons while the second involves the transfer of this energy from electrons to the lattice of the material. As early as 1957, Kaganov *et al* proposed that free electrons can be heated to a temperature that is much higher than the lattice temperature in certain situations [Kaganov 1957]. This high heating results in a double phase heating of the material. According to Qui, there exist two characteristic times for the transfer of heat: *thermalization time* and *relaxation time*. [Qui 1993c]. Thermalization time represents the time for electrons and the lattice to reach thermal equilibrium. It represents the time necessary to convert heat energy to the internal lattice. Relaxation time represents the time for electrons to change their states.

During a relatively slow heating process, the thermalization time can be thought of as instantaneous. This is modeled well by a Fourier's law model. However, for very short laser-pulse heating, these assumptions are subject to question [Qui 1993c]. In fact, because the physical dimension in microscale heat transfer is of the same order of magnitude as the electron free path, the response time is of this same magnitude. This indicates that the temperature gradient is not descriptive for a thin film of the same thickness as the mean free path [Tzou 1996].

2.3.2 Model Formulation

The model in Equation (2.10) can be described to as a *parabolic one-step* equation. This is due to the assumptions it makes. These being that heat energy is converted to lattice energy instantaneously and that heat energy is assumed to be a diffusive process [Qui 1993c]. Other, non-Fourier models have been proposed to deal with the failings of the Fourier model on a microscale. One model is based on the modified flux law [Tzou 1993]

$$Q + \tau \frac{\partial Q}{\partial t} = -\kappa \nabla T \quad (2.11)$$

Where τ is the relaxation time and Q is the heat flux. The heat flux vector in this case maintains a *memory* of the time-history of the temperature gradient. Relaxation time is the effective mean free path l , divided by the phonon speed v_s . Mathematically $\tau = l/v$. In the absence of relaxation time (or $\tau = 0$), which implies a mathematical idealization from either a zero mean free path ($l = 0$) or an infinite phonon speed ($v \rightarrow \infty$) for phonon collisions, then Equation (2.11) reduces to the classical Fourier rate equation. Therefore, an infinite speed of heat propagation is an assumption made in the classical theory of diffusion utilizing Fourier's law [Tzou 1993].

When Equation (2.11) is combined with Equation (2.10), we obtain the hyperbolic heat equation

$$\begin{aligned} C \frac{\partial T}{\partial t} &= -\nabla Q + S, \\ \tau \frac{\partial Q}{\partial t} + \kappa \nabla T + Q &= 0 \end{aligned} \quad (2.12)$$

This equation is known as a hyperbolic equation because of the additional term that modifies the parabolic Fourier heat Equation (2.10) [Tang 1996]. The double derivative terms are the wave terms. This modification predicts a finite speed of heat propagation because of the relaxation time τ , associated with heat transfer. Typical wave speeds in metals are on the order of 10^5 m/s [Özisik 1994].

While the hyperbolic model answers some issues arising from a microscale examination of heat transfer, it still leaves questions. It is not based on the details of energy transport in the material, such as the interaction of electrons and phonons [Qui 1993a]. Also, material properties may not be able to be regarded as constant. The

relaxation time and thermal conductivity are generally temperature-dependent [Tzou 1993]. In addition, the value of thermal conductivity depends on processing parameters such as laser pulse duration and intensity, during short-pulse laser heating [Qui 1993b].

These considerations have led to the dual-phase lag equation. This equation is derived from the lag equation which holds a lag in heat flux behind the temperature gradient. Compared to the hyperbolic heat equation, this model has an additional mixed derivative term. Now, as with the hyperbolic model, the time lag associated with heat flux causes wavelike behavior. However, the additional time lag creates a mixed derivative term that smoothes the sharp wave fronts caused by the first lag term. The mixed derivative term renders the equation in the form of a parabolic equation. This parabolic dual phase equation is modeled thus

$$C_e(T_e) \frac{\partial T_e}{\partial t} = \nabla(\kappa \nabla T_e) - G(T_e - T_l) + S \quad (2.13a)$$

$$C_l(T_l) \frac{\partial T_l}{\partial t} = G(T_e - T_l) \quad (2.13b)$$

Here, C_e and C_l are the volumetric electron heat capacity and the volumetric lattice heat capacity respectively, and G is the electron-lattice coupling factor. The coupling factor will be described in detail later.

Qui and Tien [Qui 1993a] derived a model described as the *hyperbolic two step* model from the Boltzmann transport for electrons. Each of these models have functionality. Each is, however, contingent upon the interrelatedness of thermalization time and relaxation time. Figure 2.3 illustrates the applicability stemming from these relationships.

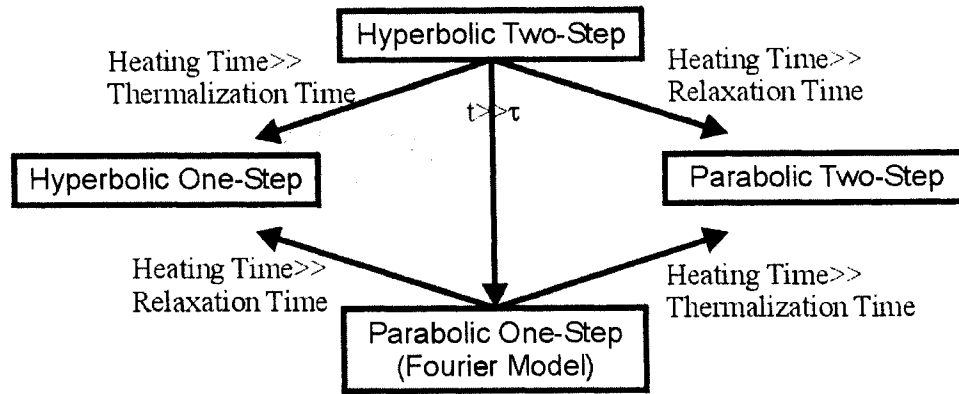


Figure 2.3 Interrelationship between laser heating models [Qui 1993a]

The complexity of solutions for Equation (2.13) lies in the temperature-dependent heat capacity of the electron gas. Tzou argues that for an electron gas temperature lower than the Fermi temperature, (of the order of 10^4 K), the electron heat capacity (C_e), is proportional to the electron temperature [Tzou 1996]. This makes the equation non-linear. In metals, the specific heat can be given by [Barron 1985]

$$C_e = \gamma_e T_e \quad (2.14)$$

Where γ_e is known as the electron specific heat coefficient and is experimentally obtainable.

In the parabolic dual-phase model, the energy exchange between phonons and electrons is characterized by the phonon-electron coupling factor G [Kaganov 1957]

$$G = \frac{\pi^2}{6} \frac{m_e n_e v_s^2}{\tau_e T_e} \text{ for } T_e \gg T_l \quad (2.15)$$

where m_e represents the electron mass, n_e the number density (concentration) of electrons per unit volume, and v_s the speed of sound

$$v_s = \frac{k}{2\pi h} (6\pi^2 n_a)^{-\frac{1}{3}} T_D \quad (2.16)$$

with the quantity h being Planck's constant, k being Boltzmann constant, n_a being the atomic number density per unit volume, and T_D representing the Debye temperature. The electron temperature (T_e) is much higher than the lattice temperature (T_l) in the early time response. The condition $T_e \gg T_l$ in Equation (2.15) for the applicability of G is thus valid in the fast-transient process of electron-phonon dynamics. Within the limits of Wiedemann-Frenz's law, which states that for metals at moderate temperatures ($T_l > 0.48T_D$), the ratio of the thermal conductivity to the electrical conductivity is proportional to the temperature and the constant of proportionality is independent of particular metal, the electron thermal conductivity can be expressed

$$\kappa_e = \frac{\pi^2 n_e k^2 \tau_e T_e}{3m_e} \quad (2.17)$$

Or simply

$$m_e = \frac{\pi^2 n_e k^2 \tau_e T_e}{3\kappa_e} \quad (2.18)$$

Substituting (2.18) into (2.15) for the electron mass yields

$$G = \frac{\pi^4 (n_e v \kappa_s)^2}{18k} \quad (2.19)$$

This coupling factor is dependent upon the thermal conductivity, (κ) and the number density of the electron gas. The coupling factor does not show a strong dependence on temperature and is not effected by relaxation time [Tzou 1996].

In order to estimate the value of G , the number density of the electron gas is a key quantity. Qui and Tien assumed one free electron per atom for noble metals and employed the s-band approximation for the valence electrons in transition metals [Qui 1993c]. Thus the value for number density of the electron gas is chosen as a fraction of

the valence electrons. The phonon-electron coupling factor is calculated, and experimentally measured values are listed in Table 2.1 for comparison.

Table 2.1 Phonon-electron coupling factor (G), for some noble and transition metals [Tzou 1996]

Metal	Calculated, x 10¹⁶ W/m³K	Measured, x 10¹⁶ W/m³K
Cu	14	4.8 ± 0.7 (Brorson et al., 1990) 10 (Elsayed-Ali et al., 1987)
Ag	3.1	2.8 (Groeneveld et al., 1990)
Au	2.6	2.8 ± 0.5 (Brorson et al. 1990)
Cr	45 ($n_e/n_a = 0.5$)	42 ± 5 (Brorson et al. 1990)
W	27 ($n_e/n_a = 1.0$)	26 ± 3 (Brorson et al. 1990)
V	648 ($n_e/n_a = 2.0$)	523 ± 37 (Brorson et al. 1990)
Nb	138 ($n_e/n_a = 2.0$)	387 ± 36 (Brorson et al. 1990)
Ti	202 ($n_e/n_a = 1.0$)	185 ± 16 (Brorson et al. 1990)
Pb	62	12.4 ± 1.4 (Brorson et al. 1990)

Equation (2.13a) is governed by diffusion in the electron gas and heat is transferred to the lattice in a lumped capacity sense through the coupling factor, G . In other words, the rate of energy increase in the metal lattice is proportional to the temperature difference between the metal lattice and the electrons. By eliminating the electron gas temperature, T_e from Equation (2.13) for constant thermal properties, one can show that

$$\frac{1}{\alpha_T} \frac{\partial T_l}{\partial t} + \frac{1}{C_T^2} \frac{\partial^2 T_l}{\partial t^2} = \nabla^2 T_l + \frac{\alpha_e}{C_T^2} \frac{\partial}{\partial t} (\nabla^2 T_l) \quad (2.20)$$

Where α_e is the thermal diffusivity of the electron gas and α_T is the equivalent thermal diffusivity represented by

$$\alpha_T = \frac{\kappa}{C_e + C_l} \quad (2.21)$$

C_T is the thermal wave speed and is represented by

$$C_T = \sqrt{\frac{\kappa G}{C_e C_l}} \quad (2.22)$$

However, for simplicity of discussion and ease of numerical analysis, this single equation form is seldom utilized. In this work, Equation (2.13) is used.

Researchers determined the parabolic two-step model to be a good estimate [Qui 1992]. To compare experimental results with a numerical model, the normalized temperature change in the electron gas is identical to the normalized reflectivity change on the film surface

$$\frac{\Delta R}{(\Delta R)_{\max}} = \frac{\Delta T_e}{(\Delta T_e)_{\max}} \quad (2.23)$$

where R denotes the reflectivity. The left side of Equation (2.23) can be measured by the front-surface-pump and back-surface-probe technique [Tzou 1996]. The right hand side of Equation (2.23) represents the solution to the numerical model for estimating heat propagation.

Figure 2.4 shows the resulting applicability of the parabolic two step model. The predicted temperature change at the surface of a thin gold film is compared with the experimental data collected.

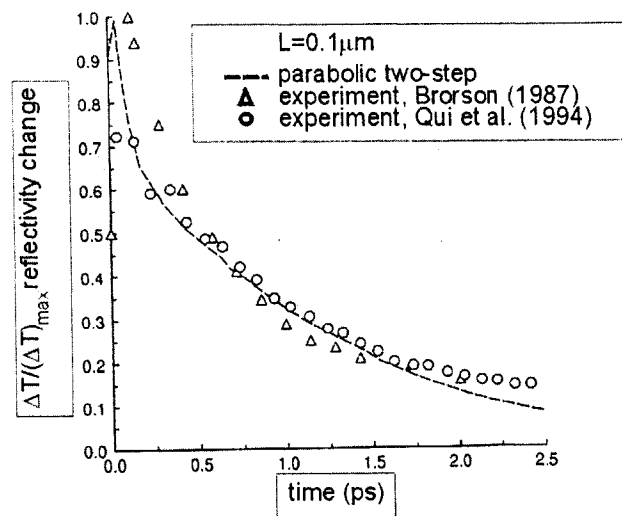


Figure 2.4 Normalized temperature change (reflectivity change) in gold film predicted by dual-phase-lag model [Tzou 1996]

2.4 Previous Work

There are many numerical solutions to the various forms of the microscale heat equation, [Tzou 1994, 1995a, 1995b, 1995c, 1995d, 1996, 1999, 2000a, 2000b, 2001, 2002] [Özsisik 1994] [Chiffell 1994] [Wang 2000, 2001a, 2001b, 2002] [Antaki 1998, 2000, 2002] [Dai 1999, 2000a, 2000b, 2000c, 2001a, 2001b, 2004a, 2004b] [Qui 1992, 1993, 1994a, 1994b] [Joshi 1993] [Chen 1999a, 1999b, 2000a, 2000b, 2001a, 2001b, 2001c, 2003] [Al-Nimr 1997a, 1997b, 1999, 2000a, 2000b, 2000c, 2001, 2003] [Tang 1996, 1999] [Lin 1997][Ho 1995, 2003] [Tsai 2003][Shen 2003]. Among these Tzou and Özsisik [Tzou 1994] considered the heat equation in only one dimension. They studied the lagging behavior by solving over a semi-infinite interval. Their solutions were obtained using the Laplace transform method and the Reimann-sum approximation for the inversion.

Özisik's [Özisik 1994] work gives a thorough overview of the thermal wave theory emphasizing its applications in the field of engineering applications. Special features in thermal wave propagation such as the sharp wavefront and rate effects, the thermal shock phenomenon, the thermal resonance phenomenon, and reflections of thermal waves across a material interface were discussed. Joshi and Majumdar [Joshi 1993] obtained numerical solutions using the explicit upstream difference method. Antaki and others [Antaki 1998, 2000, 2002] investigated the heat conduction in a semi-infinite slab. Tang and Araki [Tang 1999] derived an analytic solution in finite rigid slabs by using Green's function and a finite integral transform technique. Ho and colleagues [Ho 1995, 2003] studied heat transfer in a multilayered structure using the lattice Boltzmann method. Tsai and Hung [Tsi 2003] studied thermal wave propagation in a bi-layered composite sphere using the dual-phase-lag heat transport equation. Recently, Dai and Nassar [Dai 2004b] have developed a finite difference scheme for solving the parabolic two-step heat transport equations in a 3D double-layered rectangular thin film. Tzou and Chiu studied thermal lagging in ultra-fast laser heating [Tzou 2001]. This was implemented to describe the experimental data of femtosecond (*fs*) laser heating of gold films. An explicit finite difference scheme was developed. It was found that the lag model including temperature-dependant thermal properties yields numerical values that are consistent with the experimental data for ultra-fast heating on gold films. Wang and associates [Wang 2001b] showed that the dual-phase heat conduction equation is well-posed in a finite region under Dirichlet, Neumann or Robin boundary conditions. Later, Wang [Wang2002] showed the dual-phase heat conduction equation offers a unique solution under these same boundary conditions. Tang and Araki

[Tang 1999] introduced a generalized macroscopic model in treating the transient heat conduction problem in finite rigid slabs irradiated by short-pulse lasers. The analytical solution is derived from Green's function method and a finite integral transform technique. Energy transfer features such as wave, wavelike and diffusion behaviors were exhibited by adjusting the relaxation parameters. Their numerical methods were compared with experimental data and showed agreement. Lin and associates [Lin 1997] obtained an analytic solution using Fourier series. An exact solution, using a separation of variables technique, to the universal equation between heat flux and the temperature gradient for the one dimensional case was considered. Al-Nimr and Arpaci [Al-Nimr 1997a, 1997b, 1999, 2000a, 2000b, 2001, 2003] proposed an approach based on the physical decoupling of the hyperbolic two-step model, to describe the thermal behavior of a thin metal film exposed to picosecond thermal pulse. This approach was based upon the assumption that the metal film thermal behavior occurs in two distinct stages. In the first phase, the electron gas transmits its energy to the lattice through electron-phonon coupling. In the second phase, the electron gas and lattice are at thermal equilibrium. In this phase diffusion dominates the transfer of energy within the system. This method, which eliminates the coupling of energy equations to simplify the system, applies to metal films with the parameter $\frac{GL^2}{K_e}$ much less than one. Chen and Beraun [Chen 1999a, 1999b, 2000a, 2000b, 2001a, 2001b, 2001c, 2003] used a corrective smoothed particle method to find a numerical solution to the interaction of short laser bursts and thin metallic films. Dai and Nassar [Dai 1999, 2001, 2002, 2004] and associates have developed many finite difference models for examining a numerical solution for a dual thin film system irradiated by an ultrashort laser burst.

Thus there is considerable research covering the dual-phase model for heat conduction. Research has supported the fact that the dual-phase model is applicable in this case. The model is well-posed, it produces a unique solution, and the numerical results accurately describe experimental results. However, research concerning numerical solutions to this dual-phase equation has been bounded. In the case of analytical methodologies, single dimensional systems are the primary consideration. The numerical methodologies concentrate on finite difference models for specific geometries. These utilize many different methodologies for the specific situation. They include modified Crank-Nicholson schemes, alternating direction implicit schemes, and three level finite difference scheme in spherical coordinates.

There is a need for a generalized numerical solution to this model – one that is flexible for many geometries and dimensionalities. This work extends the body of research to the case that the double-layered thin film is irregular in the planar direction and develops an unconditionally stable FE-FD hybrid scheme for solving the parabolic two-step model.

CHAPTER THREE

MATHEMATICAL MODEL

3.1 Problem Description

In this dissertation, we consider an irregularly shaped double-layer thin film exposed to ultrashort-pulse lasers as shown in Figure 3.1. We will determine the temperature rise in the thin-film.

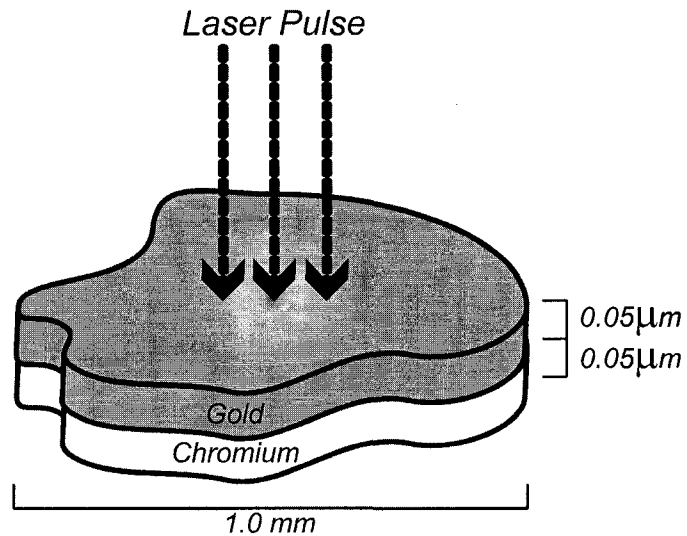


Figure 3.1 Graphical Representation of Modeled Example

The mathematical model which governs the heat transfer on the double-layered thin film exposed to ultrashort-pulse laser can be described by adding layer information to Equation (2.13).

It is expressed

$$C_e^{(m)} \frac{\partial T_e^{(m)}}{\partial t} = \nabla(\kappa_e^{(m)} \nabla T_e^{(m)}) - G^{(m)}(T_e^{(m)} - T_l^{(m)}) + S^{(m)} \quad (3.1a)$$

$$C_l^{(m)} \frac{\partial T_l^{(m)}}{\partial t} = G^{(m)}(T_e^{(m)} - T_l^{(m)}) \quad (3.1b)$$

where $C_e = \gamma T_e$, and C_e^0 initially and here $m=1,2$ and represents the two layers of the system.

In this problem, we consider the case in which the temperature of the electrons and the temperature of the lattice are initially uniform and equal to T_0 before the laser pulse is applied. Thus, the initial conditions are as follows

$$T_e(x, y, z, -2t_p) = T_l(x, y, z, -2t_p) = T_0 \quad (3.2)$$

where t_p indicates the laser pulse duration. At the top of the gold layer, ($z = 0$), and at the bottom of the chromium layer, ($z = L$), the heat transfer rate is generally very small. In this problem, the heat transfer rate at these two interfaces is considered to be zero. Thus, the Neumann boundary conditions exist

$$\nabla T_e|_0 = \nabla T_e|_L = \nabla T_l|_0 = \nabla T_l|_L = 0 \quad (3.3)$$

The temperature of the gold layer and the temperature of the chromium layer are equal at the interface between the two layers. This indicates that there is no “temperature jump” between the two layers due to the bonding of the layers. Thus, at the gold-chromium boundary, the following condition exists

$$T_e|_{Au} = T_e|_{Cr} \quad \text{and} \quad T_l|_{Au} = T_l|_{Cr} \quad (3.4)$$

In addition, the heat conducted through the gold-chromium interface from the gold is equal to the heat conducted into the chromium. Thus, at the gold-chromium interface, the additional condition arises

$$\kappa^{(1)} \nabla T_e \Big|_{Au} = \kappa^{(2)} \nabla T_e \Big|_{Cr} \quad (3.5)$$

The source term is defined as

$$S^{(m)} = 0.94 \left(\frac{1-R}{t_p \delta} \right) J \exp \left[-\frac{z}{\delta} - 2.77 \left(\frac{t-2t_p}{t_p} \right)^2 \right] \quad (3.6)$$

and R is given as 0.93, and $\delta = 15.3 \text{ nm}$. J represents the total energy carried by laser pulse divided by the laser spot cross section $t_p = 100 \text{ fs}$ and represents the full-width-at-half-maximum (FWHM) duration of laser pulse time, (t_0), or $t = 0$, is when laser arrives at metal surface [Tzou 1996]. Figure 3.2 gives an example with $J = 13.4 \text{ J/m}^2$.

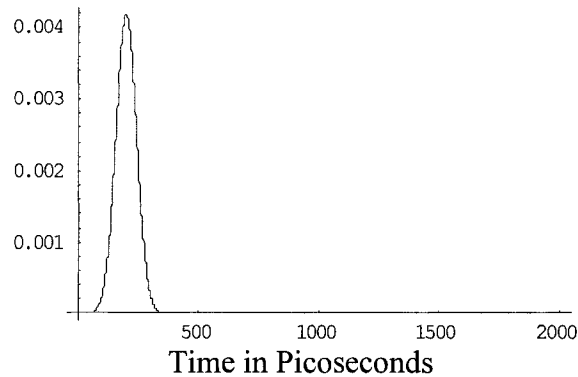


Figure 3.2 Plot of laser heat source

It is difficult to obtain an analytic solution for this problem due to the complex geometry and nonlinear coefficients. Therefore a numerical solution is sought in this study.

3.2 General Procedure

3.2.1 Approach Described

The following procedure in the numerical method will be used:

- 1) Since the thin film is irregular in shape with respect to the xy -directions, we first discretize the Equation (3.1) in the xy -direction using the finite element method. To this end, we set up global finite element formulation using a modified Galerkin Weighted Residual method. The matrix coefficients (in the x - y plane) are assembled yielding a system of parabolic partial differential equations in one direction (z -axis).
- 2) Utilize the finite difference method to discretize this PDE system in the z -direction.

3.2.2 Reasoning Behind Hybrid Approach

While there are many different means by which partial differential equation systems can be solved, many situations make the use of analytical methods which are laborious and difficult to use. One of the most powerful methods for obtaining a numerical solution is the finite element method. The basic ideas behind this methodology date back to the early 1940's, however it's principles came together during the 1960's and have grown to a better applicability due to the advent of faster computers [Comini 1996].

The finite element methodology is based on three ideas [Gockenbach 2002]:

1. The problem is written in its *weak* or *variational form*, which expresses the problem as infinitely many scalar equations. In this form, we have the boundary conditions given implicitly.
2. A discretization method (in our situation, the Galerkin Weighted Residual), is applied to solve the above equation on a finite-dimensional subspace. This results in a linear system of equations which must be solved.

3. A basis of *piecewise polynomials* is chosen for the finite-dimensional subspace so that the matrix system will be sparse and thus easier to solve.

Because of the broad choice of weighting functions, there are many residual methods by which we can apply the finite element methodology. We choose a common method known as the Galerkin Weighted Residual method [Comini 1996]. According to this method, the weighting functions are chosen to be the same as the approximating functions (basis functions). This has several advantages:

1. The avoidance of manipulating two sets of functions – one for the basis and another for the weighting function.
2. The general property of the shape functions offers a naturally sparse matrix system.
3. This method leads to symmetric matrices.
4. According to Gockenbach, “the Galerkin approximation is a *best approximation* to the true solution,” [Gockenbach 2002, pg. 181].

Perhaps of equal importance is that the finite element methodology is well suited for oddly shaped or irregularly shaped objects. The mesh generated can be done so as to minimize the unallocated space on the boundaries. The elements do not have to have a uniform shape and can thusly be “adapted” to fit the irregular geometry.

However, the finite element system is computationally intense. Also, the more dimensions, or axis, that are added, the more complicated the methodology becomes. It is also difficult to combine both a spatial and time level estimation with the finite element methodology. Often a finite difference methodology is preferred for regular or non-curved geometries or time-dependant systems.

The approach is to combine the strengths of the finite element methodology (accuracy, irregular geometry considerations, sparse matrix system generation) while avoiding the before-mentioned drawbacks. One way to do this is by taking the finite element method in two spatial dimensions while holding the third spatial dimension and time dimension to be estimated through a finite difference scheme. This is possible, even preferred, if the third dimension is a regular, non-curved geometry. This is the aim of this work.

CHAPTER FOUR

NUMERICAL METHOD

4.1 Finite Element Method

4.1.1 Modified Galerkin Weighted Residual Approach

Utilizing a modified Galerkin residual finite element approach entails establishing a residual function. This residual is then multiplied by a weighting function and then made to be, on average, zero. After this weak formulation is pronounced, the weighting and basis functions are established. These will be used to formulate the matrix coefficients for a system of partial differential equations. Derivatives with respect to time and the z-axis are deliberately carried. These quantities will be determined by the finite difference method. After the basis and weighting functions have been formulated, a triangular mesh is used to assemble the matrix system and solve the finite element portion of the scheme.

4.1.2 Formulation

For the heating of the electron gas, our residual function is described thus

$$\begin{aligned} R(x, y, z, t) &= C_e \frac{\partial T_e}{\partial t} - \kappa \nabla^2 T_e + G(T_e - T_l) - S \\ &= C_e \frac{\partial T_e}{\partial t} - \kappa \frac{\partial^2 T_e}{\partial x^2} - \kappa \frac{\partial^2 T_e}{\partial y^2} - \kappa \frac{\partial^2 T_e}{\partial z^2} + G(T_e - T_l) - S \end{aligned} \quad (4.1)$$

In this system, C_e is a function of time and space. It is represented as

$$C_e \equiv C_e(T_p(z, t)) \quad (4.2)$$

where T_p will be defined later.

This residual is multiplied by a weighting function and set to be, on average zero.

It is expressed

$$\int [Rw] d\Omega = 0 \quad (4.3)$$

where w is the weighting function. By substitution, we obtain

$$\iint \left[C_e \frac{\partial T_e}{\partial t} w - \kappa \frac{\partial^2 T_e}{\partial x^2} w - \kappa \frac{\partial^2 T_e}{\partial y^2} w - \kappa \frac{\partial^2 T_e}{\partial z^2} w + G(T_e - T_l)w - Sw \right] dx dy = 0 \quad (4.4)$$

$$\begin{aligned} \iint C_e \frac{\partial T_e}{\partial t} w dx dy - \kappa \iint \left[\left(\frac{\partial^2 T_e}{\partial x^2} + \frac{\partial^2 T_e}{\partial y^2} \right) w \right] dx dy - \kappa \iint \frac{\partial^2 T_e}{\partial z^2} w dx dy + G \iint [(T_e - T_l)w] dx dy \\ - \iint Sw dx dy = 0 \end{aligned} \quad (4.5)$$

or simply

$$\begin{aligned} C_e T_l \iint w dx dy - \kappa \iint [(T_{xx} + T_{yy})w] dx dy - \kappa T_{zz} \iint w dx dy + G(T_e - T_l) \iint w dx dy \\ - S \iint w dx dy = 0 \end{aligned} \quad (4.6)$$

Taking the second term, $-\kappa \iint [(T_{xx} + T_{yy})w] dx dy$ only we note $(wT_x)_x = w_x T_x + wT_{xx}$

and $wT_{xx} = (wT_x)_x - w_x T_x$. Hence we obtain

$$\begin{aligned} -\kappa \iint [(wT_x)_x + (wT_y)_y] dx dy + \kappa \iint [w_x T_x + w_y T_y] dx dy \\ = -\kappa \oint_{\partial D} [wT_x n_x + wT_y n_y] ds + \kappa \iint [w_x T_x + w_y T_y] dx dy \end{aligned} \quad (4.7)$$

As $w(T_x n_x + T_y n_y) = w \vec{n} \nabla T$, this term is expressed

$$-\kappa \oint_{\partial D} [w \vec{n} \nabla T] ds + \kappa \iint [w_x T_x + w_y T_y] dx dy \quad (4.8)$$

The weak formulation is therefore

$$C_e \frac{\partial T_e}{\partial t} \iint w dx dy - \kappa \oint_{\partial D} [w \vec{n} \nabla T] ds + \kappa \iint \left[\frac{\partial T}{\partial x} \frac{\partial w}{\partial x} + \frac{\partial T}{\partial y} \frac{\partial w}{\partial y} \right] dx dy - \kappa \frac{\partial^2 T_e}{\partial z^2} \iint w dx dy \quad (4.9)$$

$$+ G(T_e - T_l) \iint w dx dy - S \iint w dx dy = 0$$

The term, $-\kappa \oint_{\partial D} [w \vec{n} \nabla T] ds$, contains the information from the boundary conditions.

Next the test function is defined as

$$T_h(x, y, z, t) = \sum_{p=1}^N T(z, t) \varphi_p(x, y) \quad (4.10)$$

where $\varphi_p(x, y)$ is a basis function, and N is the number of points in our x-y cross section.

The source term is defined to be

$$S_h = \sum_{p=1}^N S_p \varphi_p(x, y) \quad (4.11)$$

The weighting function, $w = \varphi_q(x, y)$. Therefore, we obtain

$$\begin{aligned} & \sum_{p=1}^N C_e \frac{\partial T}{\partial t} \left[\iint (\varphi_p \varphi_q) dx dy \right] + \sum_{p=1}^N \kappa T_p \left[\iint \left(\frac{\partial \varphi_p}{\partial x} \frac{\partial \varphi_q}{\partial x} + \frac{\partial \varphi_p}{\partial y} \frac{\partial \varphi_q}{\partial y} \right) dx dy \right] \\ & - \sum_{p=1}^N \kappa \frac{\partial^2 T}{\partial z^2} \left[\iint (\varphi_p \varphi_q) dx dy \right] + \sum_{p=1}^N G(T_p - T_l) \left[\iint (\varphi_p \varphi_q) dx dy \right] \\ & - \sum_{p=1}^N S \left[\iint (\varphi_p \varphi_q) dx dy \right] = 0 \end{aligned} \quad (4.12)$$

Setting $m_{qp} = \iint (\varphi_p \varphi_q) dx dy$ and $k_{qp} = \kappa \iint \left(\frac{\partial \varphi_p}{\partial x} \frac{\partial \varphi_q}{\partial x} + \frac{\partial \varphi_p}{\partial y} \frac{\partial \varphi_q}{\partial y} \right) dx dy$ a matrix formulation is obtained

$$C_e \mathbf{M} \frac{\partial \bar{T}_e}{\partial t} + \kappa \mathbf{K} \bar{T}_e - \kappa \mathbf{M} \frac{\partial^2 \bar{T}_e}{\partial z^2} + G \mathbf{M} (\bar{T}_e - \bar{T}_l) = \mathbf{M} \bar{S} \quad (4.13)$$

Repeating this process for the lattice equation yields

$$R_l(x, y, z, t) = C_l \frac{\partial T_l}{\partial t} - G(T_e - T_l)$$

$$\begin{aligned}
\int [R_l w] dx dy &\Rightarrow \iint \left[C_l \frac{\partial T_l}{\partial t} - G(T_e - T_l) \right] w dx dy = 0 \\
&\Rightarrow \iint \left[C_l \frac{\partial T_l}{\partial t} w \right] dx dy - G \iint [(T_e - T_l) w] dx dy = 0
\end{aligned} \tag{4.14}$$

If $T_h(x, y, z, t) = \sum_{p=1}^N T(z, t) \varphi_p(x, y)$ and $w = \varphi_q(x, y)$

$$\sum_{p=1}^N C_l \frac{\partial T}{\partial t} \left[\iint \varphi_p \varphi_q dx dy \right] - \sum_{p=1}^N G(T_e - T_l) \left[\iint \varphi_p \varphi_q dx dy \right] = 0 \tag{4.15}$$

Letting $m_{qp} = \iint \varphi_p \varphi_q dx dy$ we have

$$C_l \mathbf{M} \frac{\partial \bar{T}_l}{\partial t} - G \mathbf{M} (\bar{T}_e - \bar{T}_l) = 0 \tag{4.16}$$

Therefore, the matrix system resulting from the Finite Element Methodology is

$$C_e \mathbf{M} \frac{\partial \bar{T}_e}{\partial t} + \kappa \mathbf{K} \bar{T}_e - \kappa \mathbf{M} \frac{\partial^2 \bar{T}_e}{\partial z^2} + G \mathbf{M} (\bar{T}_e - \bar{T}_l) = \mathbf{M} \bar{S} \tag{4.17a}$$

$$C_l \mathbf{M} \frac{\partial \bar{T}_l}{\partial t} - G \mathbf{M} (\bar{T}_e - \bar{T}_l) = 0 \tag{4.17b}$$

Adding layer information, we obtain

$$C_e^{(m)} \mathbf{M} \frac{\partial \bar{T}_e^{(m)}}{\partial t} + \kappa^{(m)} \mathbf{K} \bar{T}_e^{(m)} - \kappa^{(m)} \mathbf{M} \frac{\partial^2 \bar{T}_e^{(m)}}{\partial z^2} + G^{(m)} \mathbf{M} (\bar{T}_e^{(m)} - \bar{T}_l^{(m)}) = \mathbf{M} \bar{S}^{(m)} \tag{4.18a}$$

$$C_l^{(m)} \mathbf{M} \frac{\partial \bar{T}_l^{(m)}}{\partial t} - G^{(m)} \mathbf{M} (\bar{T}_e^{(m)} - \bar{T}_l^{(m)}) = 0 \tag{4.18b}$$

4.1.3 Establishing a Triangular Mesh

A triangular mesh is chosen for the system. This information is used to create the matrix coefficient system. Figure 4.1 indicates the triangular mesh created for the case presented herein. For linear triangle elements, we can write the element expansion in the form

$$T_h^e = T_1^e \varphi_1^e + T_2^e \varphi_2^e + T_3^e \varphi_3^e \quad (4.19)$$

where $\varphi = a^e + b^e x + c^e y$.

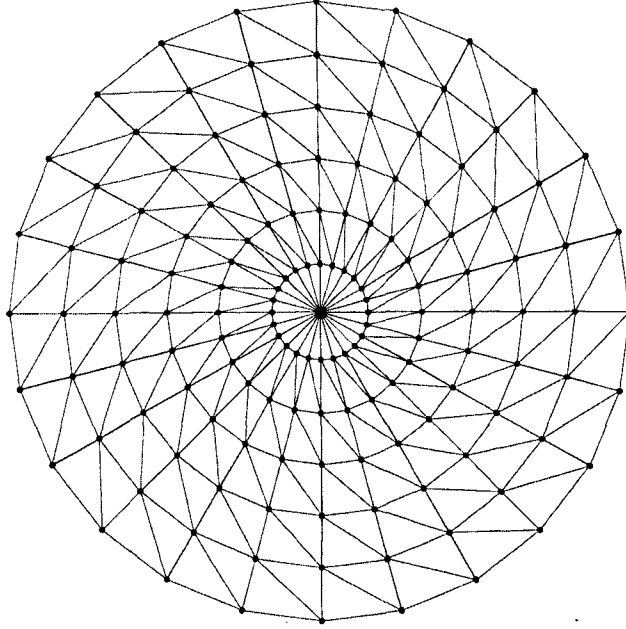


Figure 4.1 Triangular mesh for x-y plane.

After algebraic manipulation, we obtain [Comini 1996]

$$k_{qp} = \iint \left(\frac{\partial \varphi_p}{\partial x} \frac{\partial \varphi_q}{\partial x} + \frac{\partial \varphi_p}{\partial y} \frac{\partial \varphi_q}{\partial y} \right) dx dy = \frac{1}{4\Omega_e} (\beta_i \beta_j + \gamma_i \gamma_j) \quad (4.20)$$

and

$$m_{qp} = \iint (\varphi_p \varphi_q) dx dy = \frac{\Omega_e}{12} (1 + \delta_{ij}) \quad (4.21)$$

where $\Omega_e = \frac{1}{2} (\beta_2^e \gamma_3^e - \beta_3^e \gamma_2^e)$ is the area of the triangular element and δ_{ij} is the Kronecker

delta ($\delta_{ij} = 1$ for $i = j$ and $\delta_{ij} = 0$ for $i \neq j$). Also, $\beta_1^e = y_2^e - y_3^e$, $\beta_2^e = y_3^e - y_1^e$,

$\beta_3^e = y_1^e - y_2^e$ and $\gamma_1^e = x_3^e - x_2^e$, $\gamma_2^e = x_1^e - x_3^e$, $\gamma_3^e = x_2^e - x_1^e$.

This mesh enables the determination of exact values for the nodes in our mesh. This makes matrix assembly easier and helps keep track of our nodal points for the finite difference methodology to be implemented later.

The first step is to find the elemental capacitance (**M**) and elemental conductance (**K**). This is done by following the steps in Equation (4.19) and following.

At this point, the mesh is labeled by element and node. Each elemental matrix is assembled into a global matrix, (one for conductance and one for capacitance). Appendix B contains the source code for this generation. Upon completion of this assembly the Finite Element portion is complete and we move to the z-axis to formulate our temperature distribution over time.

4.2 Modified Weighted Average Finite Difference Scheme

4.2.1 Finite Difference Method Outline

A modified weighted average Finite Difference Method is used to approximate Equation (4.18). The scheme is an implicit scheme which takes three levels in time and space to obtain a higher degree of accuracy for the overall methodology. This is accomplished by averaging each point from three space levels (weighting the central point). Also, the time derivative shall be an averaging of three the time levels surrounding the current time level.

4.2.2 Notation

The previously described scheme results in the following notations

$$\bar{T}_e \approx \frac{\bar{T}_e^{n+1} + 2\bar{T}_e^n + \bar{T}_e^{n-1}}{4} \quad (4.22)$$

$$\bar{T}_i \approx \frac{\bar{T}_i^{n+1} + 2\bar{T}_i^n + \bar{T}_i^{n-1}}{4} \quad (4.23)$$

$$\frac{\partial \bar{T}_e}{\partial t} \approx \frac{\bar{T}_e^{n+1} - \bar{T}_e^{n-1}}{2\Delta t} \quad (4.24)$$

$$\frac{\partial^2 \bar{T}_e}{\partial z^2} \approx \delta_z^2 \left(\frac{\bar{T}_e^{n+1} + 2\bar{T}_e^n + \bar{T}_e^{n-1}}{4} \right) \quad (4.25)$$

$$= \frac{\bar{T}_{e(k-1)}^{n+1} - 2\bar{T}_{e(k)}^{n+1} + \bar{T}_{e(k+1)}^{n+1}}{4\Delta z^2} + \frac{\bar{T}_{e(k-1)}^n - 2\bar{T}_{e(k)}^n + \bar{T}_{e(k+1)}^n}{2\Delta z^2} + \frac{\bar{T}_{e(k-1)}^{n-1} - 2\bar{T}_{e(k)}^{n-1} + \bar{T}_{e(k+1)}^{n-1}}{4\Delta z^2} \quad (4.26)$$

$$\frac{\partial \bar{T}_i}{\partial t} \approx \frac{\bar{T}_i^{n+1} - \bar{T}_i^{n-1}}{2\Delta t} \quad (4.27)$$

4.3 Combined Hybrid Scheme

4.3.1 Formulation

Combining the two methods yields

$$C_e(T_e^n)\mathbf{M} \left[\frac{\bar{T}_e^{n+1} - \bar{T}_e^{n-1}}{2\Delta t} \right] + \kappa \mathbf{K} \left[\frac{\bar{T}_e^{n+1} + 2\bar{T}_e^n + \bar{T}_e^{n-1}}{4} \right] - \kappa \mathbf{M} \left[\delta_z^2 \left(\frac{\bar{T}_e^{n+1} + 2\bar{T}_e^n + \bar{T}_e^{n-1}}{4} \right) \right] \quad (4.28a)$$

$$+ \mathbf{GM} \left[\frac{\bar{T}_e^{n+1} + 2\bar{T}_e^n + \bar{T}_e^{n-1}}{4} - \frac{\bar{T}_i^{n+1} + 2\bar{T}_i^n + \bar{T}_i^{n-1}}{4} \right] = \mathbf{MS}^n$$

$$C_i \mathbf{M} \left[\frac{\bar{T}_i^{n+1} - \bar{T}_i^{n-1}}{2\Delta t} \right] - \mathbf{GM} \left[\frac{\bar{T}_e^{n+1} + 2\bar{T}_e^n + \bar{T}_e^{n-1}}{4} - \frac{\bar{T}_i^{n+1} + 2\bar{T}_i^n + \bar{T}_i^{n-1}}{4} \right] = 0 \quad (4.28b)$$

where δ_z^2 is the central difference-in-space operator.

The procedure for formulation of the combined computational scheme is as follows:

- 1) Set up global finite element formulation using a modified Galerkin Weighted Residual method.

- 2) Assemble the matrix coefficients (in the x-y plane) yielding a system of parabolic partial differential equations in one direction (z-axis).
- 3) Utilize Finite Difference scheme to solve this PDE system.
- 4) Formulate the algorithm to solve the system.
- 5) Implement the algorithm computationally.

4.3.2 Implementation of Scheme

Implementing the modified weighted average Finite Difference Method to approximate the PDE system yields a basic formulation:

$$\begin{aligned}
& C_e ((T_e^{(m)})^n) \mathbf{M} \left[\frac{(\bar{T}_e^{(m)})^{n+1} - (\bar{T}_e^{(m)})^{n-1}}{2\Delta t} \right] + \kappa^{(m)} \mathbf{K} \left[\frac{(\bar{T}_e^{(m)})^{n+1} + 2(\bar{T}_e^{(m)})^n + (\bar{T}_e^{(m)})^{n-1}}{4} \right] \\
& - \kappa^{(m)} \mathbf{M} \left[\delta_z^2 \left(\frac{(\bar{T}_e^{(m)})^{n+1} + 2(\bar{T}_e^{(m)})^n + (\bar{T}_e^{(m)})^{n-1}}{4} \right) \right] \\
& + G^{(m)} \mathbf{M} \left[\frac{(\bar{T}_e^{(m)})^{n+1} + 2(\bar{T}_e^{(m)})^n + (\bar{T}_e^{(m)})^{n-1}}{4} - \frac{(\bar{T}_i^{(m)})^{n+1} + 2(\bar{T}_i^{(m)})^n + (\bar{T}_i^{(m)})^{n-1}}{4} \right] \\
& = \mathbf{M} \bar{S}^n \tag{4.29a}
\end{aligned}$$

$$\begin{aligned}
& C_i \mathbf{M} \left[\frac{(\bar{T}_i^{(m)})^{n+1} - (\bar{T}_i^{(m)})^{n-1}}{2\Delta t} \right] \\
& - G^{(m)} \mathbf{M} \left[\frac{(\bar{T}_e^{(m)})^{n+1} + 2(\bar{T}_e^{(m)})^n + (\bar{T}_e^{(m)})^{n-1}}{4} - \frac{(\bar{T}_i^{(m)})^{n+1} + 2(\bar{T}_i^{(m)})^n + (\bar{T}_i^{(m)})^{n-1}}{4} \right] \\
& = 0 \tag{4.29b}
\end{aligned}$$

where $m=1,2$ and depict the gold and chromium layers respectively of the system.

At the boundary between the gold and the chromium layers, the discrete interfacial equation is

$$\kappa_{Au} \left(\frac{\left(\bar{T}_e^{(1)} \right)_{k+1}^n - \left(\bar{T}_e^{(1)} \right)_k^n}{\Delta z} \right) = \kappa_{Cr} \left(\frac{\left(\bar{T}_e^{(2)} \right)_{k+1}^n - \left(\bar{T}_e^{(2)} \right)_k^n}{\Delta z} \right) \quad (4.30)$$

Taking the second equation to solve for the third time step for the lattice temperature

$$\begin{aligned} \left(\bar{T}_l^{(m)} \right)^{n+1} &= \left(\frac{C_l}{2\Delta t} + \frac{G^{(m)}}{4} \right)^{-1} \left[\left[-\frac{G^{(m)}}{2} \left(\bar{T}_l^{(m)} \right)^n - \left(-\frac{C_l}{2\Delta t} + \frac{G^{(m)}}{4} \right) \left(\bar{T}_l^{(m)} \right)^{n-1} \right] \right. \\ &\quad \left. + \left(\frac{C_l}{2\Delta t} + \frac{G^{(m)}}{4} \right)^{-1} \left(\frac{G^{(m)}}{4} \left[\left(\bar{T}_e^{(m)} \right)^{n+1} + 2 \left(\bar{T}_e^{(m)} \right)^n + \left(\bar{T}_e^{(m)} \right)^{n-1} \right] \right) \right] \end{aligned} \quad (4.31)$$

In the above equation, the subscript (k) is omitted, but is implied throughout.

Equation (4.29a), yields

$$\begin{aligned} C_e \left(\left(\bar{T}_e^{(m)} \right)^n \right) \mathbf{M} &\left[\frac{\left(\bar{T}_e^{(m)} \right)^{n+1} - \left(\bar{T}_e^{(m)} \right)^{n-1}}{2\Delta t} \right] + \kappa^{(m)} \mathbf{K} \left[\frac{\left(\bar{T}_e^{(m)} \right)^{n+1} + 2 \left(\bar{T}_e^{(m)} \right)^n + \left(\bar{T}_e^{(m)} \right)^{n-1}}{4} \right] \\ &- \kappa^{(m)} \mathbf{M} \left[\frac{\left(\bar{T}_e^{(m)} \right)_{k-1}^{n+1} - 2 \left(\bar{T}_e^{(m)} \right)_k^{n+1} + \left(\bar{T}_e^{(m)} \right)_{k+1}^{n+1}}{4\Delta z^2} + \frac{\left(\bar{T}_e^{(m)} \right)_{k-1}^n - 2 \left(\bar{T}_e^{(m)} \right)_k^n + \left(\bar{T}_e^{(m)} \right)_{k+1}^n}{2\Delta z^2} \right. \\ &\quad \left. + \frac{\left(\bar{T}_e^{(m)} \right)_{k-1}^{n-1} - 2 \left(\bar{T}_e^{(m)} \right)_k^{n-1} + \left(\bar{T}_e^{(m)} \right)_{k+1}^{n-1}}{4\Delta z^2} \right] \\ &+ G^{(m)} \mathbf{M} \left[\frac{\left(\bar{T}_e^{(m)} \right)^{n+1} + 2 \left(\bar{T}_e^{(m)} \right)^n + \left(\bar{T}_e^{(m)} \right)^{n-1}}{4} - \frac{\left(\bar{T}_l^{(m)} \right)^{n+1} + 2 \left(\bar{T}_l^{(m)} \right)^n + \left(\bar{T}_l^{(m)} \right)^{n-1}}{4} \right] \\ &= \mathbf{M} \bar{S}^n \end{aligned} \quad (4.32)$$

For simplicity, we shall indicate $C_e \left(\left(\bar{T}_e^{(m)} \right)^n \right)$ as C_e .

Multiplying by $2\Delta t$ gives

$$C_e \mathbf{M} \left[\left(\bar{T}_e^{(m)} \right)_k^{n+1} - \left(\bar{T}_e^{(m)} \right)_k^{n-1} \right] + \frac{\Delta t \kappa^{(m)}}{2} \mathbf{K} \left[\left(\bar{T}_e^{(m)} \right)_k^{n+1} + 2 \left(\bar{T}_e^{(m)} \right)_k^n + \left(\bar{T}_e^{(m)} \right)_k^{n-1} \right]$$

$$\begin{aligned}
& -\frac{\Delta t \kappa^{(m)}}{2\Delta z^2} \mathbf{M} \begin{bmatrix} \left(\bar{T}_e^{(m)}\right)_{k-1}^{n+1} - 2\left(\bar{T}_e^{(m)}\right)_k^{n+1} + \left(\bar{T}_e^{(m)}\right)_{k+1}^{n+1} + \\ 2\left(\bar{T}_e^{(m)}\right)_{k-1}^n - 4\left(\bar{T}_e^{(m)}\right)_k^n + 2\left(\bar{T}_e^{(m)}\right)_{k+1}^n + \\ \left(\bar{T}_e^{(m)}\right)_{k-1}^{n-1} - 2\left(\bar{T}_e^{(m)}\right)_k^{n-1} + \left(\bar{T}_e^{(m)}\right)_{k+1}^{n-1} \end{bmatrix} \\
& + \frac{\Delta t G^{(m)}}{2} \mathbf{M} \begin{bmatrix} \left(\bar{T}_e^{(m)}\right)_k^{n+1} + 2\left(\bar{T}_e^{(m)}\right)_k^n + \left(\bar{T}_e^{(m)}\right)_k^{n-1} - \\ \left(\left(\bar{T}_l^{(m)}\right)_k^{n+1} + 2\left(\bar{T}_l^{(m)}\right)_k^n + \left(\bar{T}_l^{(m)}\right)_k^{n-1}\right) \end{bmatrix} \\
& = 2\Delta t \mathbf{M} \bar{S}^n
\end{aligned} \tag{4.33}$$

Combining terms yields

$$\begin{aligned}
& \left(-\frac{\kappa^{(m)} \Delta t}{2\Delta z^2} \mathbf{M}\right) \left(T_e^{(m)}\right)_{k-1}^{n-1} + \left(-\frac{\kappa^{(m)} \Delta t}{\Delta z^2} \mathbf{M}\right) \left(T_e^{(m)}\right)_{k-1}^n + \left(-\frac{\kappa^{(m)} \Delta t}{2\Delta z^2} \mathbf{M}\right) \left(T_e^{(m)}\right)_{k-1}^{n+1} \\
& + \left(-C_e \mathbf{M} + \frac{\Delta t \kappa^{(m)}}{2} \mathbf{K} + \frac{\kappa^{(m)} \Delta t}{\Delta z^2} \mathbf{M} + \frac{G^{(m)} \Delta t}{2} \mathbf{M}\right) \left(T_e^{(m)}\right)_k^{n-1} \\
& + \left(\Delta t \kappa^{(m)} \mathbf{K} + \frac{2\kappa^{(m)} \Delta t}{\Delta z^2} \mathbf{M} + G^{(m)} \Delta t \mathbf{M}\right) \left(T_e^{(m)}\right)_k^n \\
& + \left(C_e \mathbf{M} + \frac{\Delta t \kappa^{(m)}}{2} \mathbf{K} + \frac{\kappa^{(m)} \Delta t}{\Delta z^2} \mathbf{M} + \frac{G^{(m)} \Delta t}{2} \mathbf{M}\right) \left(T_e^{(m)}\right)_k^{n+1} \\
& + \left(-\frac{\kappa^{(m)} \Delta t}{2\Delta z^2} \mathbf{M}\right) \left(T_e^{(m)}\right)_{k+1}^{n-1} \\
& + \left(-\frac{\kappa^{(m)} \Delta t}{\Delta z^2} \mathbf{M}\right) \left(T_e^{(m)}\right)_{k+1}^n + \left(-\frac{\kappa^{(m)} \Delta t}{2\Delta z^2} \mathbf{M}\right) \left(T_e^{(m)}\right)_{k+1}^{n+1} \\
& - \frac{G^{(m)} \Delta t}{2} \mathbf{M} \left[\left(T_l^{(m)}\right)_k^{n+1} + 2\left(T_l^{(m)}\right)_k^n + \left(T_l^{(m)}\right)_k^{n-1}\right] = 2\Delta t \mathbf{M} \bar{S}^n
\end{aligned} \tag{4.34}$$

Putting known values to the left and unknowns to the right, multiplying by \mathbf{M}^{-1} yields

$$\begin{aligned}
& \left(\frac{\kappa^{(m)} \Delta t}{2\Delta z^2} \right) (T_e^{(m)})_{k-1}^{n-1} - \left(-C_e + \frac{\kappa^{(m)} \Delta t}{2} \mathbf{M}^{-1} \mathbf{K} + \frac{\kappa^{(m)} \Delta t}{\Delta z^2} + \frac{G^{(m)} \Delta t}{2} \right) (T_e^{(m)})_k^{n-1} + \left(\frac{\kappa^{(m)} \Delta t}{2\Delta z^2} \right) (T_e^{(m)})_{k+1}^{n-1} \\
& + \left(\frac{\kappa^{(m)} \Delta t}{\Delta z^2} \right) (T_e^{(m)})_{k-1}^n - \left(\Delta t \kappa^{(m)} \mathbf{M}^{-1} \mathbf{K} + \frac{2\kappa^{(m)} \Delta t}{\Delta z^2} + G^{(m)} \Delta t \right) (T_e^{(m)})_k^n + \left(\frac{\kappa^{(m)} \Delta t}{\Delta z^2} \right) (T_e^{(m)})_{k+1}^n \\
& - \left(\frac{G^{(m)} \Delta t}{2} \right) (T_l^{(m)})_k^{n-1} + (G^{(m)} \Delta t) (T_l^{(m)})_k^n + \left(\frac{G^{(m)} \Delta t}{2} \right) (T_l^{(m)})_k^{n+1} + 2\Delta t \bar{S}^n \\
& = \left(-\frac{\kappa^{(m)} \Delta t}{2\Delta z^2} \right) (T_e^{(m)})_{k-1}^{n+1} + \left(C_e + \frac{\Delta t \kappa^{(m)}}{2} \mathbf{M}^{-1} \mathbf{K} + \frac{\kappa^{(m)} \Delta t}{\Delta z^2} + \frac{G^{(m)} \Delta t}{2} \right) (T_e^{(m)})_k^{n+1} \\
& - \left(\frac{\kappa^{(m)} \Delta t}{2\Delta z^2} \right) (T_e^{(m)})_{k+1}^{n+1}
\end{aligned} \tag{4.35}$$

$(T_l^{(m)})_k^{n+1}$ from Equation (4.31) is substituted from the second equation. This yields

$$\begin{aligned}
& \left(\frac{\kappa^{(m)} \Delta t}{2\Delta z^2} \right) (T_e^{(m)})_{k-1}^{n-1} - \left(-C_e + \frac{\kappa^{(m)} \Delta t}{2} \mathbf{M}^{-1} \mathbf{K} + \frac{\kappa^{(m)} \Delta t}{\Delta z^2} + \frac{G^{(m)} \Delta t}{2} - \frac{\Delta t^2 (G^{(m)})^2}{4C_l + 2\Delta t G^{(m)}} \right) (T_e^{(m)})_k^{n-1} \\
& + \left(\frac{\kappa^{(m)} \Delta t}{2\Delta z^2} \right) (T_e^{(m)})_{k+1}^{n-1} + \left(\frac{\kappa^{(m)} \Delta t}{\Delta z^2} \right) (T_e^{(m)})_{k-1}^n \\
& - \left(\Delta t \kappa^{(m)} \mathbf{M}^{-1} \mathbf{K} + \frac{2\kappa^{(m)} \Delta t}{\Delta z^2} + G^{(m)} \Delta t - \frac{\Delta t^2 (G^{(m)})^2}{2C_l + \Delta t G^{(m)}} \right) (T_e^{(m)})_k^n \\
& + \left(\frac{\kappa^{(m)} \Delta t}{\Delta z^2} \right) (T_e^{(m)})_{k+1}^n - \left(-\frac{G^{(m)} \Delta t}{2} - \frac{\Delta t G^{(m)}}{2} \left(\frac{2C_l - \Delta t G^{(m)}}{2C_l + \Delta t G^{(m)}} \right) \right) (T_l^{(m)})_k^{n-1} \\
& - \left(-G^{(m)} \Delta t + \frac{\Delta t^2 (G^{(m)})^2}{2C_l + \Delta t G^{(m)}} \right) (T_l^{(m)})_k^n + 2\Delta t \bar{S}^n \\
& = \left(-\frac{\kappa^{(m)} \Delta t}{2\Delta z^2} \right) (T_e^{(m)})_{k-1}^{n+1} + \left(C_e + \frac{\Delta t \kappa^{(m)}}{2} \mathbf{M}^{-1} \mathbf{K} + \frac{\kappa^{(m)} \Delta t}{\Delta z^2} + \frac{G^{(m)} \Delta t}{2} - \frac{\Delta t^2 (G^{(m)})^2}{4C_l + 2\Delta t G^{(m)}} \right) (T_e^{(m)})_k^{n+1} \\
& - \left(\frac{\kappa^{(m)} \Delta t}{2\Delta z^2} \right) (T_e^{(m)})_{k+1}^{n+1}
\end{aligned} \tag{4.36}$$

Letting

$$A = \left(\frac{\kappa^{(m)} \Delta t}{2\Delta z^2} \right) \quad \text{and} \quad B = \left(\frac{\kappa^{(m)} \Delta t}{\Delta z^2} + \frac{G^{(m)} \Delta t}{2} - \frac{\Delta t^2 (G^{(m)})^2}{4C_l + 2\Delta t G^{(m)}} \right) \tag{4.37}$$

The following scheme is obtained

$$\begin{aligned}
& (A)(T_e^{(m)})_{k-1}^{n-1} - \left(-C_e + \frac{\kappa^{(m)}\Delta t}{2} \mathbf{M}^{-1} \mathbf{K} + B \right) (T_e^{(m)})_k^{n-1} + (A)(T_e^{(m)})_{k+1}^{n-1} \\
& + (2A)(T_e^{(m)})_{k-1}^n - (\Delta t \kappa^{(m)} \mathbf{M}^{-1} \mathbf{K} + 2B) (T_e^{(m)})_k^n + (2A)(T_e^{(m)})_{k+1}^n \\
& + \left(\frac{G^{(m)}\Delta t}{2} + \frac{\Delta t G^{(m)}}{2} \left(\frac{2C_l - \Delta t G^{(m)}}{2C_l + \Delta t G^{(m)}} \right) \right) (T_l^{(m)})_k^{n-1} + \left(G^{(m)}\Delta t - \frac{\Delta t^2 (G^{(m)})^2}{2C_l + \Delta t G^{(m)}} \right) (T_l^{(m)})_k^n \\
& + 2\Delta t \bar{S}^n \\
& = (-A)(T_e^{(m)})_{k-1}^{n+1} + \left(C_e + \frac{\Delta t \kappa^{(m)}}{2} \mathbf{M}^{-1} \mathbf{K} + B \right) (T_e^{(m)})_k^{n+1} - (A)(T_e^{(m)})_{k+1}^{n+1}
\end{aligned} \tag{4.38}$$

4.4 Stability of Model

The stability of the above scheme is now analyzed with respect to the source term.

The system produced is

$$C_e^{(m)} \mathbf{M} \frac{\partial \bar{T}_e^{(m)}}{\partial t} + \kappa^{(m)} \mathbf{K} \bar{T}_e^{(m)} - \kappa^{(m)} \mathbf{M} \frac{\partial^2 \bar{T}_e^{(m)}}{\partial z^2} + G^{(m)} \mathbf{M} (\bar{T}_e^{(m)} - \bar{T}_l^{(m)}) = \mathbf{M} \bar{S}^{(m)} \tag{4.39}$$

and

$$C_l^{(m)} \mathbf{M} \frac{\partial \bar{T}_l^{(m)}}{\partial t} - G^{(m)} (\bar{T}_e^{(m)} - \bar{T}_l^{(m)}) = 0 \tag{4.40}$$

where \mathbf{M} and \mathbf{K} are the capacitance and conductance matrices, respectively.

Equations (4.39) and (4.40) are then discretized using the finite difference method

as follows

$$\begin{aligned}
& C_e^{(m)} \mathbf{M} \frac{\left(\bar{T}_e^{(m)} \right)_k^{n+1} - \left(\bar{T}_e^{(m)} \right)_k^{n-1}}{2\Delta t} + \kappa^{(m)} \mathbf{K} \frac{\left(\bar{T}_e^{(m)} \right)_k^{n+1} + 2\left(\bar{T}_e^{(m)} \right)_k^n + \left(\bar{T}_e^{(m)} \right)_k^{n-1}}{4} \\
& - \kappa^{(m)} \mathbf{M} \delta_z^2 \left(\frac{\left(\bar{T}_e^{(m)} \right)_k^{n+1} + 2\left(\bar{T}_e^{(m)} \right)_k^n + \left(\bar{T}_e^{(m)} \right)_k^{n-1}}{4} \right) \\
& + G^{(m)} \mathbf{M} \left[\frac{\left(\bar{T}_e^{(m)} \right)_k^{n+1} + 2\left(\bar{T}_e^{(m)} \right)_k^n + \left(\bar{T}_e^{(m)} \right)_k^{n-1}}{4} - \frac{\left(\bar{T}_l^{(m)} \right)_k^{n+1} + 2\left(\bar{T}_l^{(m)} \right)_k^n + \left(\bar{T}_l^{(m)} \right)_k^{n-1}}{4} \right] = \mathbf{M} \left(\bar{S}^{(m)} \right)^n \tag{4.41}
\end{aligned}$$

$$C_l^{(m)} \mathbf{M} \frac{\left(\bar{T}_l^{(m)}\right)_k^{n+1} - \left(\bar{T}_l^{(m)}\right)_k^{n-1}}{2\Delta t} - G^{(m)} \mathbf{M} \left[\frac{\left(\bar{T}_e^{(m)}\right)_k^{n+1} + 2\left(\bar{T}_e^{(m)}\right)_k^n + \left(\bar{T}_e^{(m)}\right)_k^{n-1}}{4} - \frac{\left(\bar{T}_l^{(m)}\right)_k^{n+1} + 2\left(\bar{T}_l^{(m)}\right)_k^n + \left(\bar{T}_l^{(m)}\right)_k^{n-1}}{4} \right] = 0 \quad (4.42)$$

where $\left(\bar{T}_e^{(m)}\right)_k^n$ is the approximation of $\bar{T}_e^{(m)}(k\Delta z, n\Delta t)$, $k = 0, 1, \dots, N_z + 1$, and δ_z^2 is the second-order central difference operator. The interfacial equations are discretized as follows

$$\kappa^{(1)} \frac{\left(\bar{T}_e^{(1)}\right)_{N_z+1}^n - \left(\bar{T}_e^{(1)}\right)_{N_z}^n}{\Delta z} = \kappa^{(2)} \frac{\left(\bar{T}_e^{(2)}\right)_1^n - \left(\bar{T}_e^{(2)}\right)_0^n}{\Delta z} \quad (4.43)$$

$$\left(\bar{T}_e^{(1)}\right)_{N_z+1}^n = \left(\bar{T}_e^{(2)}\right)_0^n \quad (4.44)$$

The initial condition is

$$\left(\bar{T}_e^{(m)}\right)_k^0 = \left(\bar{T}_l^{(m)}\right)_k^0 = T_0 \quad (4.45)$$

The boundary conditions are assumed to be

$$\left(\bar{T}_e^{(m)}\right)_0^n = \left(\bar{T}_e^{(m)}\right)_1^n, \quad \left(\bar{T}_l^{(m)}\right)_0^n = \left(\bar{T}_l^{(m)}\right)_1^n, \quad \left(\bar{T}_e^{(m)}\right)_{N_z}^n = \left(\bar{T}_e^{(m)}\right)_{N_z+1}^n, \quad \left(\bar{T}_l^{(m)}\right)_{N_z}^n = \left(\bar{T}_l^{(m)}\right)_{N_z+1}^n \quad (4.46)$$

To this end, we consider the following eigenvalue problem

$$\mathbf{K}\phi_p - \lambda_p \mathbf{M}\phi_p = 0 \quad (4.47)$$

where λ_p is the eigen value corresponding to the eigenvector ϕ_p . Since \mathbf{K} and \mathbf{M} are symmetric positive definite, we assume that the eigenvectors are orthonormalized with respect to the capacitance matrix \mathbf{M} such that

$$\phi_j^T \mathbf{M} \phi_p = \delta_{pj} \quad (4.48)$$

where δ_{pj} is 1 if $p = j$ and 0 if $p \neq j$. Then multiplying Equation (4.47) by ϕ_j^T and using Equation (4.48) yields

$$\phi_j^T \mathbf{K} \phi_p - \lambda_p \delta_{pj} = 0 \quad (4.49)$$

implying that the eigenvectors are also orthogonal with respect to the matrix \mathbf{K} . Further, $\lambda_p > 0$ since \mathbf{K} is positive definite. As the eigenvectors form a basis for the semi discrete system in our system, the solution $\vec{T}^{(m)}$ may be represented as a linear combination of the eigenvectors

$$\vec{T}_e^{(m)}(x, y, z, t) = \sum_p (\alpha_e^{(m)}(z, t))_p \phi_p(x, y), \quad \vec{T}_l^{(m)}(x, y, z, t) = \sum_p (\alpha_l^{(m)}(z, t))_p \phi_p(x, y) \quad (4.50a)$$

$$\vec{S}_h^{(m)} = \sum_p S_p^{(m)}(z, t) \phi_p(x, y) \quad (4.50b)$$

where $(\alpha_e^{(m)})_p$ and $(\alpha_l^{(m)})_p$ are the generalized electron and lattice coordinates respectively. Substituting Equation (4.50) to Equations. (4.39) and (4.40), pre-multiplying by ϕ_p^T , and using the orthogonal properties in Equations. (4.47) and (4.48) leads to the result

$$\begin{aligned} C_e^{(m)} \frac{\partial (\alpha_e^{(m)})_p}{\partial t} (\phi_p^T \mathbf{M} \phi_p) + \kappa^{(m)} (\alpha_e^{(m)})_p (\phi_p^T \mathbf{K} \phi_p) - \kappa^{(m)} \frac{\partial^2 (\alpha_e^{(m)})_p}{\partial z^2} (\phi_p^T \mathbf{M} \phi_p) \\ + G^{(m)} \left((\alpha_e^{(m)})_p - (\alpha_l^{(m)})_p \right) (\phi_p^T \mathbf{M} \phi_p) = S_p^{(m)} \phi_p^T \mathbf{M} \phi_p \end{aligned} \quad (4.51)$$

and

$$C_l^{(m)} \frac{\partial (\alpha_l^{(m)})_p}{\partial t} (\phi_p^T \mathbf{M} \phi_p) - G^{(m)} \left((\alpha_e^{(m)})_p - (\alpha_l^{(m)})_p \right) (\phi_p^T \mathbf{M} \phi_p) = 0 \quad (4.52)$$

or

$$C_e^{(m)} \frac{\partial (\alpha_e^{(m)})_p}{\partial t} + (\alpha_e^{(m)})_p \lambda_p \kappa^{(m)} - \kappa^{(m)} \frac{\partial^2 (\alpha_e^{(m)})_p}{\partial z^2} + G^{(m)} \left((\alpha_e^{(m)})_p - (\alpha_l^{(m)})_p \right) = S_p^{(m)} \quad (4.53)$$

and

$$C_l^{(m)} \frac{\partial (\alpha_l^{(m)})_p}{\partial t} - G^{(m)} \left((\alpha_e^{(m)})_p - (\alpha_l^{(m)})_p \right) = 0 \quad (4.54)$$

Using a similar argument, we obtain from Equations (4.41) – (4.46)

$$C_e^{(m)} \frac{(\alpha_e^{(m)})_{pk}^{n+1} - (\alpha_e^{(m)})_{pk}^{n-1}}{2\Delta t} + \lambda_p \kappa^{(m)} \left(\frac{(\alpha_e^{(m)})_{pk}^{n-1} + 2(\alpha_e^{(m)})_{pk}^n + (\alpha_e^{(m)})_{pk}^{n+1}}{4} \right) - \frac{\kappa^{(m)}}{4\Delta z^2} \delta_z^2 \left((\alpha_e^{(m)})_{pk}^{n-1} + 2(\alpha_e^{(m)})_{pk}^n + (\alpha_e^{(m)})_{pk}^{n+1} \right) \quad (4.55)$$

$$+ \frac{G^{(m)}}{4} \left((\alpha_e^{(m)})_{pk}^{n-1} + 2(\alpha_e^{(m)})_{pk}^n + (\alpha_e^{(m)})_{pk}^{n+1} - (\alpha_l^{(m)})_{pk}^{n-1} - 2(\alpha_l^{(m)})_{pk}^n - (\alpha_l^{(m)})_{pk}^{n+1} \right) = (S^{(m)})_{pk}^n C_l^{(m)} \left(\frac{(\alpha_l^{(m)})_{pk}^{n+1} - (\alpha_l^{(m)})_{pk}^{n-1}}{2\Delta t} \right) - \frac{G^{(m)}}{4} \left((\alpha_e^{(m)})_{pk}^{n-1} + 2(\alpha_e^{(m)})_{pk}^n + (\alpha_e^{(m)})_{pk}^{n+1} - (\alpha_l^{(m)})_{pk}^{n-1} - 2(\alpha_l^{(m)})_{pk}^n - (\alpha_l^{(m)})_{pk}^{n+1} \right) = 0 \quad (4.56)$$

$$\kappa^{(1)} \frac{(\alpha_e^{(1)})_{pN_z+1}^n - (\alpha_e^{(1)})_{pN_z}^n}{\Delta z} = \kappa^{(2)} \frac{(\alpha_e^{(2)})_{p1}^n - (\alpha_e^{(2)})_{p0}^n}{\Delta z} \quad (4.57a)$$

$$(\alpha_e^{(1)})_{pN_z+1}^n = (\alpha_e^{(2)})_{p0}^n \quad (4.57b)$$

and

$$(\alpha_e^{(m)})_{pk}^0 = (\alpha_e^{(m)})_{pk}^1 = \left((\alpha_e^{(m)})_0 \right)_{pk} \quad (4.58)$$

$$(\alpha_e^{(m)})_{p0}^n = (\alpha_e^{(m)})_{p1}^n, \quad (\alpha_e^{(m)})_{pN_z+1}^n = (\alpha_e^{(m)})_{pN_z}^n \quad (4.59a)$$

$$(\alpha_l^{(m)})_{p0}^n = (\alpha_l^{(m)})_{p1}^n, \quad (\alpha_l^{(m)})_{pN_z+1}^n = (\alpha_l^{(m)})_{pN_z}^n \quad (4.59b)$$

for any time level n . Hence, the analysis of the stability of the scheme, Equations (4.41)-(4.46), can be switched to analyze the stability of the scheme Equations (4.55)-(4.59).

We now employ the discrete energy method [Lees 1961], to analyze the stability of the above scheme with respect to the source term.

Let S_h be a set of $\{u^n = \{u_{pk}^n\}, \text{ with } u_{p0}^n = u_{p1}^n \text{ and } u_{pN_z}^n = u_{pN_z+1}^n\}$. For any $u^n, v^n \in S_h$,

the inner products and norms are defined as

$$(u^n, v^n) = \Delta z \sum_{p=1}^{N_p} \sum_{k=1}^{N_z} u_{pk}^n v_{pk}^n, \quad \|u^n\|^2 = (u^n, u^n) \quad (4.60a)$$

$$\|\nabla_z u^n\|_1^2 = (\nabla_z u^n, \nabla_z u^n)_1 = \Delta z \sum_{p=1}^{N_p} \sum_{k=1}^{N_z+1} (\nabla_z u_{pk}^n)^2 \quad (4.60b)$$

We also define $\nabla_z U_k = U_{k+1} - U_k$ and $\nabla_z^- U = U_k - U_{k-1}$, the forward difference and

backward difference operators respectively. It can also be seen that the central

difference operator satisfies $\delta_z^2 U_k = \nabla_z \nabla_z^- U_k$.

Lemma 1. For any $u^n \in S_h$,

$$[u_{pk}^{n+1} + 2u_{pk}^n + u_{pk}^{n-1}][u_{pk}^{n+1} - u_{pk}^{n-1}] = [u_{pk}^{n+1} + u_{pk}^n]^2 - [u_{pk}^n + u_{pk}^{n-1}]^2 \quad (4.61)$$

Proof.

$$\begin{aligned} & [u_{pk}^{n+1} + 2u_{pk}^n + u_{pk}^{n-1}][u_{pk}^{n+1} - u_{pk}^{n-1}] \\ &= [u_{pk}^{n+1}]^2 + 2u_{pk}^{n+1}u_{pk}^n + u_{pk}^{n+1}u_{pk}^{n-1} - u_{pk}^{n+1}u_{pk}^{n-1} - 2u_{pk}^n u_{pk}^{n-1} - [u_{pk}^{n-1}]^2 \\ &= [u_{pk}^{n+1}]^2 + 2u_{pk}^{n+1}u_{pk}^n + [u_{pk}^n]^2 - \left\{ [u_{pk}^n]^2 + 2u_{pk}^n u_{pk}^{n-1} + [u_{pk}^{n-1}]^2 \right\} \\ &= [u_{pk}^{n+1} + u_{pk}^n]^2 - [u_{pk}^n + u_{pk}^{n-1}]^2 \end{aligned}$$

Lemma 2. If $(\alpha_m)_{pk}^n$, $m = 1, 2$, are the solutions of Equations (4.55)-(4.59), then

$$\begin{aligned} & \Delta z \sum_{k=1}^{N_z} \delta_z^2 \left[(\alpha_e^{(m)})_{pk}^{n+1} + 2(\alpha_e^{(m)})_{pk}^n + (\alpha_e^{(m)})_{pk}^{n-1} \right] \cdot \left[(\alpha_e^{(m)})_{pk}^{n+1} + 2(\alpha_e^{(m)})_{pk}^n + (\alpha_e^{(m)})_{pk}^{n-1} \right] \\ &= -\Delta z \sum_{k=1}^{N_z+1} \left(\nabla_z \left[(\alpha_e^{(m)})_{pk}^{n+1} + 2(\alpha_e^{(m)})_{pk}^n + (\alpha_e^{(m)})_{pk}^{n-1} \right] \right)^2 \end{aligned} \quad (4.62)$$

and

$$\begin{aligned}
& \kappa^{(1)} \Delta z \sum_{k=1}^{N_z} \delta_z^2 \left[(\alpha_e^{(1)})_{pk}^{n+1} + 2(\alpha_e^{(1)})_{pk}^n + (\alpha_e^{(1)})_{pk}^{n-1} \right] \cdot \left[(\alpha_e^{(1)})_{pk}^{n+1} + 2(\alpha_e^{(1)})_{pk}^n + (\alpha_e^{(1)})_{pk}^{n-1} \right] \\
& + \kappa^{(2)} \Delta z \sum_{k=1}^{N_z} \delta_z^2 \left[(\alpha_e^{(2)})_{pk}^{n+1} + 2(\alpha_e^{(2)})_{pk}^n + (\alpha_e^{(2)})_{pk}^{n-1} \right] \cdot \left[(\alpha_e^{(2)})_{pk}^{n+1} + 2(\alpha_e^{(2)})_{pk}^n + (\alpha_e^{(2)})_{pk}^{n-1} \right] \quad (4.63) \\
& = -\kappa^{(1)} \Delta z \sum_{k=1}^{N_z+1} \left(\nabla_z \left[(\alpha_e^{(1)})_{pk}^{n+1} + 2(\alpha_e^{(1)})_{pk}^n + (\alpha_e^{(1)})_{pk}^{n-1} \right] \right)^2 \\
& \quad - \kappa^{(2)} \Delta z \sum_{k=1}^{N_z+1} \left(\nabla_z \left[(\alpha_e^{(2)})_{pk}^{n+1} + 2(\alpha_e^{(2)})_{pk}^n + (\alpha_e^{(2)})_{pk}^{n-1} \right] \right)^2
\end{aligned}$$

Proof. Equation (4.62) can be obtained through summation by parts and substitution of Equation (4.59). We can write

$$\begin{aligned}
& \Delta z \sum_{k=1}^{N_z} \delta_z^2 \left[(\alpha_e^{(m)})_{pk}^{n+1} + 2(\alpha_e^{(m)})_{pk}^n + (\alpha_e^{(m)})_{pk}^{n-1} \right] \cdot \left[(\alpha_e^{(m)})_{pk}^{n+1} + 2(\alpha_e^{(m)})_{pk}^n + (\alpha_e^{(m)})_{pk}^{n-1} \right] \text{ as} \\
& \Delta z \sum_{k=1}^{N_z} \delta_z^2 (u_{pk}) \cdot u_{pk} \text{ by letting } u_{pk} = \left[(\alpha_e^{(m)})_{pk}^{n+1} + 2(\alpha_e^{(m)})_{pk}^n + (\alpha_e^{(m)})_{pk}^{n-1} \right]. \text{ Therefore}
\end{aligned}$$

$$\begin{aligned}
\Delta z \sum_{k=1}^{N_z} \delta_z^2 (u_{pk}) \cdot u_{pk} &= \Delta z \sum_{k=1}^{N_z} (\nabla_z \nabla_z u_{pk}) u_{pk} \\
&= \Delta z \sum_{k=1}^{N_z} (\nabla_z u_{pk+1} - \nabla_z u_{pk}) u_{pk} \\
&= \Delta z \sum_{k=1}^{N_z} ((\nabla_z u_{pk+1}) u_{pk}) - \sum_{k=1}^{N_z} ((\nabla_z u_{pk}) u_{pk}) \\
&= \Delta z \sum_{k=2}^{N_z+1} ((\nabla_z u_{pk}) u_{pk-1}) - \sum_{k=1}^{N_z} ((\nabla_z u_{pk}) u_{pk}) \\
&= \Delta z \sum_{k=1}^{N_z+1} ((\nabla_z u_{pk}) u_{pk-1}) - (\nabla_z u_{p1}) u_{p0} - \sum_{k=1}^{N_z+1} ((\nabla_z u_{pk}) u_{pk}) + (\nabla_z u_{pN_z+1}) u_{pN_z+1} \\
&= \Delta z \sum_{k=1}^{N_z+1} ((u_{pk-1} - u_{pk}) \nabla_z u_{pk}) - (\nabla_z u_{p1}) u_{p0} + (\nabla_z u_{pN_z+1}) u_{pN_z+1}
\end{aligned}$$

Substituting Equation (4.59), we obtain

$$\begin{aligned}
\Delta z \sum_{k=1}^{N_z} \delta_z^2 (u_{pk}) \cdot u_{pk} &= -\Delta z \sum_{k=1}^{N_z+1} ((u_{pk} - u_{pk-1}) \nabla_z u_{pk}) \\
&= -\Delta z \sum_{k=1}^{N_z+1} \nabla_z (u_{pk}) \nabla_z (u_{pk}) \\
&= -\Delta z \sum_{k=1}^{N_z+1} (\nabla_z (u_{pk}))^2
\end{aligned}$$

$$\begin{aligned}
& \kappa^{(1)} \Delta z \sum_{k=1}^{N_z} \delta_z^2 \left[(\alpha_e^{(1)})_{pk}^{n+1} + 2(\alpha_e^{(1)})_{pk}^n + (\alpha_e^{(1)})_{pk}^{n-1} \right] \cdot \left[(\alpha_e^{(1)})_{pk}^{n+1} + 2(\alpha_e^{(1)})_{pk}^n + (\alpha_e^{(1)})_{pk}^{n-1} \right] \\
& + \kappa^{(2)} \Delta z \sum_{k=1}^{N_z} \delta_z^2 \left[(\alpha_e^{(2)})_{pk}^{n+1} + 2(\alpha_e^{(2)})_{pk}^n + (\alpha_e^{(2)})_{pk}^{n-1} \right] \cdot \left[(\alpha_e^{(2)})_{pk}^{n+1} + 2(\alpha_e^{(2)})_{pk}^n + (\alpha_e^{(2)})_{pk}^{n-1} \right] \\
& = -\kappa^{(1)} \Delta z \sum_{k=1}^{N_z+1} \left(\nabla_z \left[(\alpha_e^{(1)})_{pk}^{n+1} + 2(\alpha_e^{(1)})_{pk}^n + (\alpha_e^{(1)})_{pk}^{n-1} \right] \right)^2 \\
& \quad - \kappa^{(2)} \Delta z \sum_{k=1}^{N_z+1} \left(\nabla_z \left[(\alpha_e^{(2)})_{pk}^{n+1} + 2(\alpha_e^{(2)})_{pk}^n + (\alpha_e^{(2)})_{pk}^{n-1} \right] \right)^2
\end{aligned} \tag{4.63}$$

Proof. Equation (4.62) can be obtained through summation by parts and substitution of Equation (4.59). We can write

$$\begin{aligned}
& \Delta z \sum_{k=1}^{N_z} \delta_z^2 \left[(\alpha_e^{(m)})_{pk}^{n+1} + 2(\alpha_e^{(m)})_{pk}^n + (\alpha_e^{(m)})_{pk}^{n-1} \right] \cdot \left[(\alpha_e^{(m)})_{pk}^{n+1} + 2(\alpha_e^{(m)})_{pk}^n + (\alpha_e^{(m)})_{pk}^{n-1} \right] \text{ as} \\
& \Delta z \sum_{k=1}^{N_z} \delta_z^2 (u_{pk}) \cdot u_{pk} \text{ by letting } u_{pk} = \left[(\alpha_e^{(m)})_{pk}^{n+1} + 2(\alpha_e^{(m)})_{pk}^n + (\alpha_e^{(m)})_{pk}^{n-1} \right]. \text{ Therefore}
\end{aligned}$$

$$\begin{aligned}
\Delta z \sum_{k=1}^{N_z} \delta_z^2 (u_{pk}) \cdot u_{pk} &= \Delta z \sum_{k=1}^{N_z} (\nabla_z \nabla_z u_{pk}) u_{pk} \\
&= \Delta z \sum_{k=1}^{N_z} (\nabla_z u_{pk+1} - \nabla_z u_{pk}) u_{pk} \\
&= \Delta z \sum_{k=1}^{N_z} ((\nabla_z u_{pk+1}) u_{pk}) - \sum_{k=1}^{N_z} ((\nabla_z u_{pk}) u_{pk}) \\
&= \Delta z \sum_{k=2}^{N_z+1} ((\nabla_z u_{pk}) u_{pk-1}) - \sum_{k=1}^{N_z} ((\nabla_z u_{pk}) u_{pk}) \\
&= \Delta z \sum_{k=1}^{N_z+1} ((\nabla_z u_{pk}) u_{pk-1}) - (\nabla_z u_{p1}) u_{p0} - \sum_{k=1}^{N_z} ((\nabla_z u_{pk}) u_{pk}) + (\nabla_z u_{pN_z+1}) u_{pN_z+1} \\
&= \Delta z \sum_{k=1}^{N_z+1} ((u_{pk-1} - u_{pk}) \nabla_z u_{pk}) - (\nabla_z u_{p1}) u_{p0} + (\nabla_z u_{pN_z+1}) u_{pN_z+1}
\end{aligned}$$

Substituting Equation (4.59), we obtain

$$\begin{aligned}
\Delta z \sum_{k=1}^{N_z} \delta_z^2 (u_{pk}) \cdot u_{pk} &= -\Delta z \sum_{k=1}^{N_z+1} ((u_{pk} - u_{pk-1}) \nabla_z u_{pk}) \\
&= -\Delta z \sum_{k=1}^{N_z+1} \nabla_z (u_{pk}) \nabla_z (u_{pk}) \\
&= -\Delta z \sum_{k=1}^{N_z+1} (\nabla_z (u_{pk}))^2
\end{aligned}$$

To obtain Equation (4.63), we let $u_{pk} = (\alpha_e^{(1)})_{pk}^{n+1} + 2(\alpha_e^{(1)})_{pk}^n + (\alpha_e^{(1)})_{pk}^{n-1}$ and

$v_{pk} = (\alpha_e^{(2)})_{pk}^{n+1} + 2(\alpha_e^{(2)})_{pk}^n + (\alpha_e^{(2)})_{pk}^{n-1}$. As such, the left hand side (LHS) of the equation can

be expressed

$$\begin{aligned}
LHS &= \kappa^{(1)} \Delta z \sum_{k=1}^{N_z} \delta_z^2 [u_{pk}] \cdot [u_{pk}] + \kappa^{(2)} \Delta z \sum_{k=1}^{N_z} \delta_z^2 [v_{pk}] \cdot [v_{pk}] \\
&= \kappa^{(1)} \Delta z \sum_{k=1}^{N_z} [(u_{pk+1} - u_{pk}) - (u_{pk} - u_{pk-1})] \cdot u_{pk} \\
&\quad + \kappa^{(2)} \Delta z \sum_{k=1}^{N_z} [(v_{pk+1} - v_{pk}) - (v_{pk} - v_{pk-1})] \cdot v_{pk} \\
&= \kappa^{(1)} \left\{ \Delta z \sum_{k=2}^{N_z+1} [(u_{pk} - u_{pk-1})] \cdot u_{pk-1} - \Delta z \sum_{k=1}^{N_z} [(u_{pk} - u_{pk-1})] \cdot u_{pk} \right\} \\
&\quad + \kappa^{(2)} \left\{ \Delta z \sum_{k=2}^{N_z+1} [(v_{pk} - v_{pk-1})] \cdot v_{pk-1} - \Delta z \sum_{k=1}^{N_z} [(v_{pk} - v_{pk-1})] \cdot v_{pk} \right\}
\end{aligned}$$

Based on Equation (4.59b), the above LHS can be further written

$$\begin{aligned}
LHS &= \kappa^{(1)} \left\{ \Delta z \sum_{k=1}^{N_z} [(u_{pk} - u_{pk-1})] \cdot u_{pk-1} - \Delta z \sum_{k=1}^{N_z+1} [(u_{pk} - u_{pk-1})] \cdot u_{pk} \right\} \\
&\quad + \kappa^{(2)} \left\{ \Delta z \sum_{k=1}^{N_z+1} [(v_{pk} - v_{pk-1})] \cdot v_{pk-1} - \Delta z \sum_{k=1}^{N_z+1} [(v_{pk} - v_{pk-1})] \cdot v_{pk} \right\} \\
&\quad + \kappa^{(1)} \Delta z \cdot (u_{pN_z+1} - u_{pN_z}) \cdot u_{pN_z+1} - \kappa^{(2)} \Delta z \cdot (v_{p1} - v_{p0}) \cdot v_{p0} \\
&\quad - \kappa^{(1)} \Delta z \cdot (u_{p1} - u_{p0}) \cdot u_{p0} - \kappa^{(2)} \Delta z \cdot (v_{pN_z+1} - v_{pN_z}) \cdot v_{pN_z+1}
\end{aligned}$$

Note that $\kappa^{(1)} \Delta z \cdot (u_{pN_z+1} - u_{pN_z}) \cdot u_{pN_z+1} - \kappa^{(2)} \Delta z \cdot (v_{p1} - v_{p0}) \cdot v_{p0} = 0$ by equation (4.57) and

$\kappa^{(1)} \Delta z \cdot (u_{p1} - u_{p0}) \cdot u_{p0} - \kappa^{(2)} \Delta z \cdot (v_{pN_z+1} - v_{pN_z}) \cdot v_{pN_z+1} = 0$ by Equation (4.59a). Thus

$$LHS = \kappa^{(1)} \Delta z \sum_{k=1}^{N_z+1} \nabla_z u_{pk} \cdot \nabla_z u_{pk} + \kappa^{(2)} \Delta z \sum_{k=1}^{N_z+1} \nabla_z v_{pk} \cdot \nabla_z v_{pk},$$

which is the RHS of Equation (4.63).

Theorem. Suppose that $(U_e^{(m)})_{pk}^n$ and $(U_l^{(m)})_{pk}^n$, $(V_e^{(m)})_{pk}^n$ and $(V_l^{(m)})_{pk}^n$ are solutions of the proposed scheme in Equations (4.55)-(4.59) with the same initial and boundary

conditions but with different source terms. We represent $(\varepsilon_e^{(m)})_{pk}^n = (U_e^{(m)})_{pk}^n - (V_e^{(m)})_{pk}^n$ and

$(\varepsilon_l^{(m)})_{pk}^n = (U_l^{(m)})_{pk}^n - (V_l^{(m)})_{pk}^n$, $m = 1, 2$. Then for any n in $0 \leq n\Delta t \leq t_0$, $(\varepsilon_e^{(m)})_{pk}^n$ and $(\varepsilon_l^{(m)})_{pk}^n$,

$m = 1, 2$

$$F(n) \leq e^{4t_0} F(0) + 2t_0 e^{4t_0} \max_{1 \leq \xi \leq n} \left\{ \|e_1(\xi)\|^2 + \|e_2(\xi)\|^2 \right\} \quad (4.64)$$

where

$$\begin{aligned} F(n) = & 2C_e^{(1)} \left\| (\varepsilon_e^{(1)})^{n+1} + (\varepsilon_e^{(1)})^n \right\|^2 + 2C_l^{(1)} \left\| (\varepsilon_l^{(1)})^{n+1} + (\varepsilon_l^{(1)})^n \right\|^2 \\ & + 2C_e^{(2)} \left\| (\varepsilon_e^{(2)})^{n+1} + (\varepsilon_e^{(2)})^n \right\|^2 + 2C_l^{(2)} \left\| (\varepsilon_l^{(2)})^{n+1} + (\varepsilon_l^{(2)})^n \right\|^2 \end{aligned} \quad (4.65)$$

and $e_m(\xi)$, $m=1,2$ are the difference of corresponding source terms in layers 1 and 2

respectively. Hence, this scheme is unconditionally stable with respect to the initial value and the source terms.

Proof. It can be seen from Equations (4.55) and (4.56) that $(\varepsilon_e^{(m)})_{pk}^n$ and $(\varepsilon_l^{(m)})_{pk}^n$, $m = 1, 2$, satisfy

$$\begin{aligned} & 2C_e^{(m)} \left[(\varepsilon_e^{(m)})_{pk}^{n+1} - (\varepsilon_e^{(m)})_{pk}^{n-1} \right] \\ & = -\lambda_p \kappa^{(m)} \Delta t \left[(\varepsilon_e^{(m)})_{pk}^{n-1} + 2(\varepsilon_e^{(m)})_{pk}^n + (\varepsilon_e^{(m)})_{pk}^{n+1} \right] + \frac{\kappa^{(m)} \Delta t}{\Delta z^2} \delta_z^2 \left[(\varepsilon_e^{(m)})_{pk}^{n-1} + 2(\varepsilon_e^{(m)})_{pk}^n + (\varepsilon_e^{(m)})_{pk}^{n+1} \right] \\ & \quad - G^{(m)} \Delta t \left[(\varepsilon_e^{(m)})_{pk}^{n-1} + 2(\varepsilon_e^{(m)})_{pk}^n + (\varepsilon_e^{(m)})_{pk}^{n+1} - \left((\varepsilon_l^{(m)})_{pk}^{n-1} + 2(\varepsilon_l^{(m)})_{pk}^n + (\varepsilon_l^{(m)})_{pk}^{n+1} \right) \right] \\ & \quad + 4\Delta t e_m(n)_{pk} \end{aligned} \quad (4.66)$$

and

$$\begin{aligned}
& 2C_l^{(m)} \left[\left(\varepsilon_l^{(m)} \right)_{pk}^{n+1} - \left(\varepsilon_l^{(m)} \right)_{pk}^{n-1} \right] \\
& = G^{(m)} \Delta t \left\{ \left(\varepsilon_e^{(m)} \right)_{pk}^{n-1} + 2 \left(\varepsilon_e^{(m)} \right)_{pk}^n + \left(\varepsilon_e^{(m)} \right)_{pk}^{n+1} - \left[\left(\varepsilon_l^{(m)} \right)_{pk}^{n-1} + 2 \left(\varepsilon_l^{(m)} \right)_{pk}^n + \left(\varepsilon_l^{(m)} \right)_{pk}^{n+1} \right] \right\} \quad (4.67)
\end{aligned}$$

and also Equations (4.57)-(4.59). Multiplying Equation (4.66) with $m = 1$ by

$$\Delta z \left[\left(\varepsilon_e^{(1)} \right)_{pk}^{n-1} + 2 \left(\varepsilon_e^{(1)} \right)_{pk}^n + \left(\varepsilon_e^{(1)} \right)_{pk}^{n+1} \right] \text{ and Equation (4.66) with } m = 2 \text{ by}$$

$$\Delta z \left[\left(\varepsilon_e^{(2)} \right)_{pk}^{n-1} + 2 \left(\varepsilon_e^{(2)} \right)_{pk}^n + \left(\varepsilon_e^{(2)} \right)_{pk}^{n+1} \right], \text{ summing over } p, k \text{ from } p = 1, \dots, N_p \text{ and } k = 1, \dots, N_z$$

respectively, and combining them together yields

$$\begin{aligned}
& 2C_e^{(1)} \left(\left(\varepsilon_e^{(1)} \right)^{n+1} - \left(\varepsilon_e^{(1)} \right)^{n-1}, \left(\varepsilon_e^{(1)} \right)^{n+1} + 2 \left(\varepsilon_e^{(1)} \right)^n + \left(\varepsilon_e^{(1)} \right)^{n-1} \right) \\
& + 2C_e^{(2)} \left(\left(\varepsilon_e^{(2)} \right)^{n+1} - \left(\varepsilon_e^{(2)} \right)^{n-1}, \left(\varepsilon_e^{(2)} \right)^{n+1} + 2 \left(\varepsilon_e^{(2)} \right)^n + \left(\varepsilon_e^{(2)} \right)^{n-1} \right) \\
& - r_z \kappa^{(1)} \left(\delta_z^2 \left[\left(\varepsilon_e^{(1)} \right)^{n+1} + 2 \left(\varepsilon_e^{(1)} \right)^n + \left(\varepsilon_e^{(1)} \right)^{n-1} \right], \left(\varepsilon_e^{(1)} \right)^{n+1} + 2 \left(\varepsilon_e^{(1)} \right)^n + \left(\varepsilon_e^{(1)} \right)^{n-1} \right) \\
& - \lambda_p \kappa^{(1)} \Delta t \left(\left(\varepsilon_e^{(1)} \right)^{n+1} + 2 \left(\varepsilon_e^{(1)} \right)^n + \left(\varepsilon_e^{(1)} \right)^{n-1}, \left(\varepsilon_e^{(1)} \right)^{n+1} + 2 \left(\varepsilon_e^{(1)} \right)^n + \left(\varepsilon_e^{(1)} \right)^{n-1} \right) \\
& - r_z \kappa^{(2)} \left(\delta_z^2 \left[\left(\varepsilon_e^{(2)} \right)^{n+1} + 2 \left(\varepsilon_e^{(2)} \right)^n + \left(\varepsilon_e^{(2)} \right)^{n-1} \right], \left(\varepsilon_e^{(2)} \right)^{n+1} + 2 \left(\varepsilon_e^{(2)} \right)^n + \left(\varepsilon_e^{(2)} \right)^{n-1} \right) \\
& - \lambda_p \kappa^{(2)} \Delta t \left(\left(\varepsilon_e^{(2)} \right)^{n+1} + 2 \left(\varepsilon_e^{(2)} \right)^n + \left(\varepsilon_e^{(2)} \right)^{n-1}, \left(\varepsilon_e^{(2)} \right)^{n+1} + 2 \left(\varepsilon_e^{(2)} \right)^n + \left(\varepsilon_e^{(2)} \right)^{n-1} \right) \\
& + \Delta t G^{(1)} \left\| \left(\varepsilon_e^{(1)} \right)^{n+1} + 2 \left(\varepsilon_e^{(1)} \right)^n + \left(\varepsilon_e^{(1)} \right)^{n-1} \right\|^2 + \Delta t G^{(2)} \left\| \left(\varepsilon_e^{(2)} \right)^{n+1} + 2 \left(\varepsilon_e^{(2)} \right)^n + \left(\varepsilon_e^{(2)} \right)^{n-1} \right\|^2 \\
& = \Delta t G^{(1)} \left(\left(\varepsilon_l^{(1)} \right)^{n+1} + 2 \left(\varepsilon_l^{(1)} \right)^n + \left(\varepsilon_l^{(1)} \right)^{n-1}, \left(\varepsilon_e^{(1)} \right)^{n+1} + 2 \left(\varepsilon_e^{(1)} \right)^n + \left(\varepsilon_e^{(1)} \right)^{n-1} \right) \\
& + \Delta t G^{(2)} \left(\left(\varepsilon_l^{(2)} \right)^{n+1} + 2 \left(\varepsilon_l^{(2)} \right)^n + \left(\varepsilon_l^{(2)} \right)^{n-1}, \left(\varepsilon_e^{(2)} \right)^{n+1} + 2 \left(\varepsilon_e^{(2)} \right)^n + \left(\varepsilon_e^{(2)} \right)^{n-1} \right) \\
& + 4 \Delta t \left(e_1(n), \left(\varepsilon_e^{(1)} \right)^{n+1} + 2 \left(\varepsilon_e^{(1)} \right)^n + \left(\varepsilon_e^{(1)} \right)^{n-1} \right) \\
& + 4 \Delta t \left(e_2(n), \left(\varepsilon_e^{(2)} \right)^{n+1} + 2 \left(\varepsilon_e^{(2)} \right)^n + \left(\varepsilon_e^{(2)} \right)^{n-1} \right) \quad (4.68)
\end{aligned}$$

where $r_z = \frac{\Delta t}{\Delta z^2}$.

By Lemmas 1 and 2, we obtain

$$\begin{aligned}
& 2C_e^{(1)} \left\| \left(\varepsilon_e^{(1)} \right)^{n+1} + \left(\varepsilon_e^{(1)} \right)^n \right\|^2 - 2C_e^{(1)} \left\| \left(\varepsilon_e^{(1)} \right)^n + \left(\varepsilon_e^{(1)} \right)^{n-1} \right\|^2 \\
& + 2C_e^{(2)} \left\| \left(\varepsilon_e^{(2)} \right)^{n+1} + \left(\varepsilon_e^{(2)} \right)^n \right\|^2 - 2C_e^{(2)} \left\| \left(\varepsilon_e^{(2)} \right)^n + \left(\varepsilon_e^{(2)} \right)^{n-1} \right\|^2
\end{aligned}$$

$$\begin{aligned}
& + r_z \kappa^{(1)} \left\| \nabla_{\bar{z}} \left[(\varepsilon_e^{(1)})^{n+1} + 2(\varepsilon_e^{(1)})^n + (\varepsilon_e^{(1)})^{n-1} \right] \right\|^2 + \lambda_p \kappa^{(1)} \Delta t \left\| (\varepsilon_e^{(1)})^{n+1} + 2(\varepsilon_e^{(1)})^n + (\varepsilon_e^{(1)})^{n-1} \right\|^2 \\
& + r_z \kappa^{(2)} \left\| \nabla_{\bar{z}} \left[(\varepsilon_e^{(2)})^{n+1} + 2(\varepsilon_e^{(2)})^n + (\varepsilon_e^{(2)})^{n-1} \right] \right\|^2 + \lambda_p \kappa^{(2)} \Delta t \left\| (\varepsilon_e^{(2)})^{n+1} + 2(\varepsilon_e^{(2)})^n + (\varepsilon_e^{(2)})^{n-1} \right\|^2 \\
& + \Delta t G^{(1)} \left\| (\varepsilon_e^{(1)})^{n+1} + 2(\varepsilon_e^{(1)})^n + (\varepsilon_e^{(1)})^{n-1} \right\|^2 + \Delta t G^{(2)} \left\| (\varepsilon_e^{(2)})^{n+1} + 2(\varepsilon_e^{(2)})^n + (\varepsilon_e^{(2)})^{n-1} \right\|^2 \\
& = \Delta t G^{(1)} \left((\varepsilon_i^{(1)})^{n+1} + 2(\varepsilon_i^{(1)})^n + (\varepsilon_i^{(1)})^{n-1}, (\varepsilon_e^{(1)})^{n+1} + 2(\varepsilon_e^{(1)})^n + (\varepsilon_e^{(1)})^{n-1} \right) \\
& \quad + \Delta t G^{(2)} \left((\varepsilon_i^{(2)})^{n+1} + 2(\varepsilon_i^{(2)})^n + (\varepsilon_i^{(2)})^{n-1}, (\varepsilon_e^{(2)})^{n+1} + 2(\varepsilon_e^{(2)})^n + (\varepsilon_e^{(2)})^{n-1} \right) \\
& \quad + 4\Delta t \left(e_1(n), (\varepsilon_e^{(1)})^{n+1} + 2(\varepsilon_e^{(1)})^n + (\varepsilon_e^{(1)})^{n-1} \right) \\
& \quad + 4\Delta t \left(e_2(n), (\varepsilon_e^{(2)})^{n+1} + 2(\varepsilon_e^{(2)})^n + (\varepsilon_e^{(2)})^{n-1} \right) \tag{4.69}
\end{aligned}$$

We now multiply Equation (4.67) with $m = 1$ by $\Delta z \left[(\varepsilon_e^{(1)})^{n-1} + 2(\varepsilon_e^{(1)})^n + (\varepsilon_e^{(1)})^{n+1} \right]$ and Equation (4.67) with $m = 2$ by $\Delta z \left[(\varepsilon_e^{(2)})^{n-1} + 2(\varepsilon_e^{(2)})^n + (\varepsilon_e^{(2)})^{n+1} \right]$, sum over p, k from $p = 1, \dots, N_p, k = 1, \dots, N_z$, respectively, and then combine them together. This yields

$$\begin{aligned}
& 2C_l^{(1)} \left((\varepsilon_i^{(1)})^{n+1} - (\varepsilon_i^{(1)})^{n-1}, (\varepsilon_i^{(1)})^{n+1} + 2(\varepsilon_i^{(1)})^n + (\varepsilon_i^{(1)})^{n-1} \right) \\
& + 2C_l^{(2)} \left((\varepsilon_i^{(2)})^{n+1} - (\varepsilon_i^{(2)})^{n-1}, (\varepsilon_i^{(2)})^{n+1} + 2(\varepsilon_i^{(2)})^n + (\varepsilon_i^{(2)})^{n-1} \right) \\
& + \Delta t G^{(1)} \left\| (\varepsilon_e^{(1)})^{n+1} + 2(\varepsilon_e^{(1)})^n + (\varepsilon_e^{(1)})^{n-1} \right\|^2 + \Delta t G^{(2)} \left\| (\varepsilon_e^{(2)})^{n+1} + 2(\varepsilon_e^{(2)})^n + (\varepsilon_e^{(2)})^{n-1} \right\|^2 \\
& = \Delta t G^{(1)} \left((\varepsilon_e^{(1)})^{n+1} + 2(\varepsilon_e^{(1)})^n + (\varepsilon_e^{(1)})^{n-1}, (\varepsilon_i^{(1)})^{n+1} + 2(\varepsilon_i^{(1)})^n + (\varepsilon_i^{(1)})^{n-1} \right) \\
& + \Delta t G^{(2)} \left((\varepsilon_e^{(2)})^{n+1} + 2(\varepsilon_e^{(2)})^n + (\varepsilon_e^{(2)})^{n-1}, (\varepsilon_i^{(2)})^{n+1} + 2(\varepsilon_i^{(2)})^n + (\varepsilon_i^{(2)})^{n-1} \right) \tag{4.70}
\end{aligned}$$

By Lemma 1, we obtain

$$\begin{aligned}
& 2C_l^{(1)} \left\| (\varepsilon_e^{(1)})^{n+1} + (\varepsilon_e^{(1)})^n \right\|^2 - 2C_l^{(1)} \left\| (\varepsilon_e^{(1)})^n + (\varepsilon_e^{(1)})^{n-1} \right\|^2 + 2C_l^{(2)} \left\| (\varepsilon_e^{(2)})^{n+1} + (\varepsilon_e^{(2)})^n \right\|^2 - 2C_l^{(2)} \left\| (\varepsilon_e^{(2)})^n + (\varepsilon_e^{(2)})^{n-1} \right\|^2 \\
& + \Delta t G^{(1)} \left\| (\varepsilon_e^{(1)})^{n+1} + 2(\varepsilon_e^{(1)})^n + (\varepsilon_e^{(1)})^{n-1} \right\|^2 + \Delta t G^{(2)} \left\| (\varepsilon_e^{(2)})^{n+1} + 2(\varepsilon_e^{(2)})^n + (\varepsilon_e^{(2)})^{n-1} \right\|^2 \\
& = \Delta t G^{(1)} \left((\varepsilon_e^{(1)})^{n+1} + 2(\varepsilon_e^{(1)})^n + (\varepsilon_e^{(1)})^{n-1}, (\varepsilon_i^{(1)})^{n+1} + 2(\varepsilon_i^{(1)})^n + (\varepsilon_i^{(1)})^{n-1} \right) \\
& + \Delta t G^{(2)} \left((\varepsilon_e^{(2)})^{n+1} + 2(\varepsilon_e^{(2)})^n + (\varepsilon_e^{(2)})^{n-1}, (\varepsilon_i^{(2)})^{n+1} + 2(\varepsilon_i^{(2)})^n + (\varepsilon_i^{(2)})^{n-1} \right) \tag{4.71}
\end{aligned}$$

Adding both Equations (4.68) and (4.70) we have

$$2C_e^{(1)} \left\| (\varepsilon_e^{(1)})^{n+1} + (\varepsilon_e^{(1)})^n \right\|^2 + 2C_l^{(1)} \left\| (\varepsilon_i^{(1)})^{n+1} + (\varepsilon_i^{(1)})^n \right\|^2$$

$$\begin{aligned}
& + 2C_e^{(2)} \left\| \left(\varepsilon_e^{(2)} \right)^{n+1} + \left(\varepsilon_e^{(2)} \right)^n \right\|^2 + 2C_l^{(2)} \left\| \left(\varepsilon_l^{(2)} \right)^{n+1} + \left(\varepsilon_l^{(2)} \right)^n \right\|^2 \\
& - \left[2C_e^{(1)} \left\| \left(\varepsilon_e^{(1)} \right)^n + \left(\varepsilon_e^{(1)} \right)^{n-1} \right\|^2 + 2C_l^{(1)} \left\| \left(\varepsilon_l^{(1)} \right)^n + \left(\varepsilon_l^{(1)} \right)^{n-1} \right\|^2 \right] \\
& - \left[2C_e^{(2)} \left\| \left(\varepsilon_e^{(2)} \right)^n + \left(\varepsilon_e^{(2)} \right)^{n-1} \right\|^2 + 2C_l^{(2)} \left\| \left(\varepsilon_l^{(2)} \right)^n + \left(\varepsilon_l^{(2)} \right)^{n-1} \right\|^2 \right] \\
& + r_z \kappa^{(1)} \left\| \nabla_{\bar{z}} \left[\left(\varepsilon_e^{(1)} \right)^{n+1} + 2 \left(\varepsilon_e^{(1)} \right)^n + \left(\varepsilon_e^{(1)} \right)^{n-1} \right] \right\|^2 \\
& + \lambda_p \kappa^{(1)} \Delta t \left\| \left(\varepsilon_e^{(1)} \right)^{n+1} + 2 \left(\varepsilon_e^{(1)} \right)^n + \left(\varepsilon_e^{(1)} \right)^{n-1} \right\|^2 \\
& + r_z \kappa^{(2)} \left\| \nabla_{\bar{z}} \left[\left(\varepsilon_e^{(2)} \right)^{n+1} + 2 \left(\varepsilon_e^{(2)} \right)^n + \left(\varepsilon_e^{(2)} \right)^{n-1} \right] \right\|^2 \\
& + \lambda_p \kappa^{(2)} \Delta t \left\| \left(\varepsilon_e^{(2)} \right)^{n+1} + 2 \left(\varepsilon_e^{(2)} \right)^n + \left(\varepsilon_e^{(2)} \right)^{n-1} \right\|^2 \\
& + \Delta t G^{(1)} \left\{ \left\| \left(\varepsilon_e^{(1)} \right)^{n+1} + 2 \left(\varepsilon_e^{(1)} \right)^n + \left(\varepsilon_e^{(1)} \right)^{n-1} \right\|^2 + \left\| \left(\varepsilon_l^{(1)} \right)^{n+1} + 2 \left(\varepsilon_l^{(1)} \right)^n + \left(\varepsilon_l^{(1)} \right)^{n-1} \right\|^2 \right. \\
& \quad \left. - 2 \left(\left(\varepsilon_l^{(1)} \right)^{n+1} + 2 \left(\varepsilon_l^{(1)} \right)^n + \left(\varepsilon_l^{(1)} \right)^{n-1}, \left(\varepsilon_e^{(1)} \right)^{n+1} + 2 \left(\varepsilon_e^{(1)} \right)^n + \left(\varepsilon_e^{(1)} \right)^{n-1} \right) \right\} \\
& + \Delta t G^{(2)} \left\{ \left\| \left(\varepsilon_e^{(2)} \right)^{n+1} + 2 \left(\varepsilon_e^{(2)} \right)^n + \left(\varepsilon_e^{(2)} \right)^{n-1} \right\|^2 + \left\| \left(\varepsilon_l^{(2)} \right)^{n+1} + 2 \left(\varepsilon_l^{(2)} \right)^n + \left(\varepsilon_l^{(2)} \right)^{n-1} \right\|^2 \right. \\
& \quad \left. - 2 \left(\left(\varepsilon_l^{(2)} \right)^{n+1} + 2 \left(\varepsilon_l^{(2)} \right)^n + \left(\varepsilon_l^{(2)} \right)^{n-1}, \left(\varepsilon_e^{(2)} \right)^{n+1} + 2 \left(\varepsilon_e^{(2)} \right)^n + \left(\varepsilon_e^{(2)} \right)^{n-1} \right) \right\} \\
& \quad = 4 \Delta t \left(e_1(n), \left(\varepsilon_e^{(1)} \right)^{n+1} + 2 \left(\varepsilon_e^{(1)} \right)^n + \left(\varepsilon_e^{(1)} \right)^{n-1} \right) \\
& \quad + 4 \Delta t \left(e_2(n), \left(\varepsilon_e^{(2)} \right)^{n+1} + 2 \left(\varepsilon_e^{(2)} \right)^n + \left(\varepsilon_e^{(2)} \right)^{n-1} \right) \tag{4.72}
\end{aligned}$$

Since

$$\begin{aligned}
& \left\| \left(\varepsilon_e^{(1)} \right)^{n+1} + 2 \left(\varepsilon_e^{(1)} \right)^n + \left(\varepsilon_e^{(1)} \right)^{n-1} \right\|^2 + \left\| \left(\varepsilon_l^{(1)} \right)^{n+1} + 2 \left(\varepsilon_l^{(1)} \right)^n + \left(\varepsilon_l^{(1)} \right)^{n-1} \right\|^2 \\
& - 2 \left(\left(\varepsilon_l^{(1)} \right)^{n+1} + 2 \left(\varepsilon_l^{(1)} \right)^n + \left(\varepsilon_l^{(1)} \right)^{n-1}, \left(\varepsilon_e^{(1)} \right)^{n+1} + 2 \left(\varepsilon_e^{(1)} \right)^n + \left(\varepsilon_e^{(1)} \right)^{n-1} \right) \geq 0 \tag{4.73}
\end{aligned}$$

and

$$\begin{aligned}
& \left\| \left(\varepsilon_e^{(2)} \right)^{n+1} + 2 \left(\varepsilon_e^{(2)} \right)^n + \left(\varepsilon_e^{(2)} \right)^{n-1} \right\|^2 + \left\| \left(\varepsilon_l^{(2)} \right)^{n+1} + 2 \left(\varepsilon_l^{(2)} \right)^n + \left(\varepsilon_l^{(2)} \right)^{n-1} \right\|^2 \\
& - 2 \left(\left(\varepsilon_l^{(2)} \right)^{n+1} + 2 \left(\varepsilon_l^{(2)} \right)^n + \left(\varepsilon_l^{(2)} \right)^{n-1}, \left(\varepsilon_e^{(2)} \right)^{n+1} + 2 \left(\varepsilon_e^{(2)} \right)^n + \left(\varepsilon_e^{(2)} \right)^{n-1} \right) \geq 0 \tag{4.74}
\end{aligned}$$

Dropping out the last six terms on the left-hand side of Equation (4.72) the following is

obtained

$$\begin{aligned}
& 2C_e^{(1)} \left\| (\varepsilon_e^{(1)})^{n+1} + (\varepsilon_e^{(1)})^n \right\|^2 + 2C_l^{(1)} \left\| (\varepsilon_l^{(1)})^{n+1} + (\varepsilon_l^{(1)})^n \right\|^2 \\
& \quad + 2C_e^{(2)} \left\| (\varepsilon_e^{(2)})^{n+1} + (\varepsilon_e^{(2)})^n \right\|^2 + 2C_l^{(2)} \left\| (\varepsilon_l^{(2)})^{n+1} + (\varepsilon_l^{(2)})^n \right\|^2 \\
& \quad - \left[2C_e^{(1)} \left\| (\varepsilon_e^{(1)})^n + (\varepsilon_e^{(1)})^{n-1} \right\|^2 + 2C_l^{(1)} \left\| (\varepsilon_l^{(1)})^n + (\varepsilon_l^{(1)})^{n-1} \right\|^2 \right] \\
& \quad - \left[2C_e^{(2)} \left\| (\varepsilon_e^{(2)})^n + (\varepsilon_e^{(2)})^{n-1} \right\|^2 + 2C_l^{(2)} \left\| (\varepsilon_l^{(2)})^n + (\varepsilon_l^{(2)})^{n-1} \right\|^2 \right] \\
& \leq 4\Delta t \left(e_1(n), (\varepsilon_e^{(1)})^{n+1} + 2(\varepsilon_e^{(1)})^n + (\varepsilon_e^{(1)})^{n-1} \right) \\
& \quad + 4\Delta t \left(e_2(n), (\varepsilon_e^{(2)})^{n+1} + 2(\varepsilon_e^{(2)})^n + (\varepsilon_e^{(2)})^{n-1} \right)
\end{aligned} \tag{4.75}$$

By the generalized Cauchy-Schwarz's inequality, we have

$$\begin{aligned}
& 2\Delta t \left(e_1(n), (\varepsilon_e^{(1)})^{n+1} + 2(\varepsilon_e^{(1)})^n + (\varepsilon_e^{(1)})^{n-1} \right) \\
& \leq 2C_e^{(1)} \left\| (\varepsilon_e^{(1)})^{n+1} + (\varepsilon_e^{(1)})^n \right\|^2 + 2C_e^{(1)} \left\| (\varepsilon_e^{(1)})^n + (\varepsilon_e^{(1)})^{n-1} \right\|^2 + \frac{1}{C_e^{(1)}} \|e_1(n)\|^2
\end{aligned} \tag{4.76}$$

and

$$\begin{aligned}
& 2\Delta t \left(e_2(n), (\varepsilon_e^{(2)})^{n+1} + 2(\varepsilon_e^{(2)})^n + (\varepsilon_e^{(2)})^{n-1} \right) \\
& \leq 2C_e^{(2)} \left\| (\varepsilon_e^{(2)})^{n+1} + (\varepsilon_e^{(2)})^n \right\|^2 + 2C_e^{(2)} \left\| (\varepsilon_e^{(2)})^n + (\varepsilon_e^{(2)})^{n-1} \right\|^2 + \frac{1}{C_e^{(2)}} \|e_2(n)\|^2
\end{aligned} \tag{4.77}$$

Substituting the above inequalities, we have

$$\begin{aligned}
& 2C_e^{(1)} \left\| (\varepsilon_e^{(1)})^{n+1} + (\varepsilon_e^{(1)})^n \right\|^2 + 2C_l^{(1)} \left\| (\varepsilon_l^{(1)})^{n+1} + (\varepsilon_l^{(1)})^n \right\|^2 \\
& \quad + 2C_e^{(2)} \left\| (\varepsilon_e^{(2)})^{n+1} + (\varepsilon_e^{(2)})^n \right\|^2 + 2C_l^{(2)} \left\| (\varepsilon_l^{(2)})^{n+1} + (\varepsilon_l^{(2)})^n \right\|^2 \\
& \quad - \left[2C_e^{(1)} \left\| (\varepsilon_e^{(1)})^n + (\varepsilon_e^{(1)})^{n-1} \right\|^2 + 2C_l^{(1)} \left\| (\varepsilon_l^{(1)})^n + (\varepsilon_l^{(1)})^{n-1} \right\|^2 \right] \\
& \quad - \left[2C_e^{(2)} \left\| (\varepsilon_e^{(2)})^n + (\varepsilon_e^{(2)})^{n-1} \right\|^2 + 2C_l^{(2)} \left\| (\varepsilon_l^{(2)})^n + (\varepsilon_l^{(2)})^{n-1} \right\|^2 \right] \\
& \leq 2\Delta t \left(2C_e^{(1)} \left\| (\varepsilon_e^{(1)})^{n+1} + (\varepsilon_e^{(1)})^n \right\|^2 + 2C_e^{(1)} \left\| (\varepsilon_e^{(1)})^n + (\varepsilon_e^{(1)})^{n-1} \right\|^2 + \frac{1}{C_e^{(1)}} \|e_1(n)\|^2 \right) \\
& \quad + 2\Delta t \left(2C_e^{(2)} \left\| (\varepsilon_e^{(2)})^{n+1} + (\varepsilon_e^{(2)})^n \right\|^2 + 2C_e^{(2)} \left\| (\varepsilon_e^{(2)})^n + (\varepsilon_e^{(2)})^{n-1} \right\|^2 + \frac{1}{C_e^{(2)}} \|e_2(n)\|^2 \right)
\end{aligned} \tag{4.78}$$

Using the notation $F(n)$ as defined in Equation (4.65), the above inequality is simplified as

$$(1 - 2\Delta t)F(n) \leq (1 + 2\Delta t)F(n+1) + 2c\Delta t \left(\|e_1(n)\|^2 + \|e_2(n)\|^2 \right) \quad (4.79)$$

where $c = \max \left\{ \frac{1}{C_e^{(1)}}, \frac{1}{C_e^{(2)}} \right\}$. Hence when $1 - 2\Delta t > \frac{\Delta t}{2}$, we have

$$F(n) \leq \left(\frac{1 + 2\Delta t}{1 - 2\Delta t} \right) F(n-1) + \left(\frac{2c\Delta t}{1 - 2\Delta t} \right) \left(\|e_1(n)\|^2 + \|e_2(n)\|^2 \right) \quad (4.80)$$

Therefore

$$\begin{aligned} F(n) &\leq \frac{(1 + 2\Delta t)}{(1 - 2\Delta t)} F(n-1) + \frac{2c\Delta t}{(1 - 2\Delta t)} \left(\|e_1(n)\|^2 + \|e_2(n)\|^2 \right) \\ &\leq \frac{(1 + 2\Delta t)}{(1 - 2\Delta t)} \left[\frac{(1 + 2\Delta t)}{(1 - 2\Delta t)} F(n-2) + \frac{2c\Delta t}{(1 - 2\Delta t)} \left(\|e_1(n)\|^2 + \|e_2(n)\|^2 \right) \right] + \frac{2c\Delta t}{(1 - 2\Delta t)} \left(\|e_1(n)\|^2 + \|e_2(n)\|^2 \right) \\ &\leq \left(\frac{1 + 2\Delta t}{1 - 2\Delta t} \right)^n F(0) \\ &\quad + \frac{2c\Delta t}{(1 - 2\Delta t)} \left[1 + \left(\frac{1 + 2\Delta t}{1 - 2\Delta t} \right) + \left(\frac{1 + 2\Delta t}{1 - 2\Delta t} \right)^2 + \dots + \left(\frac{1 + 2\Delta t}{1 - 2\Delta t} \right)^{n-1} \right] \max_{0 \leq \xi \leq n} \left\{ \|e_1(\xi)\|^2 + \|e_2(\xi)\|^2 \right\} \\ &\leq \left(\frac{1 + 2\Delta t}{1 - 2\Delta t} \right)^n F(0) + \frac{2c\Delta t}{(1 - 2\Delta t)} \left[\frac{1 - \left(\frac{1 + 2\Delta t}{1 - 2\Delta t} \right)^n}{1 - \left(\frac{1 + 2\Delta t}{1 - 2\Delta t} \right)} \right] \max_{0 \leq \xi \leq n} \left\{ \|e_1(\xi)\|^2 + \|e_2(\xi)\|^2 \right\} \\ &\leq \left(\frac{1 + 2\Delta t}{1 - 2\Delta t} \right)^n F(0) + \frac{c}{2} \left[1 - \left(\frac{1 + 2\Delta t}{1 - 2\Delta t} \right)^n \right] \max_{0 \leq \xi \leq n} \left\{ \|e_1(\xi)\|^2 + \|e_2(\xi)\|^2 \right\} \\ &\leq \left(\frac{1 + 2\Delta t}{1 - 2\Delta t} \right)^n \left[F(0) + c \max_{0 \leq \xi \leq n} \left\{ \|e_1(\xi)\|^2 + \|e_2(\xi)\|^2 \right\} \right] \end{aligned} \quad (4.81)$$

Using the inequalities, $(1 + x)^n \leq e^{nx}$ $x > 0$, and $(1 - x)^{-1} \leq e^{2x}$ when $x < 1/2$ and letting $x = 2\Delta t$ and Δt be sufficiently small, we see $\left(\frac{1 + 2\Delta t}{1 - 2\Delta t} \right)^n \leq e^{2n\Delta t} e^{4n\Delta t} \leq e^{6n\Delta t}$ and hence

$$\begin{aligned}
F(n) &\leq e^{\delta n \Delta t} F(0) + c e^{\delta n \Delta t} \max_{1 \leq \xi \leq n} \left\{ \|e_1(\xi)\|^2 + \|e_2(\xi)\|^2 \right\} \\
&\leq e^{6t_0} \left(F(0) + c \max_{1 \leq \xi \leq n} \left\{ \|e_1(\xi)\|^2 + \|e_2(\xi)\|^2 \right\} \right)
\end{aligned} \tag{4.82}$$

which completes the proof.

4.5 Algorithm for Solution.

The algorithm will consist of the following main blocks:

- 1) Establish the coefficient sparse matrices **M** and **K**.
- 2) Assume $\bar{T}_i^{(0)} = \bar{T}_i^{(1)}$ and find $\bar{T}_i^{(2)}$. This is possible because of the lag in energy exchange.
- 3) Use this information to solve the system, dealing with layer boundaries as they arrive.
- 4) Repeat until desired time has been met and record the results for evaluation.

4.5.1 Computational Algorithms

Taking the initial conditions for both the lattice and electron temperatures, the lattice temperature for first time step $(T_l^{(m)})_k^{n+1}$ is determined from the Equation (4.31). This value is then substituted into Equation (4.38) and implicitly solved for the electron temperature at the next time step $(T_e^{(m)})_k^{n+1}$. This process is repeated, and the results are plotted, until the desired time is achieved. At the beginning of each time-step iteration, the non-linear term C_e is recalculated and applied to the system. A conjugant-gradient method is employed to solve the linear system. The interface equations are incorporated into the global matrix system of equations. However, it is possible to form a parallel implementation of this algorithm and therefore increase efficiency. This is accomplished by implicitly solving the gold layer (top layer) with one CPU performing the operations,

and the chromium layer (padding layer) with another CPU. These two then feed information to a CPU which combines them with the interface equations to arrive at the new time step temperature values. *Mathematica* was chosen as the software in which the algorithm was coded.

4.5.2 Mathematica as a Programming Language

For this problem, we will implement the computational power of the program suite *Mathematica*. *Mathematica* is a computer-based software system for doing mathematics (symbolic calculations), numerical analysis, and visualizing and plotting data. In the December 17, 1999, issue of Science, the excitement and possibilities of *Mathematica* were captured in John Wass's review of *Mathematica* 4.0. In that review he states: "It is hard to imagine a scientific software tool that is equally useful to a math professor, a cardiologist, a protein chemist, a population biologist, a civil engineer, an architect, and an atmospheric scientist. *Mathematica* is just such a program....With a powerful programming language and a dizzying array of functions, the program can be adapted to perform diverse calculations for almost any scientific need."

Data elements in *Mathematica* are strongly typed, but the language system performs many types of automatic conversion, especially on numbers. All numbers in *Mathematica* are unlimited precision: integers, reals, rationals, and complex. Programmers define their own data types, after a fashion. In a sense, *Mathematica* has only one non-primitive data type: the "basic form." All aggregate data and symbolic expressions in *Mathematica* are internally stored as a head and a body, where the head defines the data type. Programmers can create their own head types, and do, and in that sense they are defining new data types.

When input is made into *Mathematica*, a data structure is created in the memory of the computer to represent the expression entered. In general, different pieces of the expression will be stored at different places in memory. Thus, for example, for a list such as $\{2, x, y + z\}$ the “backbone” of the list will be stored at one place, while each of the actual elements will be stored at a different place. The backbone of the list then consists just of three “pointers” that specify the addresses in computer memory at which the actual expressions that form the elements of the list are to be found. These expressions then in turn contain pointers to their subexpressions. The chain of pointers ends when one reaches an object such as a number or a string, which is stored directly as a pattern of bits in computer memory.

Crucial to the operation of *Mathematica* is the notion of symbols such as x . Whenever x appears in an expression, *Mathematica* represents it by a pointer. But the pointer is always to the same place in computer memory—an entry in a central table of all symbols defined in your *Mathematica* session. This table is a repository of all information about each symbol. It contains a pointer to a string giving the symbol's name, as well as pointers to expressions which give rules for evaluating the symbol.

Every piece of memory used by *Mathematica* maintains a count of how many pointers currently point to it. When this count drops to zero, *Mathematica* knows that the piece of memory is no longer being referenced, and immediately makes the piece of memory available for something new. This strategy essentially ensures that no memory is ever wasted, and that any piece of memory that *Mathematica* uses is actually storing data that you need to access in your *Mathematica* session. [Wolfram 1999]

Within the front end of *Mathematica*, the labor is divided into three groups: Packages, Notebooks and Cells. The packages are much like object oriented designed packages in that they can contain many sub units which form a total “program.” The “code” is created in notebooks. These ASCII based text documents are subdivided into cells which block, or partition the code in the notebook.

Mathematica is built on the powerfully unifying idea that everything can be represented as a symbolic expression. *Mathematica* handles many different kinds of things: mathematical formulas, lists and graphics, etc. Although they are different in appearance, all of these are handled in one uniform way. They are all *expressions*.

Each expression takes the form of $h[e_1, e_2, \dots e_i]$. Here, h refers to a *head* which contains a listing of expressions. *Mathematica* takes a string typed in its interface and converts it to a standard form. Everything in *Mathematica* is treated as an expression to be evaluated. [Wolfram 1999].

At the heart of *Mathematica* is a simple procedure known as the *evaluator*, which takes every function that appears in an expression and evaluates that function. When the function is one of the thousand or so that are built into *Mathematica*, the evaluator executes directly the internal code in the *Mathematica* system. This code is set up to perform the operations corresponding to the function, and then builds a new expression representing the result.

A crucial feature of the built-in functions in *Mathematica* is that they support *universal computation*. *Universal Computation* indicates that out of the many functions, programs may be constructed that perform various operations possible for a computer. In fact, small subsets of *Mathematica*'s built-in functions would be sufficient to support

universal computation. But having the whole collection of functions makes it in practice easier to construct the programs one needs. The underlying point, however, is that because *Mathematica* supports universal computation the built-in functions do not have to be modified. A combination of functions in an appropriate way is what is necessary to perform a particular task.

Universal computation is the basis for all standard computer languages. But many of these languages rely on the idea of *compilation*. In C or Fortran, for example, the program must first be written, then compiled to generate machine code that can actually be executed on your computer. *Mathematica* does not require the compilation step. Once input an expression has been typed, the functions in the expression can immediately be executed.

The source code for the kernel, save a fraction of a percent, is identical for all computer systems on which *Mathematica* runs. For the front end, however, a significant amount of specialized code is needed to support each different type of user interface environment. The front end contains about 600,000 lines of system-independent C source code, of which roughly 150,000 lines are concerned with expression formatting. Then there are between 50,000 and 100,000 lines of specific code customized for each user interface environment.

Mathematica uses a client-server model of computing. The front end and kernel are connected via *MathLink*—the same system as is used to communicate with other programs. Within the C code portion of the *Mathematica* kernel, modularity and consistency are achieved by having different parts communicate primarily by exchanging complete *Mathematica* expressions.

There are many detailed differences between different kinds of computer systems. But one of the important features of *Mathematica* is that it allows you to work and create material without being concerned about such differences.

The commands that are given to the *Mathematica* kernel, for example, are absolutely identical on every computer system. This means that when a program is written using these commands, it can be run on any computer that supports *Mathematica*.

The structure of *Mathematica* notebooks is also the same on all computer systems. And as a result, if a notebook is created on one computer system, it can be used on any other system.

CHAPTER FIVE

NUMERICAL EXAMPLES

5.1 Description

Three different examples are chosen to demonstrate the applicability of the scheme. Initial and boundary conditions as discussed in section 3.1.1 are chosen for all examples. The first case examines a disk radiated by a short pulse laser only at the center of the top surface of the disk. Secondly, the laser is pulsed twice over the same center point on the disk. Finally, the laser is pulsed at various positions on the surface of the disk.

Table 5.1 indicates the known parameters for the given system. These values have been garnered experimentally and reported in several sources [Qui 1993a] [Tzou 1996] [Barron 1985].

Table 5.1 Known parameters for the system

	Gold	Chromium
T_0	300 K	300 K
κ	315 W/mK	94 W/mK
γ	70 J/m ³ K ²	193.33 J/m ³ K ²
C_e^0	2.1x10 ⁴ J/m ³ K	5.8x10 ⁴ J/m ³ K
C_1	2.5x10 ⁶ J/m ³ K	3.3x10 ⁶ J/m ³ K
G	2.6x10 ¹⁶ W/m ³ K	42x10 ¹⁶ W/m ³ K

5.2 Case One – Base Case

For this case, a two-layered thin film disk is irradiated by a picosecond laser as illustrated in Figure 5.1.

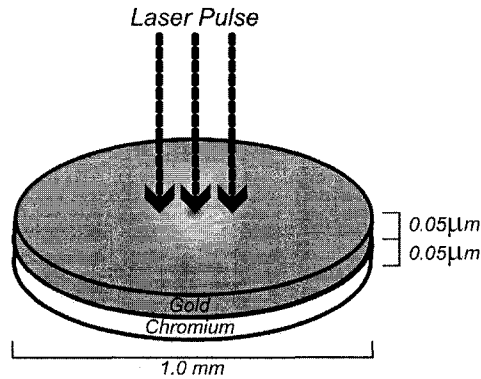


Figure 5.1 Schematic representation for case one

Three different x - y planar meshes were chosen – these being planar meshes with thirty-three nodes, one with sixty-five nodes and a final mesh with one hundred twenty-nine nodes. A z -directional grid size of 10^{-6} microns was chosen and a time step of 0.001 picoseconds. Qualities for the Gold and Chromium were chosen from Table 4.1. The laser source was assumed to be the same as in equation (3.6) [Qui 1994]. Figures 5.2 and 5.3 give the normalized temperature profiles at the surface directly beneath the heat source. Figure 5.2 depicts the normalized electron temperature on the surface over time. The maximum temperature of T_e on the surface was roughly 1100 Kelvin. Evident are three distinct intervals for this plot. In the first time interval (0.0 - 0.25 ps), there is a very fast rise of the electron temperature, up to the maximum temperature. In the second interval (0.26 -1.5 ps), thermal equilibrium is quickly reached within the electrons causing the temperature to drop quickly. It is during this time that heat energy is being

transferred to the lattice through lattice-electron coupling. In the final interval (1.6 – 2.0 ps), the electron temperature is roughly uniform as thermal equilibrium is being reached with the lattice.

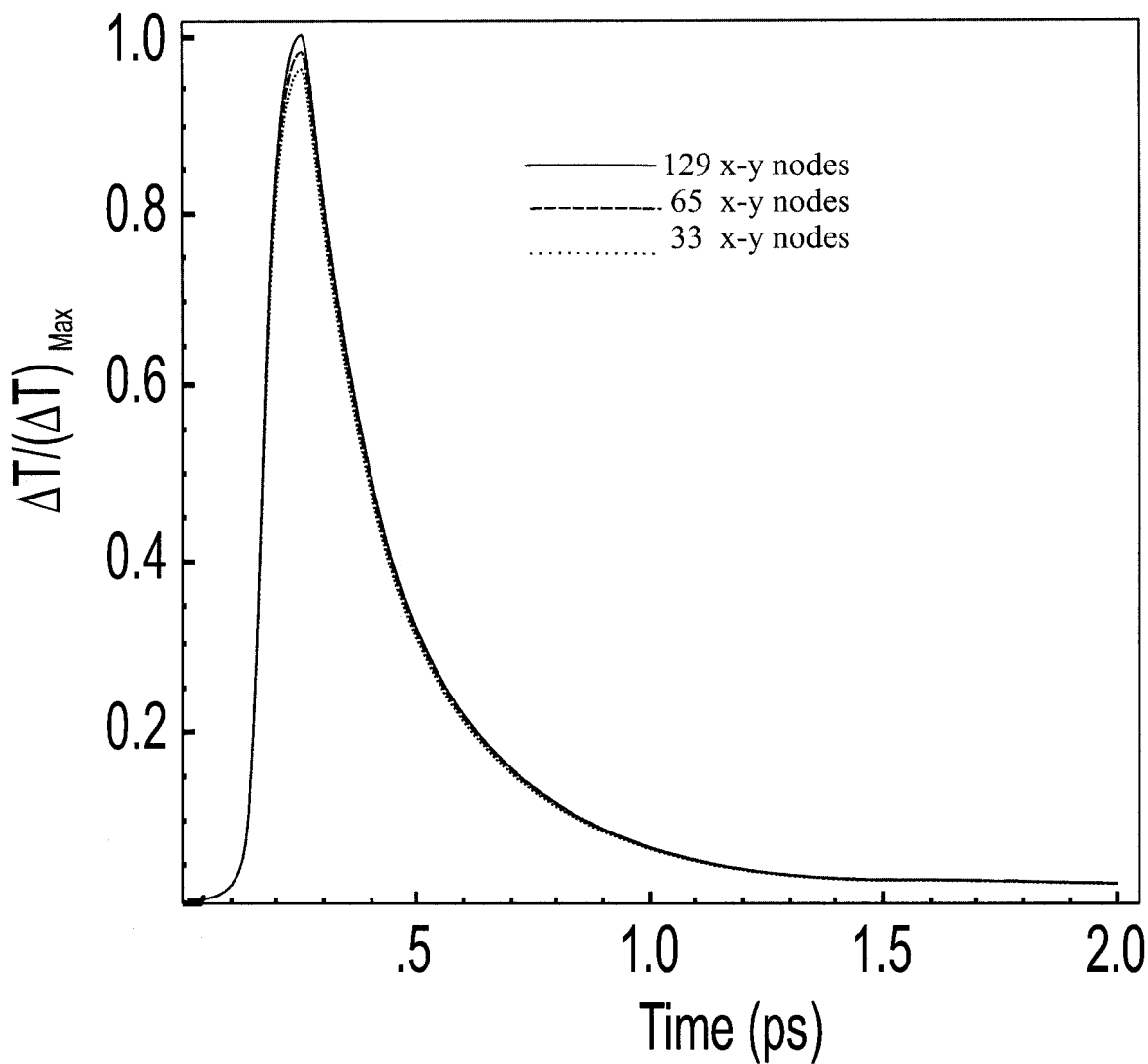


Figure 5.2 Normalized electron temperature change on surface

This plot shows good agreement with the one obtained by [Tzou 1996]. The results also show good agreement with Dai and Nassar [Dai 2000a].

In that work

$$L_{pre}^{(l)}[(\bar{T})_{jkn}^{(l)}]^{n+1} =$$

$$\begin{aligned}
L_{pre}^{(l)} [(\bar{T}^{(l)})_{jkm}^{n+1}]^{(i)} - \omega \left\{ \frac{[(T^{(l)})_{jkm}^{n+1}]^{(i)} - T_{jkm}^n}{\Delta t} - \frac{\kappa^{(l)}}{2\rho^{(l)}C_p^{(l)}} (\delta_x^2 + \delta_y^2) [(T^{(l)})_{jkm}^{n+1}]^{(i)} - (T^{(l)})_{jkm}^n \right\} \\
+ \frac{\kappa^{(l)}}{2\rho^{(l)}C_p^{(l)}\Delta z^2} \left(\frac{1}{2} + \frac{\tau_q^{(l)}}{\Delta t}\right)^{-1} \left(\frac{1}{2} + \frac{\tau_T^{(l)}}{\Delta t}\right) [(T^{(l)})_{jkm+1}^n - 2(T^{(l)})_{jkm}^{n+1}]^{(i)} + [(T^{(l)})_{jkm-1}^{n+1}]^{(i)} \\
- \frac{\kappa^{(l)}}{2\rho^{(l)}C_p^{(l)}\Delta z^2} \left(\frac{1}{2} + \frac{\tau_q^{(l)}}{\Delta t}\right)^{-1} \left(\frac{1}{2} - \frac{\tau_T^{(l)}}{\Delta t}\right) [(T^{(l)})_{jkm+1}^n - 2(T^{(l)})_{jkm}^n + (T^{(l)})_{jkm-1}^n] \\
+ \frac{1}{2\rho^{(l)}C_p^{(l)}\Delta z} \left[1 + \left(\frac{1}{2} + \frac{\tau_q^{(l)}}{\Delta t}\right)^{-1} \left(\frac{1}{2} + \frac{\tau_T^{(l)}}{\Delta t}\right)\right] [(q^{(l)})_{jkm}^n - (q^{(l)})_{jkm-1}^n] - \frac{1}{\rho^{(l)}C_p^{(l)}} Q_{jkm}^{n+\frac{1}{2}}, \\
l=1, 2, \quad i=0, 1, 2, \dots \quad (5.1)
\end{aligned}$$

and

$$\begin{aligned}
(q^{(l)})_{jkm}^{n+1} &= \left(\frac{1}{2} + \frac{\tau_q^{(l)}}{\Delta t}\right)^{-1} \left(-\frac{1}{2} + \frac{\tau_q^{(l)}}{\Delta t}\right) (q^{(l)})_{jkm}^n \\
&\quad - \left(\frac{1}{2} + \frac{\tau_q^{(l)}}{\Delta t}\right)^{-1} \left(-\frac{\kappa^{(l)}}{\Delta z} \left(\frac{1}{2} + \frac{\tau_T^{(l)}}{\Delta t}\right) [(T^{(l)})_{jkm}^{n+1} - (T^{(l)})_{jkm-1}^{n+1}]\right) \\
&\quad + \left(\frac{1}{2} + \frac{\tau_q^{(l)}}{\Delta t}\right) [(T^{(l)})_{jkm}^n - (T^{(l)})_{jkm-1}^n] \quad l=1, 2, \quad (5.2)
\end{aligned}$$

There is only slight variation between the x-y mesh sizes which is a further indicator of stability. The results shown in Figure 5.3 depict the normalized lattice temperature profiles at the surface directly beneath the heat source. The maximum temperature rise of T_l was roughly 10.99 Kelvin which is again in good agreement with other numerical studies. The three time intervals are also evident. The first interval (0.0 - 0.25ps), shows little or no increase in heat energy for the lattice due to the quick electron excitement with little transfer to the lattice. In the second interval (0.26 - 1.5 ps), the metal lattice temperature starts to rise quickly as the electron-lattice coupling begins. In the final domain (1.6 – 2.0 ps), the lattice temperature is leveling showing the

approach of equilibrium with the electrons. Again, mesh size in the x-y plane shows little impact on the results implying stability in the scheme.

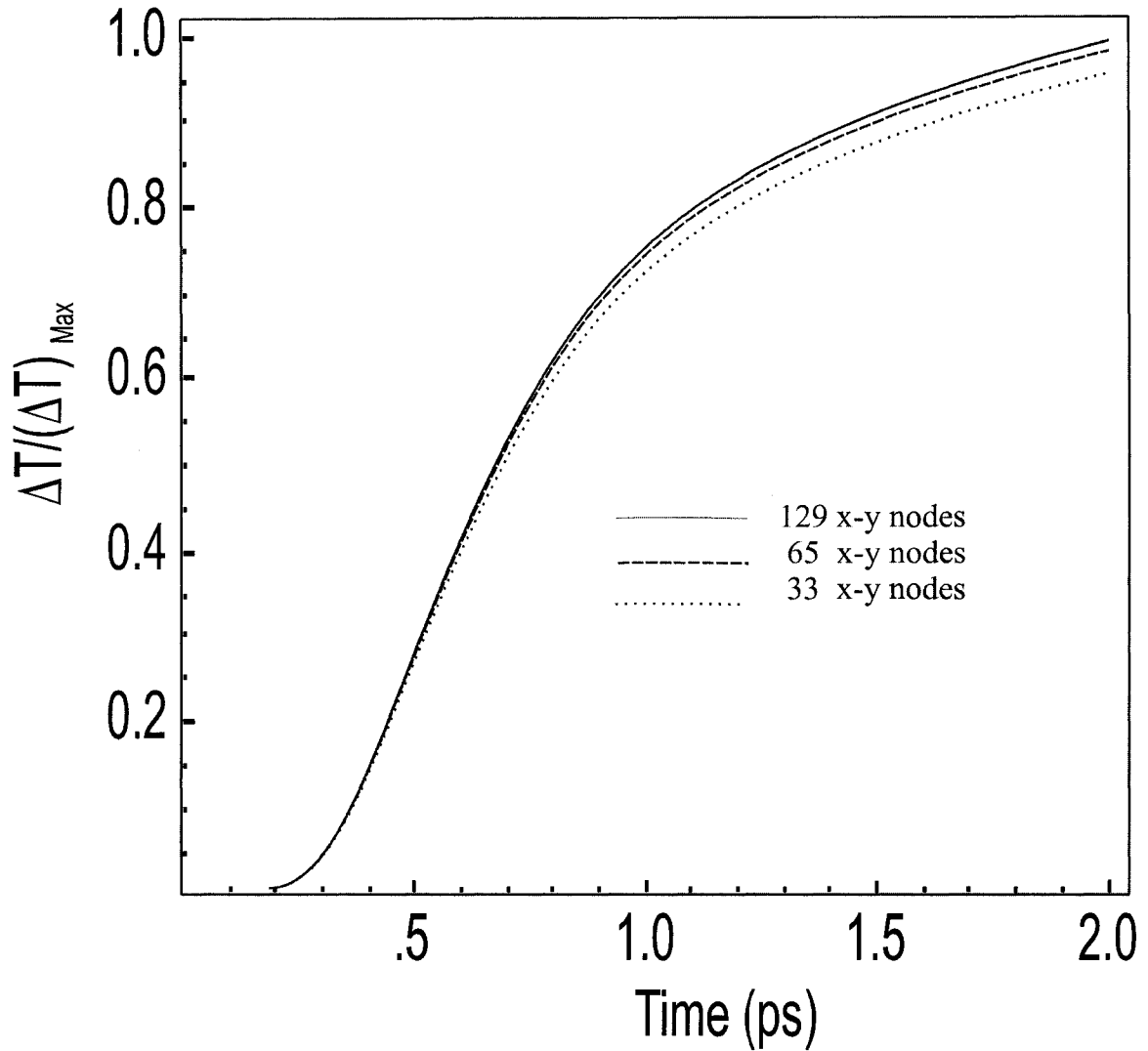


Figure 5.3 Normalized lattice temperature change on surface

Figures 5.4 and 5.5 give the change for both electron and lattice temperatures along the z axis for time $t = 0.2$ ps, $t = 0.25$ ps, and $t = 0.5$ ps. Results are shown and are in good agreement with numerical studies.

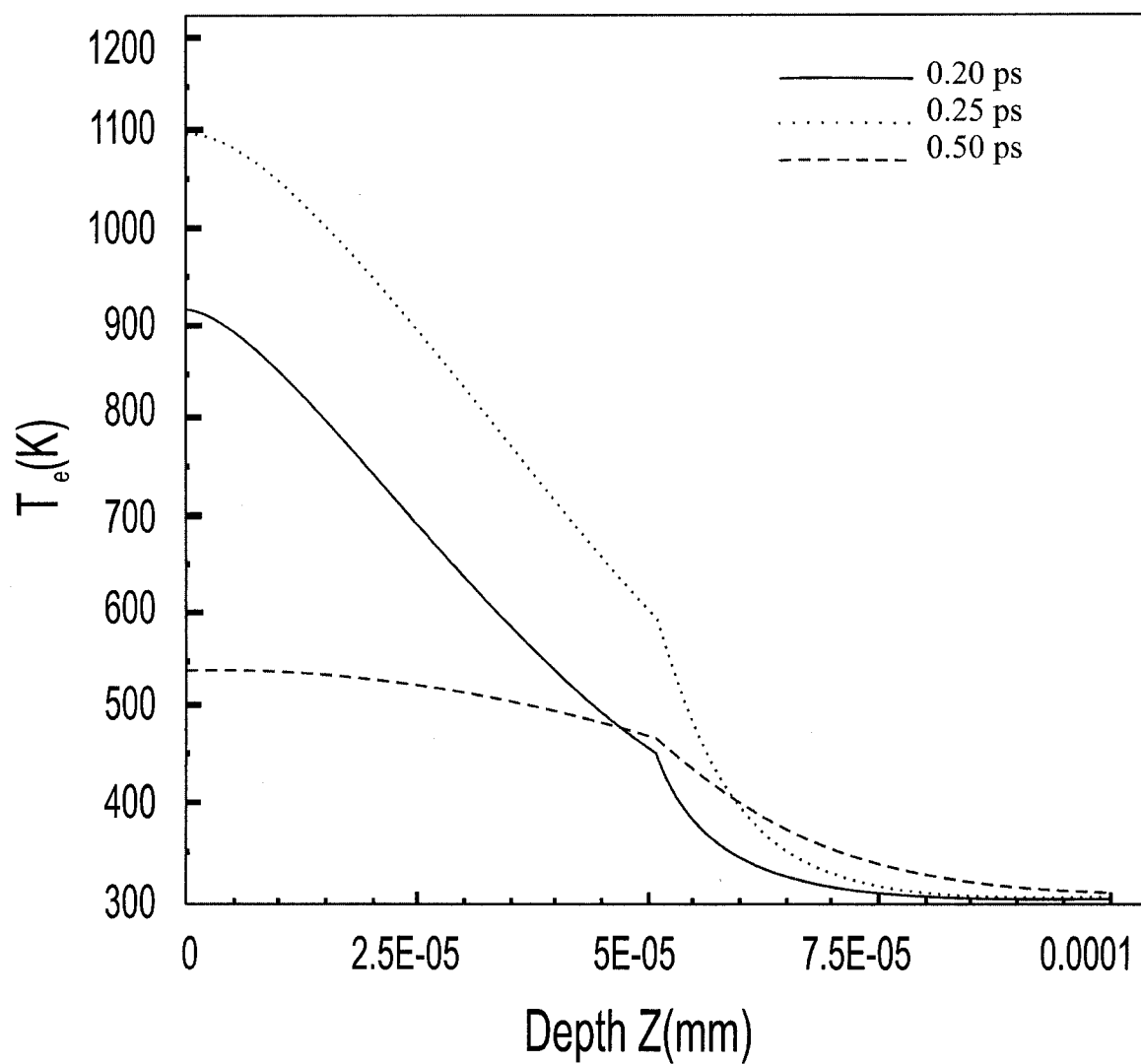


Figure 5.4 Electron temperature profile (z-direction)

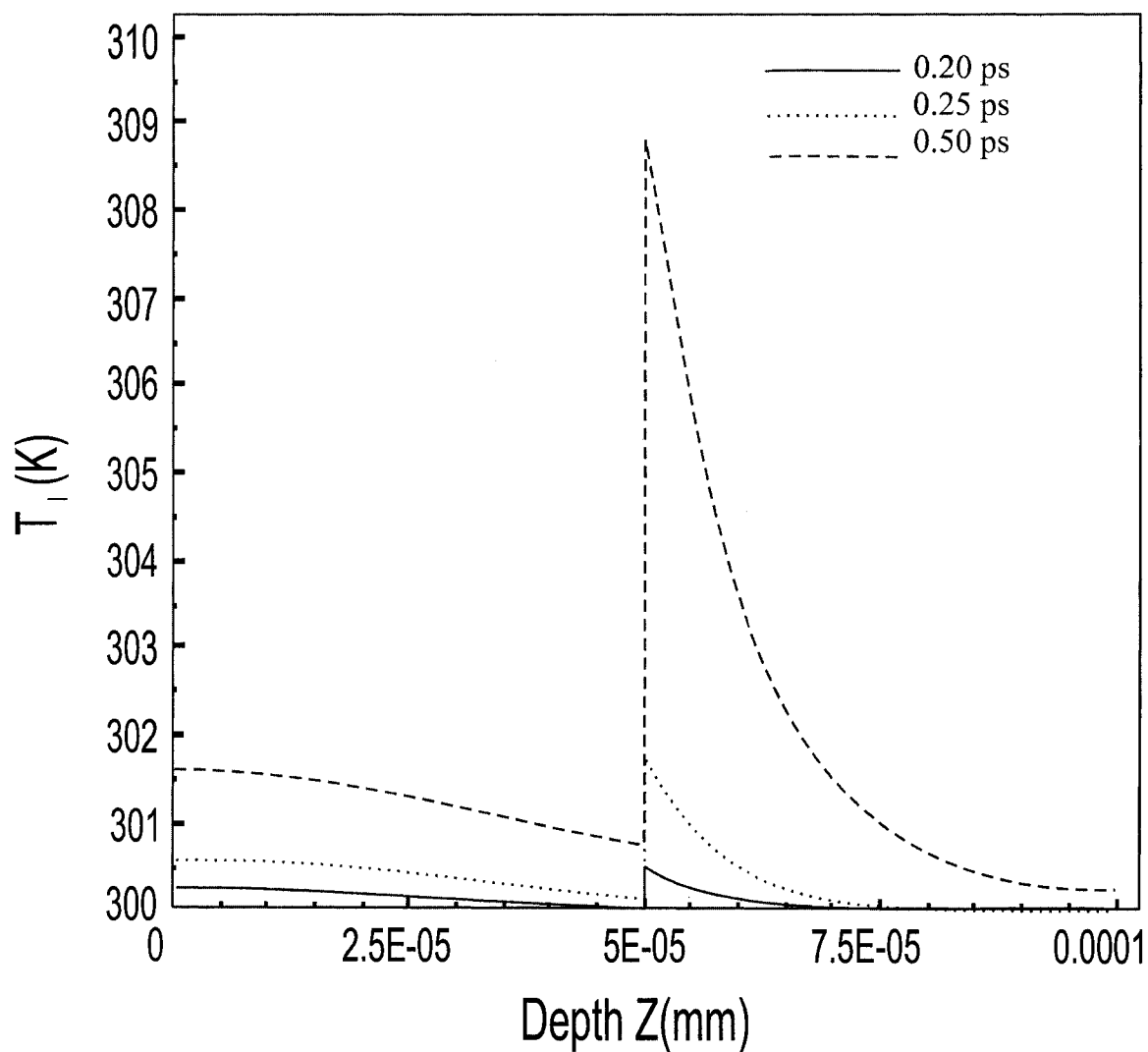


Figure 5.5 Lattice temperature profile (z-direction)

Figures 5.6 and 5.7 give contour plots at time $t=0.2$ ps, $t=0.25$ ps, and $t=0.5$ ps for the electron and lattice temperatures respectively along the x-z plane.

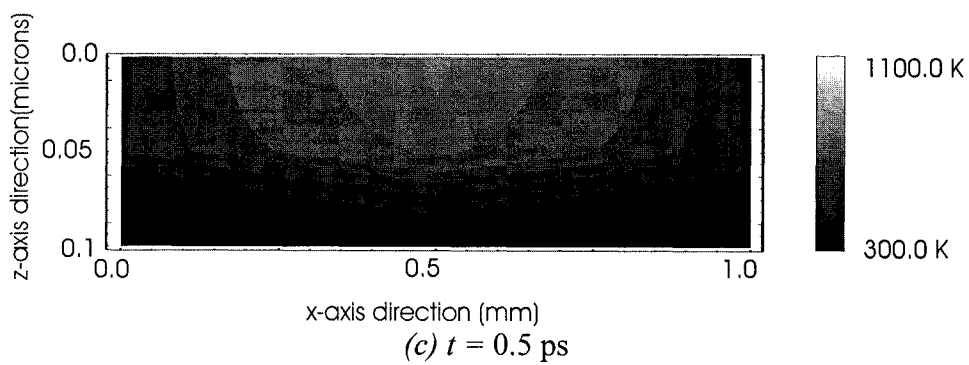
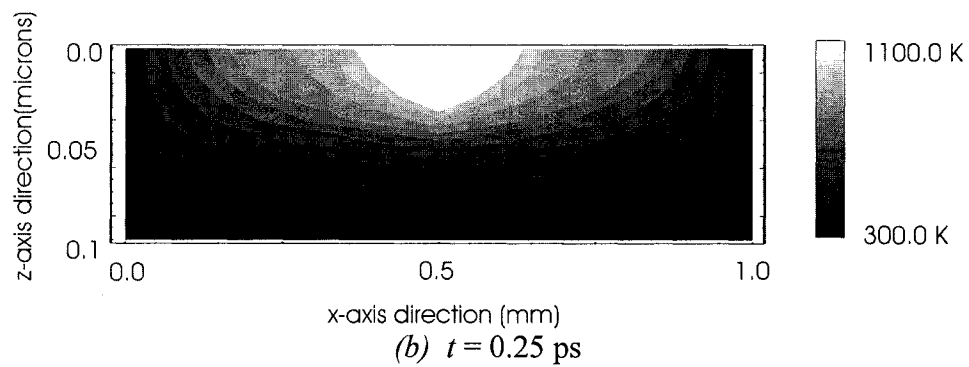
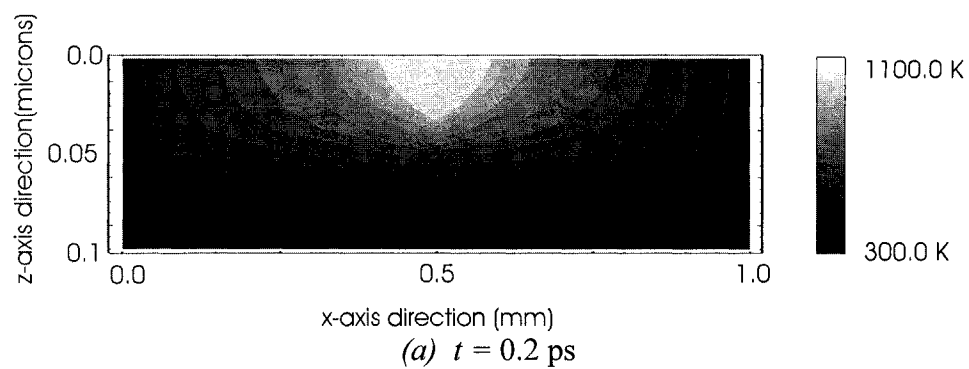


Figure 5.6 Electron temperature distribution in the x-z plane

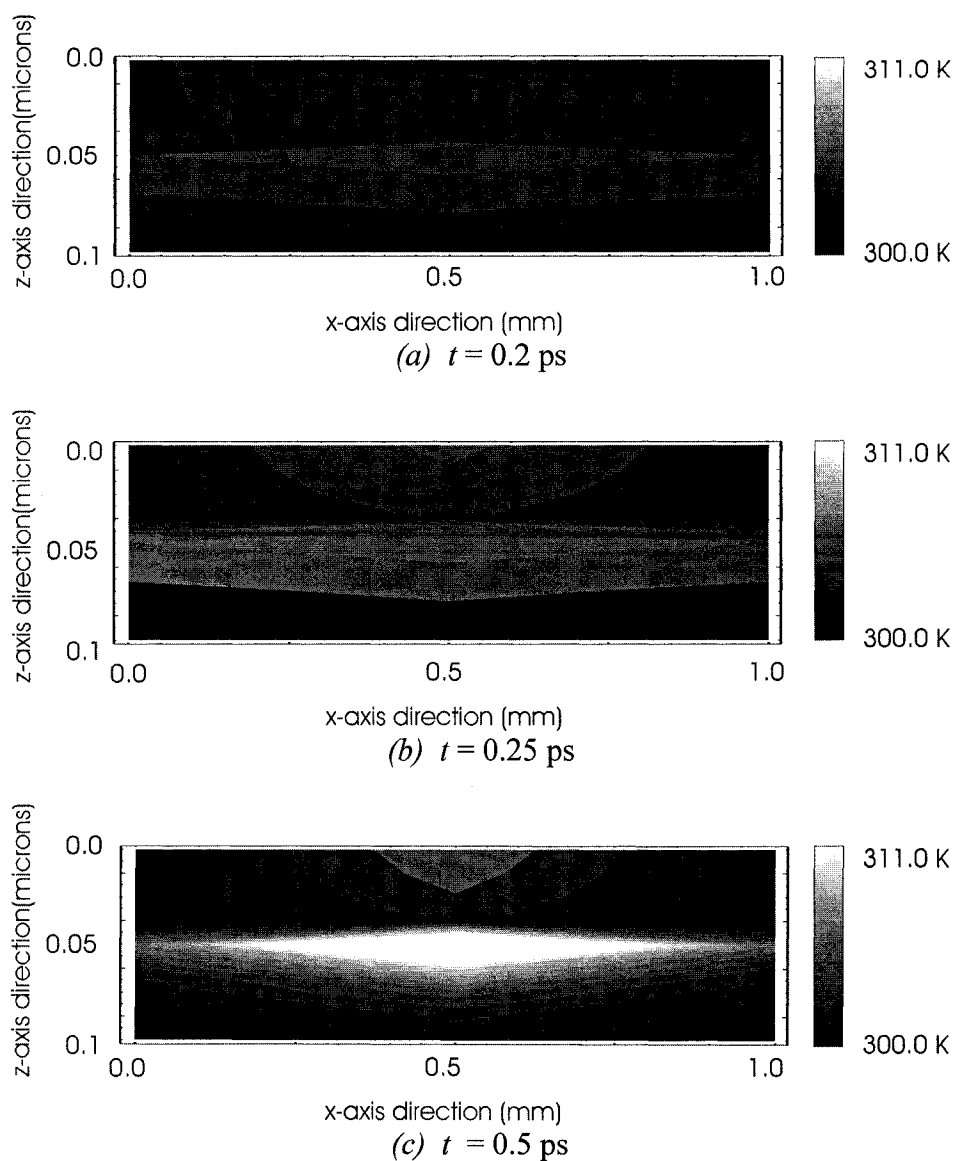


Figure 5.7 Lattice temperature distribution in the x-z plane

Figure 5.8 shows a comparison of the surface contours for both the electron and lattice temperatures at time $t=0.25$ ps. This time interval represents the peak electron heating. The lag in coupling electron and lattice energy exchange is evident. This contour comparison reveals a high electron temperature and only a slight variation in the lattice/bulk temperature at the close of the first time interval (0.0 - 0.25ps).

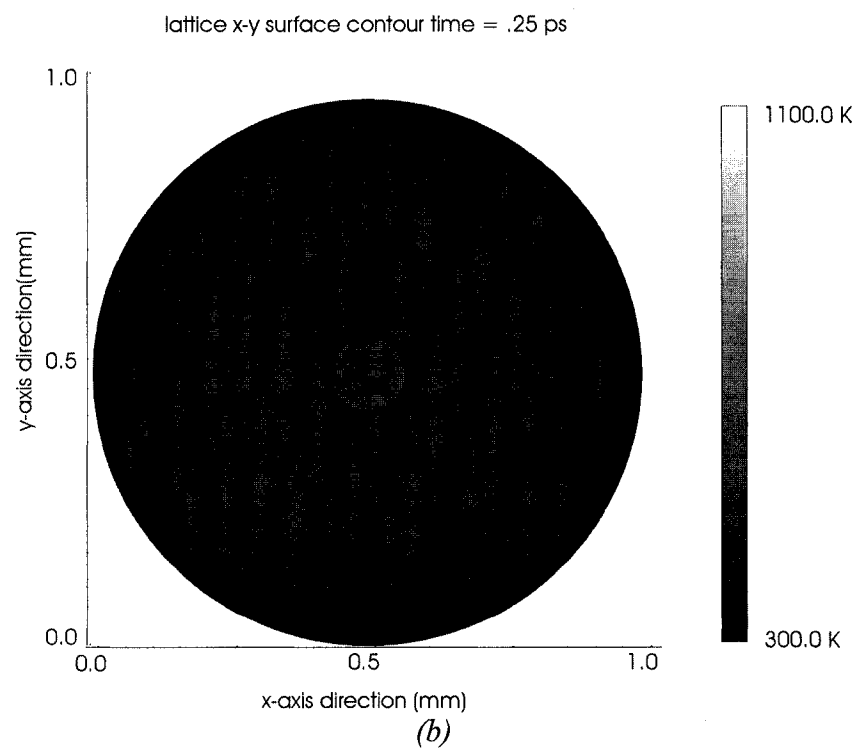
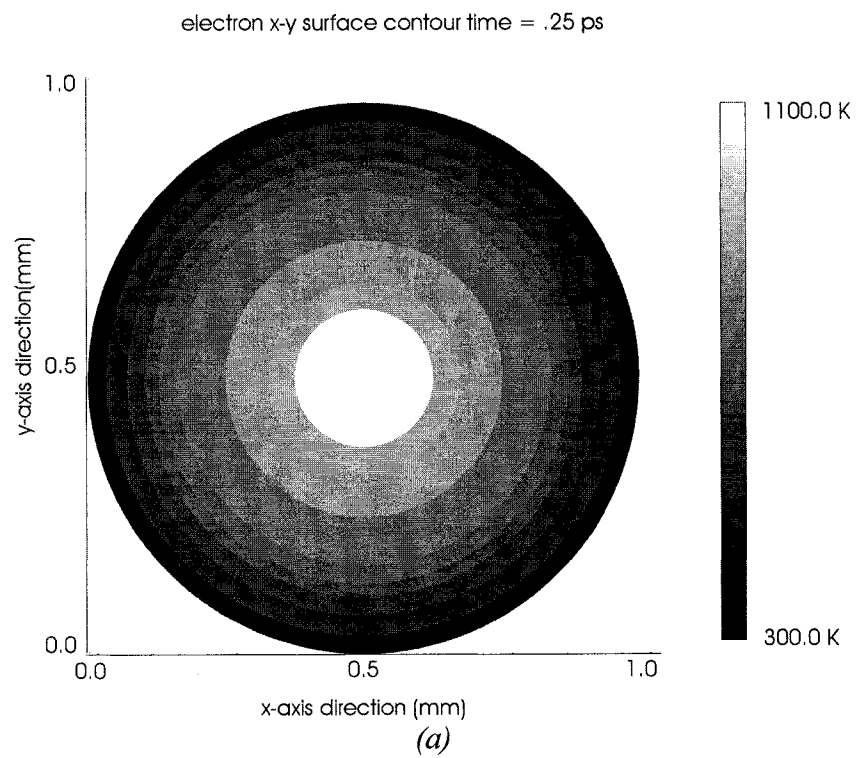


Figure 5.8 Electron and lattice temperature distribution in the x-y plane (0.25 ps)

5.3 Case Two – Double Pulse Heat Source

The second case represents a double pulse of the laser heat source. The same center section is irradiated. The heat source for this case is chosen to be

$$S_p = 0.94J \left(\frac{1-R}{t_p \delta} \right) e^{-\frac{z}{\delta}} \cdot \left[e^{-2.77 \left(\frac{t-2t_p}{t_p} \right)^2} + e^{-2.77 \left(\frac{t-4t_p}{t_p} \right)^2} \right] \quad (5.3)$$

where $J=13.4 \text{ J/m}^2$, R is given to be 0.93, $t_p=100 \text{ fs}$, and $\delta=15.3 \text{ nm}$. The dense mesh of the finite element representation was chosen for highest accuracy and the same time and z -directional (depth) values as in Case One were chosen. Figure 5.9 shows the normalized change in electron temperature ($\Delta T_e / (\Delta T_e)_{\text{max}}$) on the surface of the gold/chromium disk.

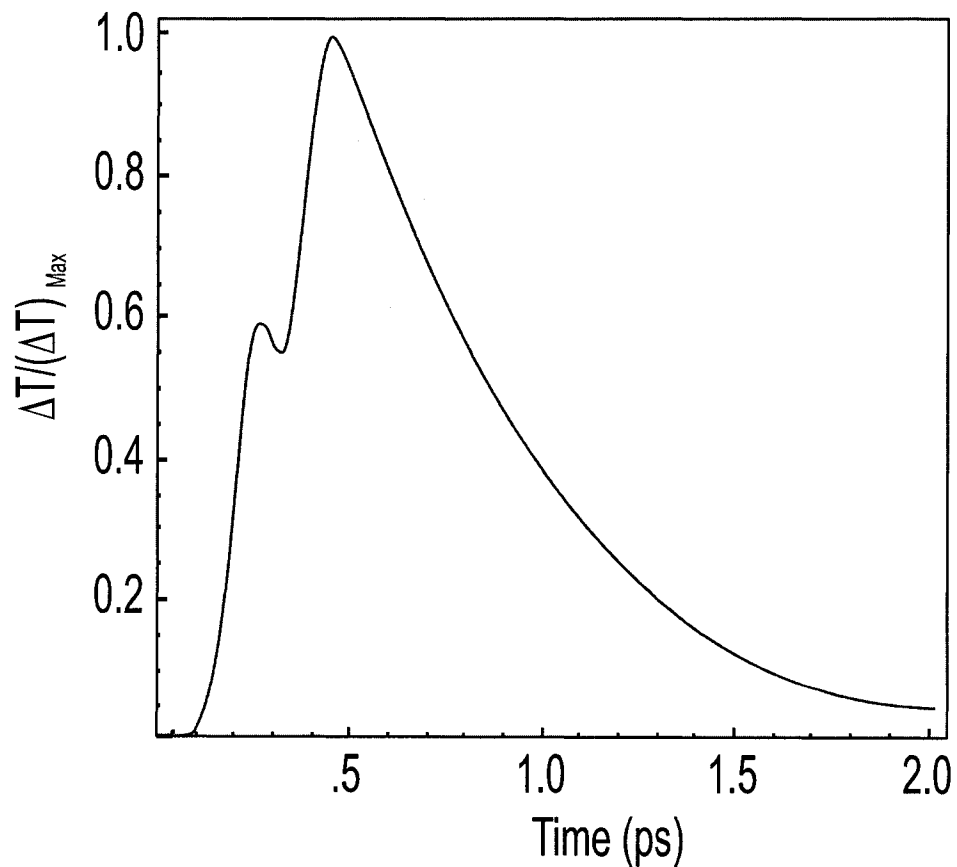


Figure 5.9 Normalized electron temperature change on surface (double pulse)

It can be seen from Figure 5.9 that there are two peaks in electron temperature due to the two laser pulses. Figure 5.10 gives the normalized temperature distribution for the lattice.

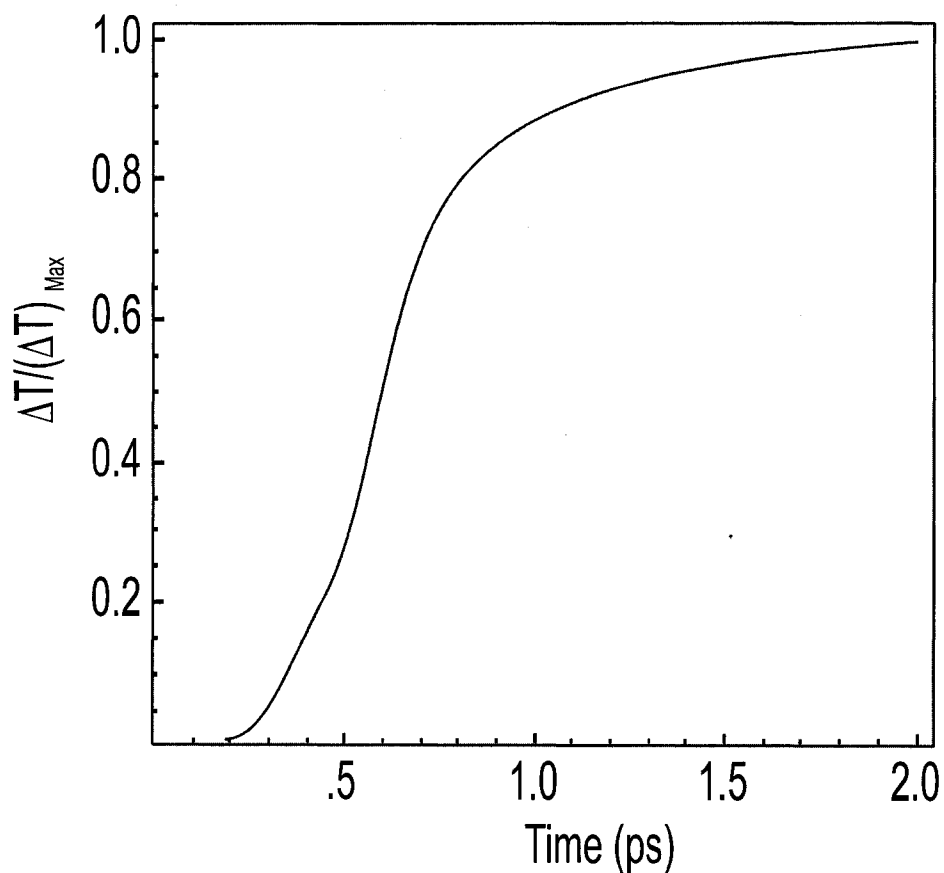


Figure 5.10 Normalized lattice temperature change on surface (double pulse)

A slight bend is evident at time $t=0.5$ ps, as the second electron temperature peak begins to transfer energy to the lattice. Figure 5.11 demonstrates the temperature distribution through the disk along the z -direction through the film. The same three times as in case one were chosen ($t=0.2$ ps, $t=0.25$ ps and $t=0.5$ ps).

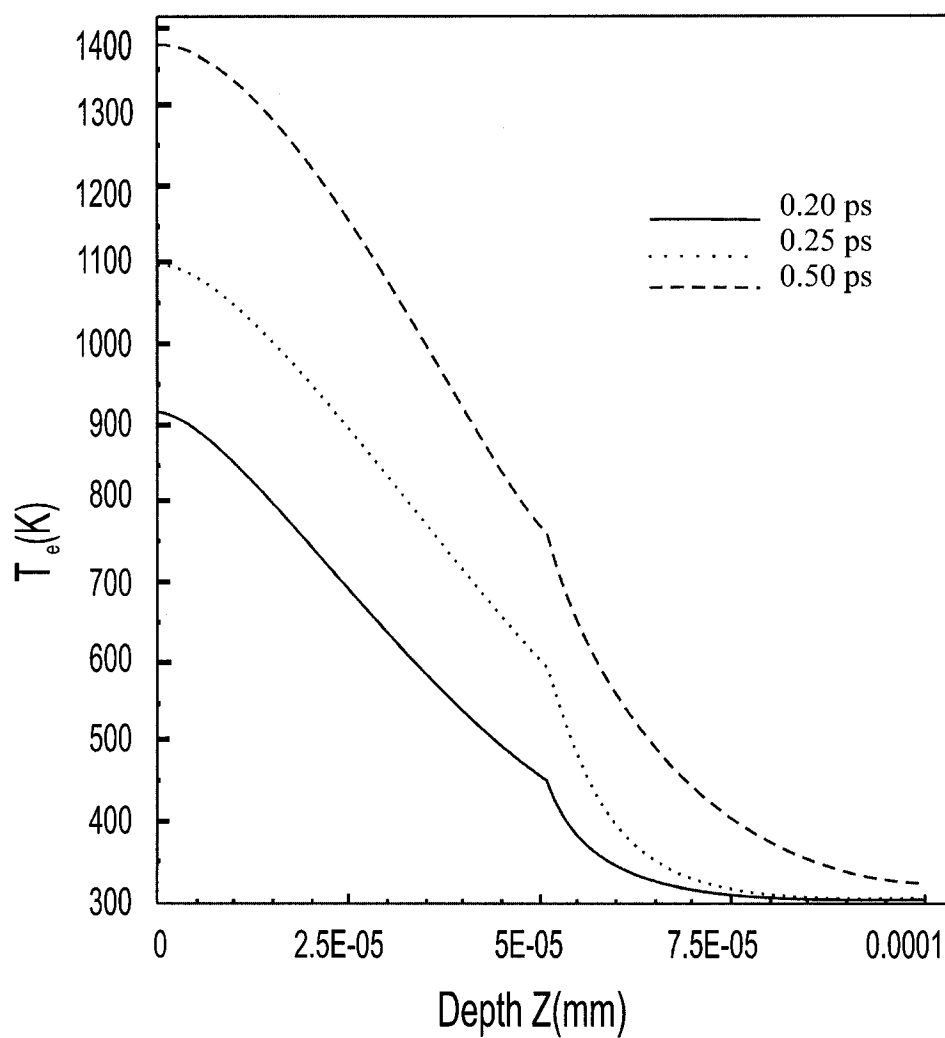


Figure 5.11 Electron temperature distribution (double pulse)

This figure shows a peak temperature at time $t=0.5$ ps of nearly 1400 Kelvin.

Figure 5.12 demonstrated the lattice temperature distribution through the film in the z -direction.

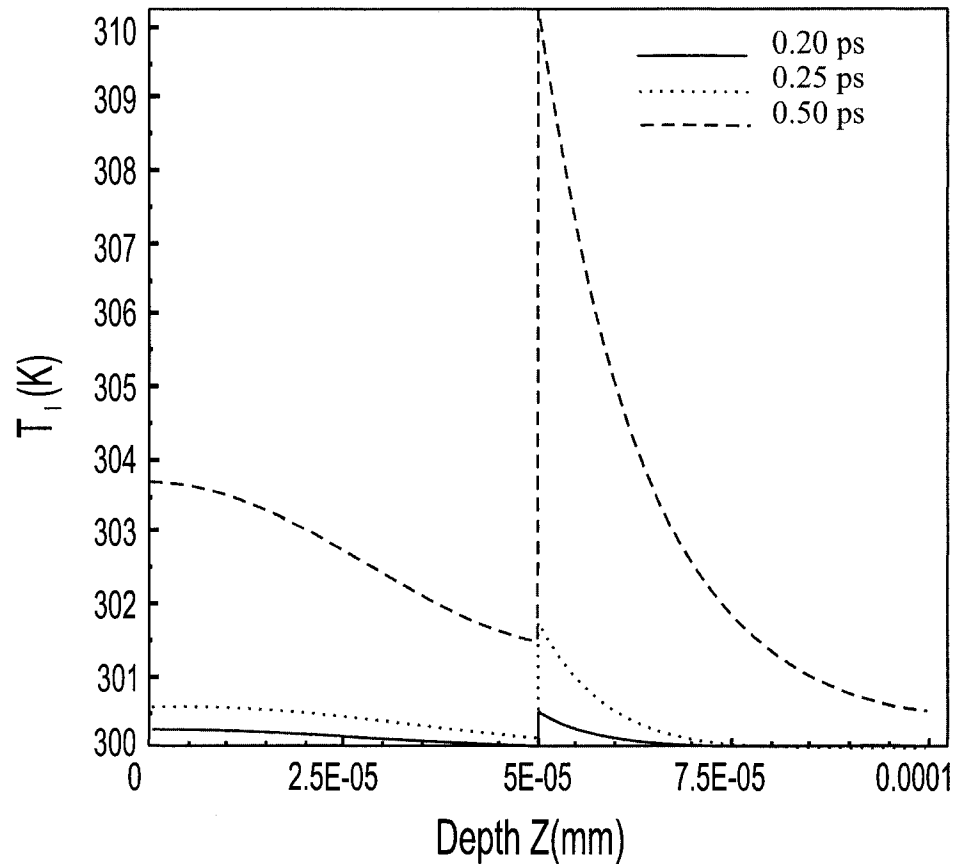


Figure 5.12 Lattice temperature distribution (double pulse)

Again, the temperature profile is similar to the ones in case one, except that the peak is higher due to the second pulse of the laser.

5.4 Case Three – Moving Heat Source

This case demonstrates a moving source. The laser is pulsed five times at even time intervals about the center of the disk. The first pulse is focused on the center of the disk. The second pulse moves along the x -axis in the positive direction. The third pulse is located the same distance from the center along the positive direction of the y -axis. The fourth and fifth pulses are located likewise along the negative directions of the x - and y -axis respectively. Figure 5.13 gives a graphical representation.

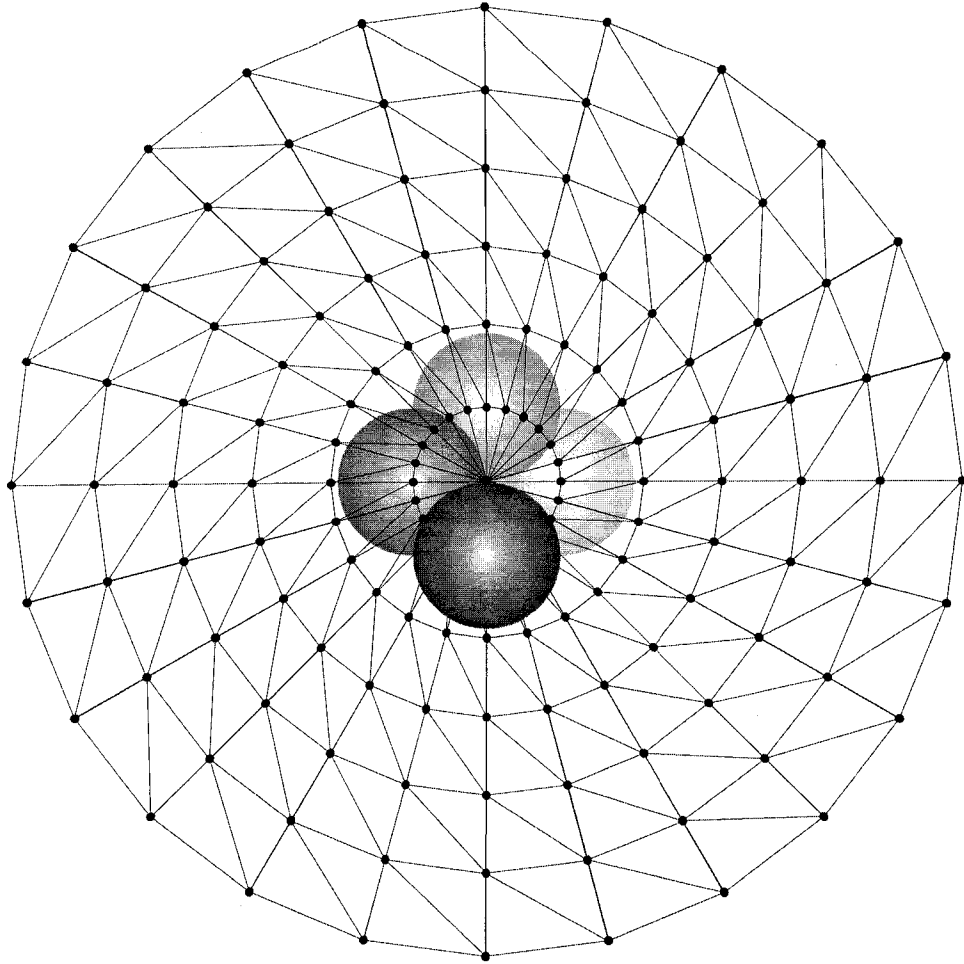


Figure 5.13 Graphical representation of pulsed laser on thin film surface

Figure 5.14 demonstrates the normalized electron temperature change for the central point of the top of the thin film's surface. The distinct laser pulses are evident as the electron temperature rises sharply with each pulse.

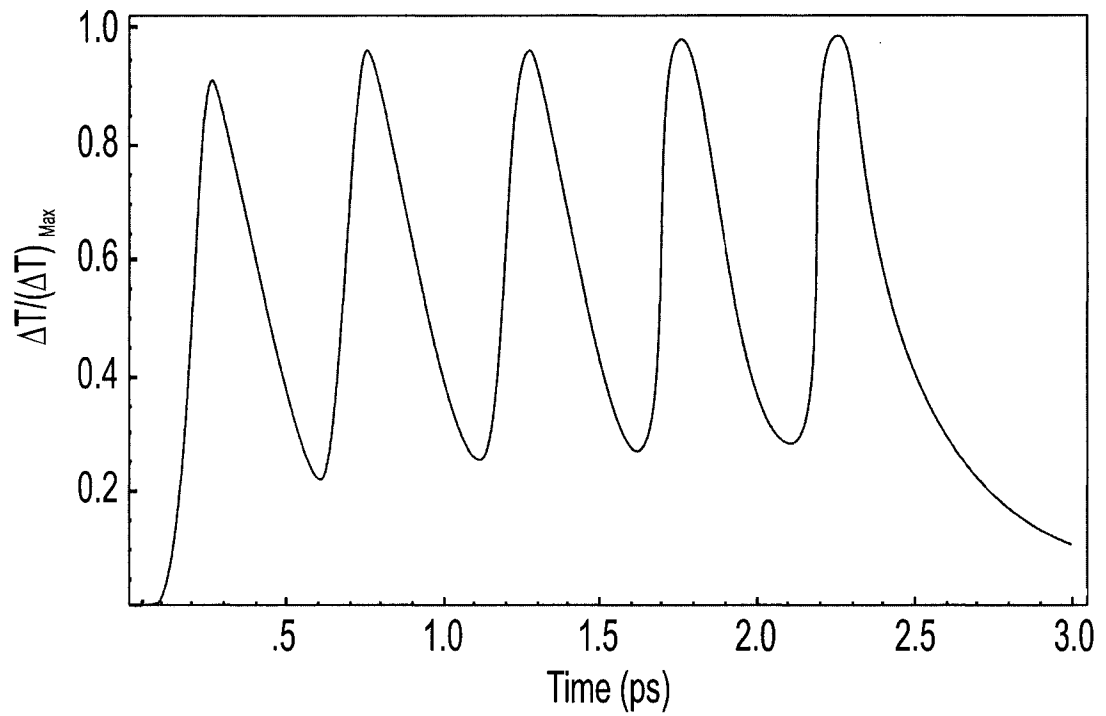


Figure 5.14 Normalized electron temperature distribution center surface of disk (moving source)

Figure 5.15 demonstrates the normalized lattice temperature for the same point. Again, a steady climb is evident with changes caused by each pulse as the energy is transferred from the electron cloud to the lattice.

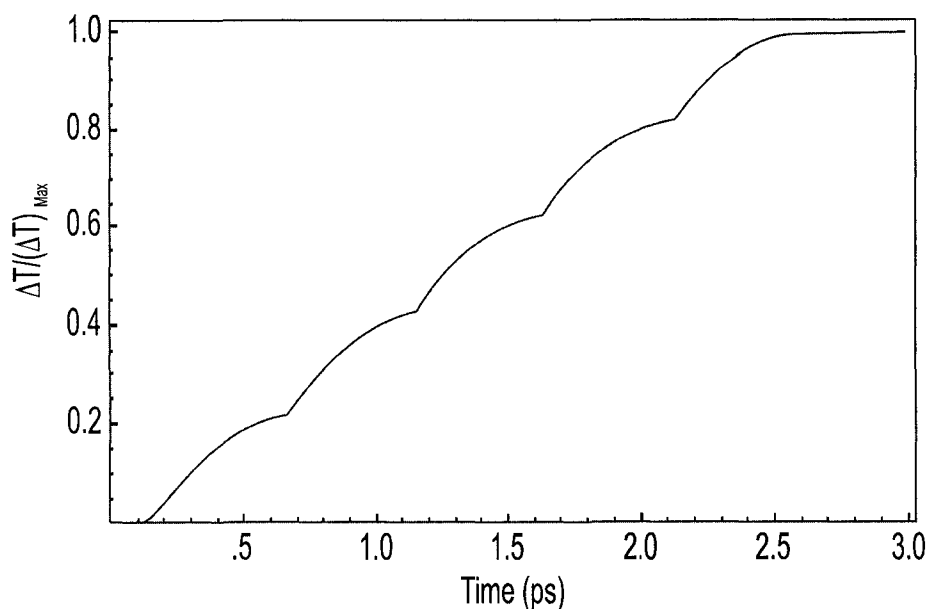
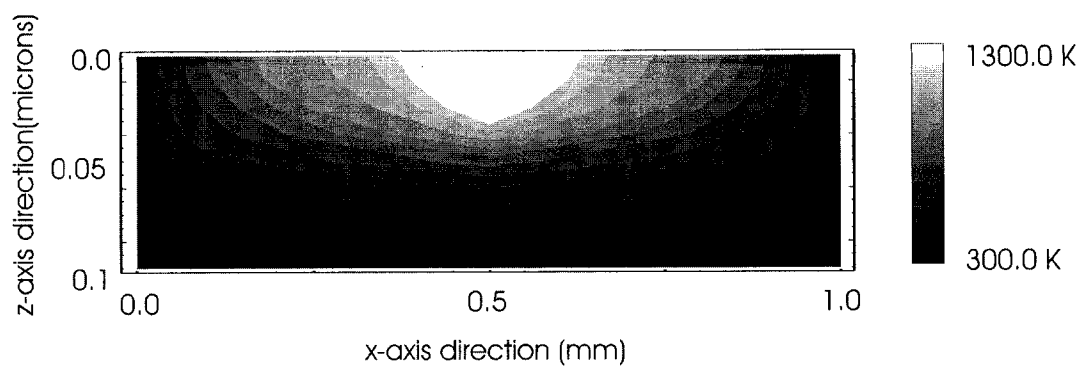
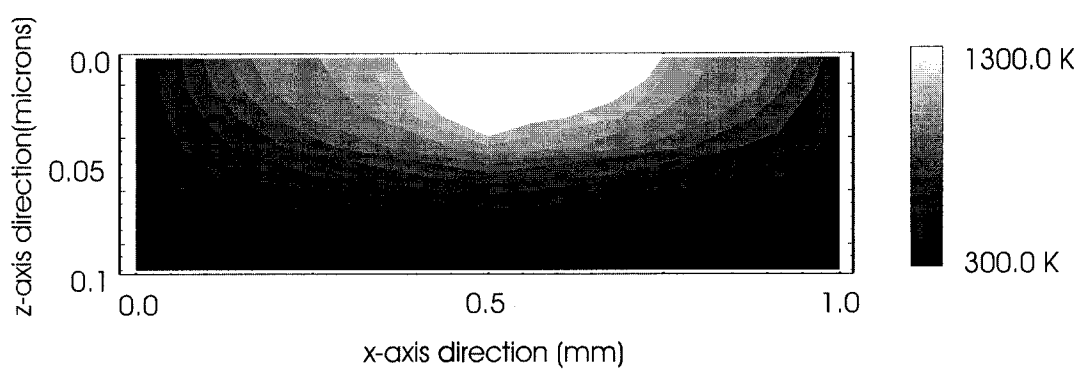


Figure 5.15 Normalized lattice temperature distribution center surface of disk (moving source)

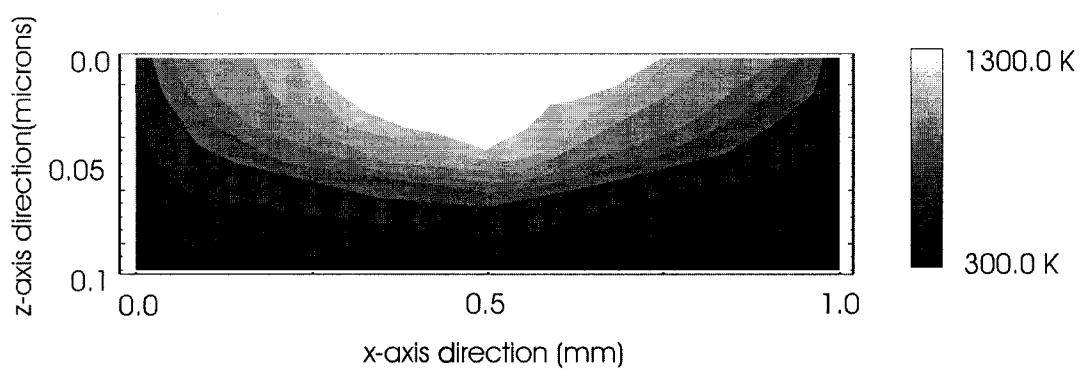
Contours for the electron temperature distribution through the thin films are shown in Figure 5.16. The first contour is after time $t=0.25$ ps. This is at the peak electron temperature profile for the first laser pulse. The second contour demonstrates the temperature distribution through the thin films after time $t=0.75$ ps. This represents the peak electron temperature rise for the second pulse. It is evident that the temperature distribution moves slightly toward the positive x -direction. The final contour demonstrates the electron temperature distribution through the thin films after time $t=1.75$ ps. This represents the peak electron temperature rise for the fourth laser pulse. This pulse is located along the negative x -axis. A shift in temperature toward that point is evident in this contour. Figures 5.17, 5.18 and 5.19 show the temperature distribution profile on the surface (xy -plane) at time $t=0.25$ ps, $t=0.75$ ps and $t=1.75$ ps respectively. The heat propagation from the moving source is evident in these figures.



(a) $t = 0.25$ ps



(a) $t = 0.75$ ps



(a) $t = 1.75$ ps

Figure 5.16 Contour electron temperature distributions for moving source case

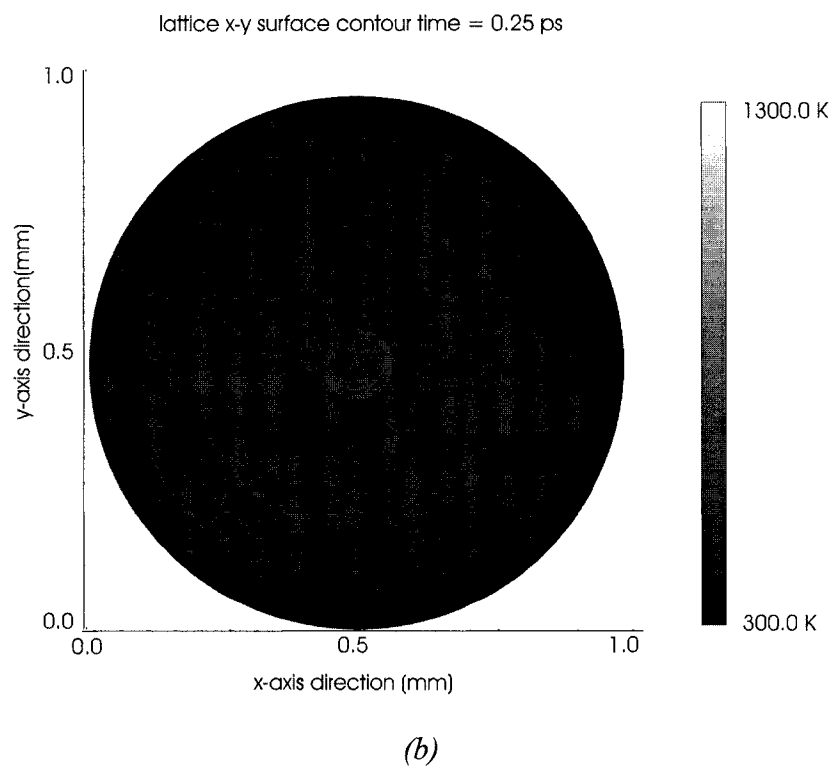
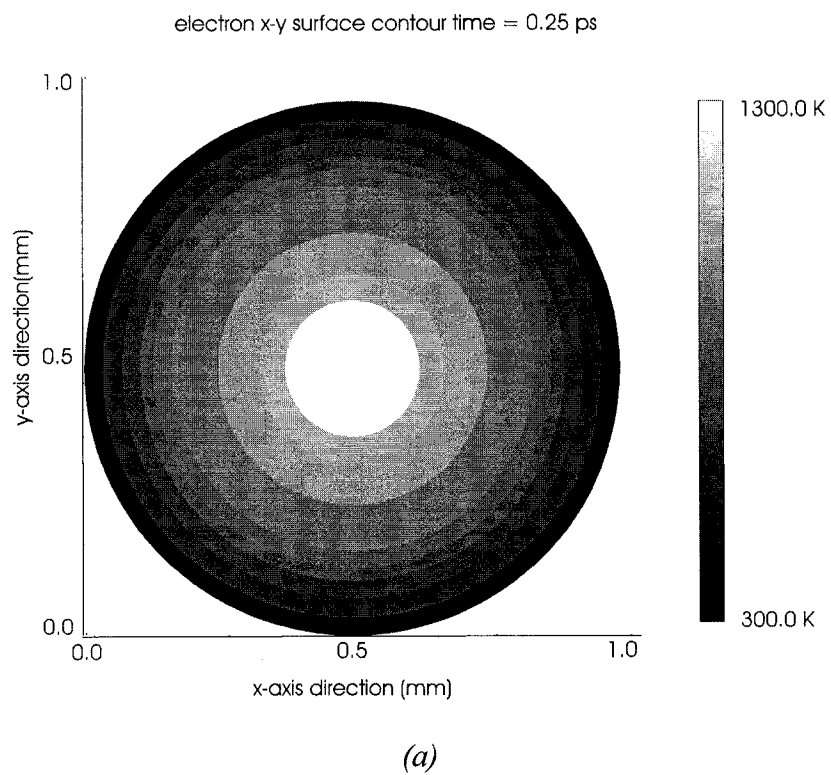


Figure 5.17 Electron and lattice temperature distribution in the x-y plane (0.25 ps)

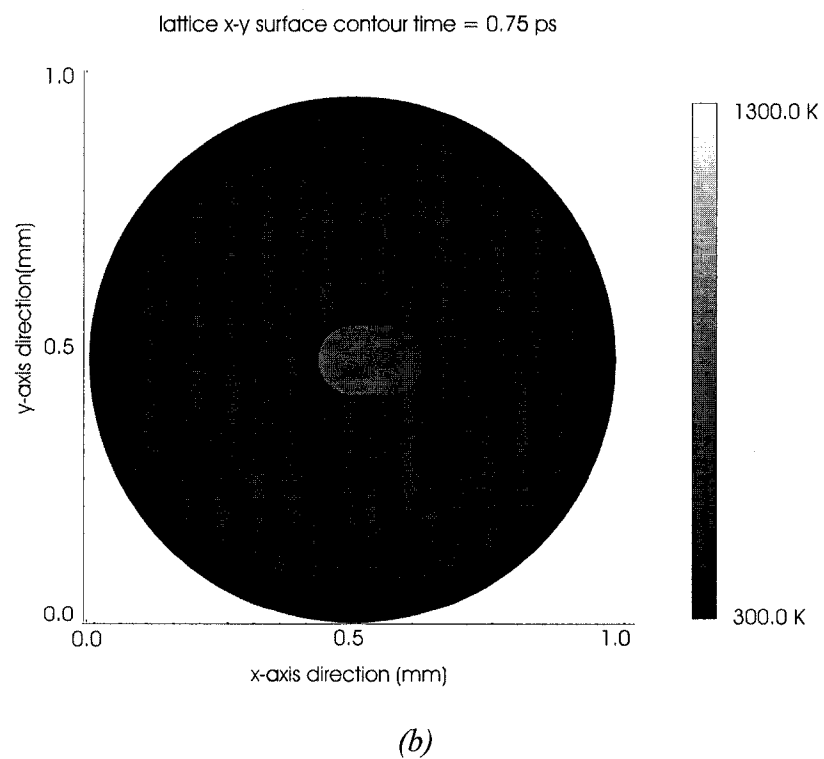
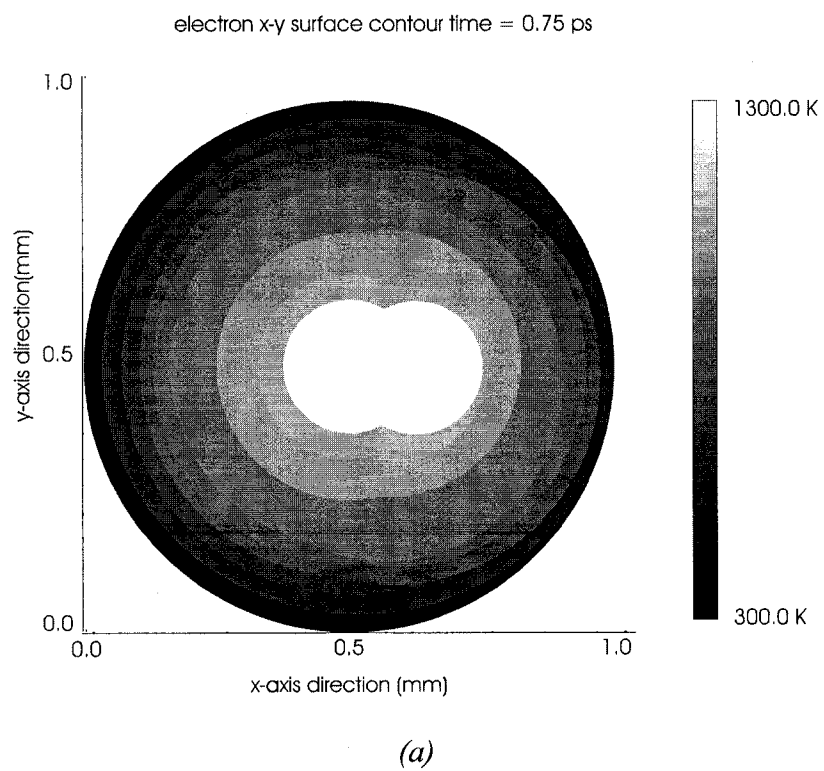


Figure 5.18 Electron and lattice temperature distribution in the x-y plane (0.75 ps)

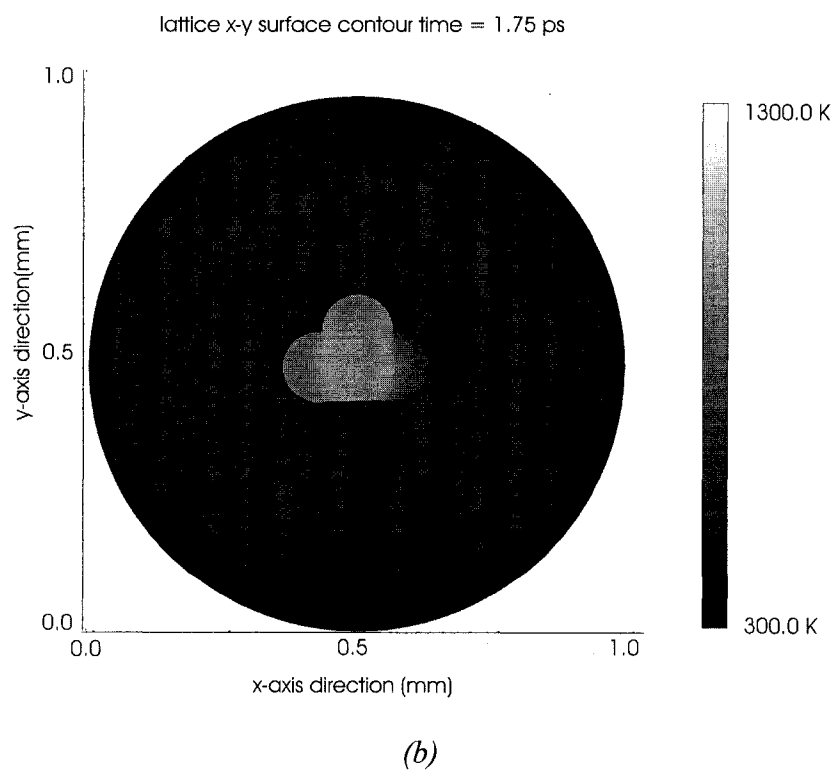
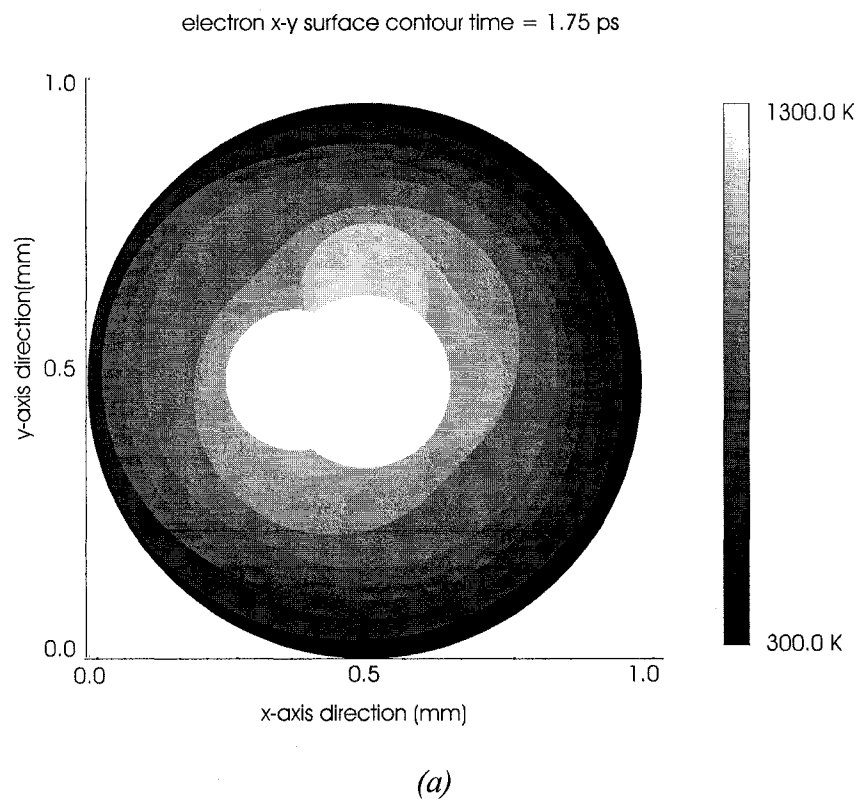


Figure 5.19 Electron and lattice temperature distribution in the x-y plane (1.75 ps)

CHAPTER SIX

CONCLUSION AND FUTURE RESEARCH

6.1 CONCLUSIONS

This dissertation has reviewed the fundamentals of heat transfer at both the macro and micro scale along with the dual-phase-lagging model for examining micro scale heat transfer. The dual-phase-lagging heat conduction equation originates from the first law of thermodynamics and heat flux density. It is developed through the examination of energy transport of the high-rate heating in which the non-equilibrium thermodynamic transition and microstructural effect become important associated with shortening of the response time.

A hybrid finite element-finite difference method has been developed for solving this parabolic two-step micro heat transport equations in a three dimensional double-layered thin film exposed to ultrashort pulsed lasers. First the geometry was discretized along the xy -direction using a finite element method to generate matrix coefficients for the system of equations. Secondly, the z -direction was discretized using a weighted average finite difference method. The system was encoded using *Mathematica* software and the results were examined. It was shown that the scheme is unconditionally stable with respect to the initial condition and the heat source. Numerical results for thermal analysis of a gold layer on a chromium padding layer are obtained. These results are examined for three distinct cases. The first case examined the thermal properties of a thin

double-layered disk exposed to a single ultrashort laser pulse. Secondly, this disk apparatus was exposed to an ultrashort double-pulse laser and the thermal properties examined. Finally, the ultrashort laser heat source was moved about the central point of the double-layered thin disk and the thermal properties examined. The method derived can be readily applied to multiple layers and irregularly shaped geometries.

6.2 Future Work

The future work related to this research may involve the development of an unconditionally stable scheme for thin films with varying interstitial conditions. This dissertation accounted for a perfect conduction between the gold and chromium layers. Future work should consider imperfect interstitial conditions or the thermal contact resistance between the layers. Another area for future research would be the addition of stress between the two layers. This work examines the heat distribution only. It is possible, albeit complicated, to consider tensile and compressive stresses caused by such a temperature variation. Such an examination would offer a more complete understanding of microscale heat transfer for thin films irradiated by short-pulsed-high-intensity lasers.

APPENDIX A

POSITIVE EIGENVALUES

Enclosed is a table indicating the eigenvalues of and a representation of the conductance and capacitance matrices.

APPENDIX B

SOURCE CODE

(* Parabolic Two Step Model Two Layers *)

<< LinearAlgebra`MatrixManipulation`

(* assembler Portion *)

Needs["Inpak`Geometry`Triangle`"];

(* Finding coordinate / node positions *)

Unset[k]; Unset[m]; Unset[t];

pta = Abs[($\frac{1}{16}$ * Cos[$\frac{\pi}{8}$])];

ptb = Abs[($\frac{1}{16}$ * Sin[$\frac{\pi}{8}$])];

ptc = $\frac{\sqrt{2}}{2}$;

(* variable terms for element slice -- bracket notation: [element number, element node] *)

X[1, 1] = 0; X[1, 2] = $\frac{1}{16}$; X[1, 3] = pta;

Y[1, 1] = 0; Y[1, 2] = 0; Y[1, 3] = ptb;

X[2, 1] = $\frac{1}{16}$; X[2, 2] = 2 pta; X[2, 3] = pta;

Y[2, 1] = 0; Y[2, 2] = 2 ptb; Y[2, 3] = ptb;

X[3, 1] = $\frac{1}{16}$; X[3, 2] = $\frac{2}{16}$; X[3, 3] = 2 pta;

Y[3, 1] = 0; Y[3, 2] = 0; Y[3, 3] = 2 ptb;

X[4, 1] = $\frac{2}{16}$; X[4, 2] = 3 pta; X[4, 3] = 2 pta;

Y[4, 1] = 0; Y[4, 2] = 3 ptb; Y[4, 3] = 2 ptb;

X[5, 1] = $\frac{2}{16}$; X[5, 2] = $\frac{3}{16}$; X[5, 3] = 3 pta;

Y[5, 1] = 0; Y[5, 2] = 0;

Y[5, 3] = 3 ptb;

X[6, 1] = $\frac{3}{16}$; X[6, 2] = 4 pta; X[6, 3] = 3 pta;

Y[6, 1] = 0; Y[6, 2] = 4 ptb; Y[6, 3] = 3 ptb;

X[7, 1] = $\frac{3}{16}$; X[7, 2] = $\frac{4}{16}$; X[7, 3] = 4 pta;

Y[7, 1] = 0; Y[7, 2] = 0; Y[7, 3] = 4 ptb;

X[8, 1] = $\frac{4}{16}$; X[8, 2] = 5 pta; X[8, 3] = 4 pta;

Y[8, 1] = 0; Y[8, 2] = 5 ptb;

Y[8, 3] = 4 ptb;

X[9, 1] = $\frac{4}{16}$; X[9, 2] = $\frac{5}{16}$; X[9, 3] = 5 pta;

Y[9, 1] = 0; Y[9, 2] = 0;

Y[9, 3] = 5 ptb;

$$X[10, 1] = \frac{5}{16}; X[10, 2] = 6 \text{ pta}; X[10, 3] = 5 \text{ pta};$$

$$Y[10, 1] = 0; Y[10, 2] = 6 \text{ ptb};$$

$$Y[10, 3] = 5 \text{ ptb};$$

$$Y[11, 1] = 0; Y[11, 2] = 0; Y[11, 3] = 6 \text{ ptb};$$

$$X[12, 1] = \frac{6}{16}; X[12, 2] = 8 \text{ pta}; X[12, 3] = 6 \text{ pta};$$

$$Y[12, 1] = 0; Y[12, 2] = 8 \text{ ptb}; Y[12, 3] = 6 \text{ ptb};$$

$$X[13, 1] = \frac{6}{16}; X[13, 2] = \frac{8}{16}; X[13, 3] = 8 \text{ pta};$$

$$Y[13, 1] = 0; Y[13, 2] = 0;$$

$$Y[13, 3] = 8 \text{ ptb};$$

For[z = 1, z ≤ 13, z++,

$\Omega_z = \text{Area} [\{ \{ X[z, 1], Y[z, 1] \}, \{ X[z, 2], Y[z, 2] \}, \{ X[z, 3], Y[z, 3] \} \}] ;$

(*Print[" Ω ["k,"]=", Ω_k];*)

$\beta[z, 1] = Y[z, 2] - Y[z, 3];$

$\beta[z, 2] = Y[z, 3] - Y[z, 1];$

$\beta[z, 3] = Y[z, 1] - Y[z, 2];$

$\text{gamma}[z, 1] = X[z, 3] - X[z, 2];$

$\text{gamma}[z, 2] = X[z, 1] - X[z, 3];$

$\text{gamma}[z, 3] = X[z, 2] - X[z, 1];$

];

(* Iterating for elemental matrices -- z indicates element, i indicates row, j indicates column *)

For[z = 1, z ≤ 13, z++,

For[j = 1, j ≤ 3, j++,

For[i = 1, i ≤ 3, i++,

$$k_z[i, j] = \left(\frac{1}{4\Omega_z} \right) * (\beta[z, i] * \beta[z, j] + \text{gamma}[z, i] * \text{gamma}[z, j]);$$

If[i = j, $\delta = 1$, $\delta = 0$];

$$m_z[i, j] = \frac{\Omega_z}{12} * (1 + \delta);$$

];

];

(* Creating elemental matrices *)

$$k[z] = \begin{matrix} k_z[1, 1] & k_z[1, 2] & k_z[1, 3] \\ k_z[2, 1] & k_z[2, 2] & k_z[2, 3] \\ k_z[3, 1] & k_z[3, 2] & k_z[3, 3] \end{matrix}; \quad m[z] = \begin{matrix} m_z[1, 1] & m_z[1, 2] & m_z[1, 3] \\ m_z[2, 1] & m_z[2, 2] & m_z[2, 3] \\ m_z[3, 1] & m_z[3, 2] & m_z[3, 3] \end{matrix};$$

Print[" "];

Print["k["z,"]=", k[z] // MatrixForm]; Print["m["z,"]=", m[z] // MatrixForm];

];

(* Element Relationship for 208 Elements *)

(* Elements at the horizontal diameter need special definition *)

t[16] = {{113, 112, 97}};

t[32] = {{112, 81, 97}};

t[48] = {{112, 96, 81}};

t[64] = {{86, 65, 81}};

t[80] = {{96, 80, 65}};

t[96] = {{80, 49, 65}};

t[112] = {{80, 64, 49}};

t[128] = {{64, 33, 49}};

t[144] = {{64, 48, 33}};

t[160] = {{48, 17, 33}};

t[176] = {{48, 32, 17}};

t[192] = {{32, 1, 17}};

t[208] = {{32, 16, 1}};

(* Iterating for other elemental relationships *)

For[i = 1, i < 15, i++,

t[i] = {{113, 96+i, 97+i}};

t[16+i] = {{96+i, 81+i, 97+i}};

t[32+i] = {{96+i, 80+i, 81+i}};

t[48+i] = {{80+i, 65+i, 81+i}};

t[64+i] = {{80+i, 64+i, 65+i}};

t[80+i] = {{64+i, 49+i, 65+i}};

t[96+i] = {{64+i, 48+i, 49+i}};

t[112+i] = {{48+i, 33+i, 49+i}};

t[128+i] = {{48+i, 32+i, 33+i}};

t[144+i] = {{32+i, 17+i, 33+i}};

t[160+i] = {{32+i, 16+i, 17+i}};

t[176+i] = {{16+i, 1+i, 17+i}};

t[192+i] = {{16+i, i, i+1}};

]

For[i = 1, i < 208, i++,

Print["t[" , i, "]" = ", t[i]];

];

(* Assembler Portion *)

(* Set Up Blank Matrices *)

K = Table[0., {i, 113}, {j, 113}];

M = Table[0, {i, 113}, {j, 113}];

```

(* Main Iteration *)
For[l = 1, l ≤ 208, l++,
  For[j = 1, j ≤ 3, j++,
    For[i = 1, i ≤ 3, i++,
      If[l ≤ 16, elem = 1];
      If[16 < l ≤ 32, elem = 2];
      If[32 < l ≤ 48, elem = 3];
      If[48 < l ≤ 64, elem = 4];
      If[64 < l ≤ 80, elem = 5];
      If[80 < l ≤ 96, elem = 6];
      If[96 < l ≤ 112, elem = 7];
      If[144 < l ≤ 160, elem = 8];

      If[160 < l ≤ 176, elem = 9];
      If[176 < l ≤ 192, elem = 10];
      If[192 < l ≤ 208, elem = 11];

      u[l, j] = Extract[t[l], {1, j}];
      u[l, i] = Extract[t[l], {1, i}];
      vk[j, i] = Extract[k[elem], {j, i}];
      vm[j, i] = Extract[m[elem], {j, i}];

      (* K Matrix *)
      prev = Extract[K, {u[l, j], u[l, i]}];
      K = ReplacePart[K, prev + vk[j, i], {u[l, j], u[l, i]}];

      (* M Matrix *)
      prev = Extract[M, {u[l, j], u[l, i]}];
      M = ReplacePart[M, prev + vm[j, i], {u[l, j], u[l, i]}];
    ]];
  ];
];

(* Print Results *)
Print["K=", K// MatrixForm];
Print["M=", M// MatrixForm];
MK = Inverse[M].K;
Print["MK=", MK// MatrixForm];
For[i = 1, i ≤ 208, i++,
  Unset[t[i]];
];
];

```

```

(* DEFINING VARIABLES *)
(* ENDTIME = ( Total Time / Δt ) = 2 ps / 0.001 ps = 2000 *)
(* L = ( Total Distance in z direction / Δz ) = 1 * 10-4 mm / 1.0 * 10-6 mm = 100 *)
(* p indicates nodal number *)

t = 0.001; (* time step Δt *)
m = 1; (* gold/chromium layer index *)
z = 0.10 * 10-6; (* Δz value *)
P = 208; (* Number of Nodes *)
L = 100; (* Total Depth Steps *)
ENDTIME = 3000; (* Total Time Step *)
DUMAX = 0; (* DIMax *)
DOLMAX = 0;

MDZ = Table[ 0., {i, P}, {j, P} ];
C1[1] = 2.5 * 10-3; (* Lattice Heat Cap -- gold *)
C1[2] = 3.3 * 10-3; (* Lattice Heat Cap -- chro *)
γ[1] = 70 * 10-9; (* gamma -- gold *)
γ[2] = 193.33333 * 10-9; (* gamma -- chro *)
G[1] = 2.6 * 10-5; (* Coupling Factor gold *)
G[2] = 42. * 10-5; (* Coupling Factor chromium *)
κ[1] = 315 * 10-15; (* gold *)
κ[2] = 94 * 10-15; (* chromium *)

(* COEFFICIENTS FOR SYSTEM *)
h1 = ( κ[1] * t / ( 2 * z2 ) );
h2 = ( κ[2] * t / ( 2 * z2 ) );
f1 = ( t * G[1] / 2 - ( t2 * (G[1])2 / ( 4 * (C1[1]) + ((G[1]) * 2 * t) ) + κ[1] * t / z2 ) );
f2 = ( t * G[2] / 2 - ( t2 * (G[2])2 / ( 4 * (C1[2]) + ((G[2]) * 2 * t) ) + κ[2] * t / z2 ) );

f[1] = List[];
f[2] = List[];
h[1] = List[];
h[2] = List[];

```

```

For[p=1, p<=P, p++,
  f[1] = AppendTo[f[1], f1];
  f[2] = AppendTo[f[2], f2];
  h[1] = AppendTo[h[1], h1];
  h[2] = AppendTo[h[2], h2];
];
f[1] = DiagonalMatrix[f[1]];
f[2] = DiagonalMatrix[f[2]];
h[1] = DiagonalMatrix[h[1]];
h[2] = DiagonalMatrix[h[2]];
o = ZeroMatrix[P];
(* Setting Initial Conditions *)
For[p=1, p<=P, p++,
  For[k=0, k<=L, k++,
    U[p, k, -2] = 300;
    U[p, k, -1] = 300;
    U[p, k, 0] = 300;

    (* Setting Initial Conditions *)
    For[p=1, p<=P, p++,
      For[k=0, k<=L, k++,
        U[p, k, -2] = 300;
        U[p, k, -1] = 300;
        U[p, k, 0] = 300;
        U1[p, k, -2] = 300;
        U1[p, k, -1] = 300;
        U1[p, k, 0] = 300;
        U1[p, k, 1] = 300;
      ];
    ];

    (* Defining Vectors *)
    For[n=-2, n<=1, n++,
      For[k=0, k<=L, k++,
        T0[k, n] = List[];
        T1[k, n] = List[];
        For[p=1, p<=P, p++,
          T0[k, n] = AppendTo[T0[k, n], {U[p, k, n]}];
          T1[k, n] = AppendTo[T1[k, n], {U1[p, k, n]}];
        ];
      ];
    ];
];

```

(* List Creation for Final Results Plots *)

```
plotHeat2 = List[];
plotHeat25 = List[];
plotHeat5 = List[];
plotHeatU2 = List[];
plotHeatU25 = List[];
plotHeatU5 = List[];
plotCenter = List[];
plotElectron = List[];
plotSource = List[];
```

(* Start Main Iteration *)

```
For[n = 0, n ≤ ENDTIME, n++,
  If[Mod[n, 500] = 0, Print["n=", n]];
  b[n] = List[];
```

```
For[k = 1, k ≤ (L-1), k++,
```

```
  If[k ≥  $\frac{L}{2}$ , m = 2, m = 1];
```

(* Source File for Case One*)

$$S_n = 0.94 \left(\frac{.07 * 13.4}{0.1 * 15.3} \right) * e^{\left(-\left(\frac{kx}{15.3 * 10^{-6}} \right) - \left(2.77 * \left(\frac{(nt) - (0.2)}{0.1} \right)^2 \right) \right)};$$

(* Source File for Double Pulse *)

$$S_n = 0.94 \left(\frac{.07 * 13.4}{0.1 * 15.3} \right) * \left(e^{\left(-\left(\frac{kx}{15.3 * 10^{-6}} \right) - \left(2.77 * \left(\frac{(nt) - (0.2)}{0.1} \right)^2 \right) \right)} + e^{\left(-\left(\frac{kx}{15.3 * 10^{-6}} \right) - \left(2.77 * \left(\frac{(nt) - (0.4)}{0.1} \right)^2 \right) \right)} \right);$$

(* Source Vector *)

```
S[n, k] = List[];
For[p = 1, p ≤ P, p++,
  If[p ≤ 180, s = 0, s = S_n];
  S[n, k] = AppendTo[S[n, k], {s}];
];
```

(* Source File for Bouncing Source *)

If[n < 500,

$$S_n = 0.94 \left(\frac{.07 * 13.4 * 2.6}{0.1 * 15.3} \right) * e^{\left(-\left(\frac{k * z}{15.3 * 10^{-6}} \right) - \left(2.77 * \left(\frac{(n * t) - (0.2)}{0.1} \right)^2 \right) \right)}$$

S[n, k] = List[];

For[p = 1, p ≤ P, p++,

 If[p ≤ 32, s = 0, s = S_n];

 S[n, k] = AppendTo[S[n, k], {s}];

];

];

If[500 ≤ n < 1000,

$$S_n = 0.94 \left(\frac{.07 * 13.4 * 2.6}{0.1 * 15.3} \right) * \left\{ e^{\left(-\left(\frac{k * z}{15.3 * 10^{-6}} \right) - \left(2.77 * \left(\frac{((n - 500) * t) - (0.2)}{0.1} \right)^2 \right) \right)} \right\};$$

S[n, k] = List[];

For[p = 1, p ≤ P - 1, p++,

 If[p = 17, s = S_n, s = 0];

 S[n, k] = AppendTo[S[n, k], {s}];

];

S[n, 33] = AppendTo[S[n, k], {S_n}];

];

If[1000 ≤ n < 1500,

$$S_n = 0.94 \left(\frac{.07 * 13.4 * 2.6}{0.1 * 15.3} \right) * e^{-\left(\frac{k * z}{15.3 * 10^{-6}} \right) - \left(2.77 * \left(\frac{((n-1000) * t) - (0.2)}{0.1} \right)^2 \right)};$$

```
S[n, k] = List[];
For[p = 1, p ≤ P - 1, p++,
  If[p = 21, s = S_n, s = 0];
  S[n, k] = AppendTo[S[n, k], {s}];
];
S[n, 33] = AppendTo[S[n, k], {S_n}];
];
```

If[1500 ≤ n < 2000,

$$S_n = 0.94 \left(\frac{.07 * 13.4 * 2.6}{0.1 * 15.3} \right) * e^{-\left(\frac{k * z}{15.3 * 10^{-6}} \right) - \left(2.77 * \left(\frac{((n-1500) * t) - (0.2)}{0.1} \right)^2 \right)};$$

```
S[n, k] = List[];
For[p = 1, p ≤ P - 1, p++,
  If[p = 25, s = S_n, s = 0];
  S[n, k] = AppendTo[S[n, k], {s}];
];
S[n, 33] = AppendTo[S[n, k], {S_n}];
];
```

If[2000 ≤ n < 2500,

$$S_n = 0.94 \left(\frac{.07 * 13.4 * 2.6}{0.1 * 15.3} \right) * e^{-\left(\frac{k * z}{15.3 * 10^{-6}} \right) - \left(2.77 * \left(\frac{((n-2000) * t) - (0.2)}{0.1} \right)^2 \right)};$$

```
S[n, k] = List[];
For[p = 1, p ≤ P - 1, p++,
  If[p = 29, s = S_n, s = 0];
  S[n, k] = AppendTo[S[n, k], {s}];
];
S[n, 33] = AppendTo[S[n, k], {S_n}];
];
```

If[n ≥ 2500,

$$S_n = 0.94 \left(\frac{.07 * 13.4 * 2.6}{0.1 * 15.3} \right) * e^{-\left(\frac{k * z}{15.3 * 10^{-6}} \right) - \left(2.77 * \left(\frac{((n) * t) - (0.2)}{0.1} \right)^2 \right)};$$

```
S[n, k] = List[];
For[p = 1, p ≤ P, p++,
  If[p ≤ 32, s = 0, s = S_n];
  S[n, k] = AppendTo[S[n, k], {s}];
];
```

(* Non linear heat capacity *)

$C_0[k, n] = \text{List}[];$

For[p=1, p<P, p++,

$C_0[k, n] = \text{AppendTo}[C_0[k, n], \gamma[m] * U[p, k, n]];$

];

$C_0[k, n] = \text{DiagonalMatrix}[C_0[k, n]];$

(* Right Hand Matrix System Representation *)

$$\begin{aligned} b_k = & (h[m] \cdot T_0[k-1, n-1]) - \left((-C_0[k, n] + \left(\frac{t \cdot x[m]}{2} * MK \right) + f[m]) \cdot T_0[k, n-1] \right) + \\ & (h[m] \cdot T_0[k+1, n-1]) + (2 * (h[m] \cdot T_0[k-1, n])) - \left(\left((t \cdot x[m]) * MK \right) + (2 * f[m]) \right) \cdot T_0[k, n] + \\ & (2 * (h[m] \cdot T_0[k+1, n])) + \left(\left(\frac{t \cdot G[m]}{2} + \left(\frac{t \cdot G[m]}{2} * \left(\frac{2 * C_1[m] - t \cdot G[m]}{2 * C_1[m] + t \cdot G[m]} \right) \right) \right) * T_1[k, n-1] \right) + \\ & \left(\left(t \cdot G[m] - \left(\frac{t^2 * (G[m])^2}{2 * C_1[m] + t \cdot G[m]} \right) \right) * T_1[k, n] \right) + (2 * t * S[n, k]); \end{aligned}$$

(* Left Hand Matrix System Representation *)

$$sb[k, 1, 1] = \left((C_0[k, n] + \left(\frac{t \cdot x[1]}{2} * MK \right) + f[1]) - h[1] \right);$$

$$sb[k, 1, 2] = (C_0[k, n] + \left(\frac{t \cdot x[1]}{2} * MK \right) + f[1]);$$

$$sb[k, 1, 3] = \left(\left((C_0[k, n] + \left(\frac{t \cdot x[1]}{2} * MK \right) + f[1]) * \left(\frac{x[1]}{x[1] + x[2]} \right) \right) - h[1] \right);$$

$$sb[k, 2, 1] = \left((C_0[k, n] + \left(\frac{t \cdot x[2]}{2} * MK \right) + f[2]) - h[2] \right);$$

$$sb[k, 2, 2] = (C_0[k, n] + \left(\frac{t \cdot x[2]}{2} * MK \right) + f[2]);$$

$$sb[k, 2, 3] = \left(\left((C_0[k, n] + \left(\frac{t \cdot x[2]}{2} * MK \right) + f[2]) * \left(\frac{x[2]}{x[1] + x[2]} \right) \right) - h[2] \right);$$

$$sb[k, 2, 4] = \left(- \left(\frac{x[2]}{x[1] + x[2]} \right) * h[2] \right);$$

$$sb[k, 1, 4] = \left(- \left(\frac{x[1]}{x[1] + x[2]} \right) * h[1] \right);$$

]; (* END OF Z DIRECTIONAL (K) LOOP *)

```

(* CREATING THE "B" OF Ax=B *)
For[k=1, k<=(L-1), k++,
  For[p=1, p<=P, p++,
    AppendTo[b[n], {Extract[b_k, {p, 1}]}];
  ];
];

(* CREATING THE "A" OF Ax=B *)

(* Setting up zero portions *)
ZERO[1] = 0;
For[i=1, i<=L-1, i++,
  For[j=1, j<i, j++,
    ZERO[i] = AppendRows[ZERO[i-1], 0];
  ];
]; (* Left Padding *)

r[1] = AppendRows[sb[1, 1, 1], -h[1]];
For[k=3, k<=L-1, k++,
  r[1] = AppendRows[r[1], 0];
]; (* First Row Complete *)

r[2] = AppendRows[-h[1], sb[2, 1, 2], -h[1]];
For[i=4, i<=L-1, i++,
  r[2] = AppendRows[r[2], 0];
];

A[n] = AppendColumns[r[1], r[2]];

(* Getting to the middle of the matrix *)
For[k=3, k<=  $\frac{L}{2}$ , k++,
  r[k] = AppendRows[ZERO[k-2], -h[1], sb[k, 1, 2], -h[1], ZERO[L-(k+2)]];
  A[n] = AppendColumns[A[n], r[k]];
];

(* Interstitial Layer
  r[ $\frac{L}{2}$ ] = AppendRows[ZERO[ $\frac{L}{2}$ -2], -h[1], sb[ $\frac{L}{2}$ , 1, 2], -h[1], ZERO[L-( $\frac{L}{2}$ +2)]];
  A[n] = AppendColumns[A[n], r[ $\frac{L}{2}$ ]];
  r[ $\frac{L}{2}$ +1] = AppendRows[ZERO[ $\frac{L}{2}$ -1], -h[2], sb[ $\frac{L}{2}$ +1, 2, 2], -h[2], ZERO[L-( $\frac{L}{2}$ +3)]];
  A[n] = AppendColumns[A[n], r[ $\frac{L}{2}$ +1]];
*)

```

```
(* Getting to the end of the matrix *)
For[k = ( $\frac{L}{2} + 1$ ), k ≤ L-3, k++,
  r[k] = AppendRows[ZERO[k-2], -h[2], sb[k, 2, 2], -h[2], ZERO[L-(k+2)]];
  A[n] = AppendColumns[A[n], r[k]];
];
```

```
(* Second to Last Row *)
```

```
r[L-2] = AppendRows[ZERO[L-4], -h[2], sb[L-2, 2, 2], -h[2]];
A[n] = AppendColumns[A[n], r[L-2]];
```

```
(* Last Row *)
```

```
r[L-1] = AppendRows[ZERO[L-3], -h[2], sb[L-1, 2, 1]];
A[n] = AppendColumns[A[n], r[L-1]];
```

```
(* solving for all values of  $T_0[k, n+1]$  *)
```

```
Q[n] = List[];
Q[n] = LinearSolve[A[n], b[n]];
For[k = 1, k ≤ (L-1), k++,
  For[p = 1, p ≤ P, p++,
    U[p, k, n+1] = Extract[Q[n], {(p+(k-1)*P), 1}];
  ];
];
```

```
(* Defining  $T_0[k, n+1]$  vectors *)
```

```
For[k = 1, k ≤ (L-1), k++,
  T_0[k, n+1] = List[];
  T_1[k, n+1] = List[];
  For[p = 1, p ≤ P, p++,
    T_0[k, n+1] = AppendTo[T_0[k, n+1], {U[p, k, n+1]}];
    T_1[k, n+1] = AppendTo[T_1[k, n+1], {U_1[p, k, n+1]}];
  ];
];
```

(* Setting the values at the surface and bottom *)

```

T0[L, n+1] = List[];
T0[0, n+1] = List[];
T1[L, n+1] = List[];
T1[0, n+1] = List[];
For[p=1, p<=P, p++,
  T0[L, n+1] = AppendTo[T0[L, n+1], {U[p, L-1, n+1]}];
  T0[0, n+1] = AppendTo[T0[0, n+1], {U[p, 1, n+1]}];
  T1[L, n+1] = AppendTo[T1[L, n+1], {U1[p, L-1, n+1]}];
  T1[0, n+1] = AppendTo[T1[0, n+1], {U1[p, 1, n+1]}];
];

```

(* SECOND EQUATION T₁[k,n+1] *)

```

m = 1;
For[k=1, k<=(L-1), k++,
  If[k >=  $\frac{L}{2}$ , m = 2, m = 1];
  Q1[n] = List[];
  Q1[n] = { {  $\left( \frac{t \cdot G[m]}{(2 \cdot C_1[m]) + (t \cdot G[m])} \right) \cdot T_0[k, n-1] \right) + \left( \left( \frac{2 \cdot t \cdot G[m]}{(2 \cdot C_1[m]) + (t \cdot G[m])} \right) \cdot T_0[k, n] \right) +$ 
    {  $\left( \frac{t \cdot G[m]}{(2 \cdot C_1[m]) + (t \cdot G[m])} \right) \cdot T_0[k, n+1] \right) + \left( \left( \frac{(2 \cdot C_1[m]) - (t \cdot G[m])}{(2 \cdot C_1[m]) + (t \cdot G[m])} \right) \cdot T_1[k, n-1] \right) +$ 
    {  $\left( \frac{-4 \cdot t \cdot G[m]}{(4 \cdot C_1[m]) + (2 \cdot t \cdot G[m])} \right) \cdot T_1[k, n] \right) };
  For[p=1, p<=P, p++,
    U1[p, k, n+1] = Extract[Q1[n], {p, 1}];
  ];
  T1[k, n+1] = List[];
  For[p=1, p<=P, p++,
    T1[k, n+1] = AppendTo[T1[k, n+1], {U1[p, k, n+1]}];
  ];
];
(* end of T1 loop *)$ 
```

```

(* Getting DUMAX *)
If[(U[P, 1, n] - 300) > DUMAX, DUMAX = (U[P, 1, n] - 300)];
DU[n] = (U[P, 1, n] - 300);
If[(U1[P, 1, n] - 300) > DUDMAX, DUDMAX = (U1[P, 1, n] - 300)];
DUL[n] = (U1[P, 1, n] - 300);

(* Plotting temp over time*)
AppendTo[plotElectron, {n, U[P, 1, n]}];
AppendTo[plotSource, {n, Sn}];

If[n == 200,
  For[k = 1, k ≤ (L-1), k++,
    AppendTo[plotHeat2, {k, U1[P, k, 200]}]
  ]
];

If[n == 250,
  For[k = 1, k ≤ (L-1), k++,
    AppendTo[plotHeat25, {k, U1[P, k, 250]}]
  ]
];

If[n = 200,
  Con200 = List[];
  For[i = L-1, i ≥ 1, i--,
    Con200 = AppendTo[Con200, {U[3, i, 200], U[5, i, 200], U[1, i, 200]}];
  ];
  ConL200 = List[];
  For[i = L-1, i ≥ 1, i--,
    ConL200 = AppendTo[ConL200, {U1[3, i, 200], U1[5, i, 200], U1[1, i, 200]}];
  ];
];

If[n = 250,
  Con250 = List[];
  For[i = L-1, i ≥ 1, i--,
    Con250 = AppendTo[Con250, {U[3, i, 250], U[5, i, 250], U[1, i, 250]}];
  ];
  ConL250 = List[];
  For[i = L-1, i ≥ 1, i--,
    ConL250 = AppendTo[ConL250, {U1[3, i, 250], U1[5, i, 250], U1[1, i, 250]}];
  ];
];

```

```

If[n = 500,
  Con500 = List[];
  For[i = L - 1, i ≥ 1, i--,
    Con500 = AppendTo[Con500, {U[3, i, 500], U[5, i, 500], U[1, i, 500]}];
  ];
  ConL500 = List[];
  For[i = L - 1, i ≥ 1, i--,
    ConL500 = AppendTo[ConL500, {U1[3, i, 500], U1[5, i, 500], U1[1, i, 500]}];
  ];
];

```

```

If[n = 500,
  For[k = 1, k ≤ (L - 1), k++,
    AppendTo[plotHeat5, {k, U1[P, k, 500]}];
  ];
];

```

```

If[n == 200,
  For[k = 1, k ≤ (L - 1), k++,
    AppendTo[plotHeatU2, {k, U[P, k, 200]}];
  ];
];

```

```

If[n == 250,
  For[k = 1, k ≤ (L - 1), k++,
    AppendTo[plotHeatU25, {k, U[P, k, 250]}];
  ];
];

```

```

If[n = 500,
  For[k = 1, k ≤ (L - 1), k++,
    AppendTo[plotHeatU5, {k, U[P, k, 500]}];
  ];
];

```

(* Clearing Memory *)

```

Unset[b[n]];
Unset[A[n]];
Unset[Q[n]];
Unset[Qi[n]];

```

```

For[k=1, k<=L-1, k++,
  Unset[Cn[k, n]];
  Unset[S[n, k]];
  Unset[Tn[k, n-1]];
  Unset[T1[k, n-1]];
  sb[k, 1, 1];
  sb[k, 1, 2];
  sb[k, 2, 1];
  sb[k, 2, 2];
  For[p=1, p<=P, p++,
    Unset[U1[p, k, n-1]];
    Unset[U[p, k, n-1]];
  ];
]; (* end memory clearing *)

]; (* end of time (n) loop *)

Print["Electron Contour at 200"]; ListPlot3D[Con200, Mesh->False];
ListContourPlot[Con200, Contours->15, ContourLines->False];
ListContourPlot[Con200, Contours->15, ContourShading->False];
Print["Lattice Contour at 200"]; ListPlot3D[ConL200, Mesh->False];
ListContourPlot[ConL200, Contours->15, ContourLines->False];
ListContourPlot[ConL200, Contours->15, ContourShading->False];
Print["Electron Contour at 250"]; ListPlot3D[Con250, Mesh->False];
ListContourPlot[Con250, Contours->15, ContourLines->False];
ListContourPlot[Con250, Contours->15, ContourShading->False];
Print["Lattice Contour at 250"]; ListPlot3D[ConL250, Mesh->False];
ListContourPlot[ConL250, Contours->15, ContourLines->False];
ListContourPlot[ConL250, Contours->15, ContourShading->False];
Print["Electron Contour at 500"]; ListPlot3D[Con500, Mesh->False];
ListContourPlot[Con500, Contours->15, ContourLines->False];
ListContourPlot[Con500, Contours->15, ContourShading->False];
Print["Lattice Contour at 500"]; ListPlot3D[ConL500, Mesh->False];
ListContourPlot[ConL500, Contours->15, ContourLines->False];
ListContourPlot[ConL500, Contours->15, ContourShading->False];

Print["DUMAX=", DUMAX];
Print["DULMAX=", DULMAX];

plotDUMAX= List[];
plotDUMAX= List[];

```

```

For[n = 1, n <= ENDTIME, n++,
  AppendTo[plotDMAX, {n, (DU[n] / DUMAX)}];
  AppendTo[plotDIMAX, {n, (DUL[n] / DUMAX)}];
];

(* Plotting Graphs *)
ListPlot[plotSource, PlotJoined -> True, PlotRange -> All]; Print["Laser Heat Source"];
ListPlot[plotElectron, PlotJoined -> True, PlotRange -> All]; Print["Surface Heat"];
ListPlot[plotDMAX, PlotJoined -> True, PlotRange -> All]; Print["DMAX Plot"];
ListPlot[plotDIMAX, PlotJoined -> True, PlotRange -> All]; Print["DIMAX Plot"];

<< Graphics`MultipleListPlot`
MultipleListPlot[plotHeat2, plotHeat25, plotHeat5, SymbolShape -> {False},
  PlotRange -> All, PlotJoined -> {True, True, True}, PlotLegend -> {"2 ps", "2.5 ps", "5 ps"}]
MultipleListPlot[plotHeatU2, plotHeatU25, plotHeatU5, SymbolShape -> {False},
  PlotRange -> All, PlotJoined -> {True, True, True}, PlotLegend -> {"2 ps", "2.5 ps", "5 ps"}]

```

REFERENCES

- [Al-Nimr 1997a] M. A. Al-Nimr and S. Masoud, Non-equilibrium laser heating of metal films, *ASME Journal of Heat Transfer* 119(1997) 188-190.
- [Al-Nimr 1997b] M. A. Al-Nimr, Heat transfer mechanisms during laser heating of thin metal films, *International Journal Thermophysics* 18(1997) 1257-1268.
- [Al-Nimr 1999] M. A. Al-Nimr, Arpaci vs. picosecond thermal pulses in thin metal films, *Journal of Applied Physics* 85(1999) 2517-2521.
- [Al-Nimr 2000a] M. K. Al-Nimr and V. S. Arpaci, The thermal behavior of thin metal films in the hyperbolic two-step model, *International Journal of Heat and Mass Transfer* 43(2000) 2021-2028.
- [Al-Nimr 2000b] M. A. Al-Nimr and M. Naji, On the phase-lag effect on the non-equilibrium entropy production, *Microscale Thermophysics Engineering* 4(2000) 231-243.
- [Al-Nimr 2000c] M. A. Al-Nimr and M. Naji, Arpaci vs. non-equilibrium entropy production under the effect of the dual-phase-lag heat conduction model, *ASME Journal of Heat Transfer* 122(2000) 217-222.
- [Al-Nimr 2001] M. A. Al-Nimr and S. Kiwan, Effect of thermal losses on the microscopic two-step heat conduction model, *International Journal of Heat and Mass Transfer* 44(2001) 1013-1018.
- [Al-Nimr 2003] M. A. Al-Nimr, M. Hader and M. Naji, Use of the microscopic parabolic heat conduction model in place of the macroscopic model validation criterion under harmonic boundary heating, *International Journal of Heat and Mass Transfer* 46(2003) 333-339.
- [Antaki 1998] P. J. Antaki, Solution for non-Fourier dual phase lag heat conduction in a semi-infinite slab with surface heat flux, *International Journal of Heat and Mass Transfer* 41(1998) 2253-2258.
- [Antaki 2000] P. J. Antaki, Effect of dual-phase-lag heat conduction on ignition of a solid, *Journal of Thermophysics Heat Transfer* 14(2000) 276-278.

- [Antaki 2002] P. J. Antaki, Importance of nonequilibrium thermal conductivity on ignition of a solid, *International Journal of Heat and Mass Transfer* 45(2002) 4063-4067.
- [Barron 1985] R. Barron, *Cryogenic Systems*, 2nd ed. (Oxford Science Publications, New York, 1985).
- [Chen 1999a] J. K. Chen, J. E. Beraun and J. K. Tzou, A dual-phase-lag diffusion model for interfacial layer growth in metal matrix composites, *Journal of Material Science* 34(1999) 6183-6187.
- [Chen 1999b] J. K. Chen, J. E. Beraun and T. C. Carney, A corrective smoothed particle method for boundary value problems in heat conduction, *International Journal of numerical Methods Engineering* 46(1999) 231-252.
- [Chen 2000a] J. K. Chen and J. E. Beraun, A generalized smoothed particle hydrodynamics method for nonlinear dynamic problems, *Computational Methods in Applied Mechanical Engineering* 190(2000) 225-239.
- [Chen 2000b] J. K. Chen, J. E. Beraun and D. Y. Tzou, A dual-phase-lag diffusion model for predicting thin film growth, *Semiconductor Science Technology* 15(2000) 235-241.
- [Chen 2001a] J. K. Chen, J. E. Beraun and C. J. Jih, A corrective smoothed particle method for transient elastoplastic dynamics, *Computer Mechanics* 27(2001) 177-187.
- [Chen 2001b] J. K. Chen and J. E. Beraun, Numerical study of ultrashort laser pulse interactions with metal films, *Numerical Heat Transfer A* 40(2001) 1-20.
- [Chen 2001c] J. K. Chen, J. E. Beraun and D. Y. Tzou, A dual-phase-lag diffusion model for predicting inter-metallic compound layer growth in solder joints, *ASME Journal of Electronic Packaging* 112(2001) 52-57.
- [Chen 2003] J. K. Chen, J. E. Beraun and C. L. Tham, Investigation of thermal response caused by pulse laser heating, *Numerical Heat Transfer A* 44(2003) 705-722.
- [Chiffell 1994] R. J. Chiffell, On the wave behavior and rate effect of thermal and thermomechanical waves. M. S. Thesis, University of New Mexico, Albuquerque, NM (1994).
- [Comini 1994] G. Comini, S. Del Giudice and C. Nonino, *Finite Element Analysis in Heat Transfer: Basic Formulation and Linear Problems*. (Taylor & Francis, New York, 1994).
- [Dai 1999] W. Dai and R. Nassar, A finite difference method for solving the heat transport equation at the microscale, *Numerical Methods for Partial Differential Equations* 15(1999) 697-708.

- [Dai 2000a] W. Dai, Y. Zhang, and R. Nassar, A Hybrid Finite Element-Alternating Direction Implicit Method for Solving Parabolic Differential Equations on Multilayers with Irregular Geometry. *Journal of Computational and Applied Mathematics* 117 (2000).
- [Dai 2000b] W. Dai and R. Nassar, A domain decomposition method for solving three dimensional heat transport equations in double layered thin films with microscale thickness, *Numerical Heat Transfer* 38(2000) 243-256.
- [Dai 2000c] W. Dai and R. Nassar, A compact finite difference scheme for solving a three-dimensional heat transport equation in a thin film, *Numerical Methods for Partial Differential Equations* 16(2000) 441-458.
- [Dai 2001a] W. Dai, and R. Nassar, A finite difference scheme for solving three-dimensional heat transport equation in a thin film with microscopic thickness. *International Journal of Numerical Method in Engineering* 50(2001) 1865-1880.
- [Dai 2001b] W. Dai and R. Nassar, A domain decomposition method for solving 3-D heat transfer equations in double layered thin film with microscale thickness and nonlinear interfacial conditions, *Numerical Heat Transfer A* 39(2001) 21-33.
- [Dai 2002] W. Dai and R. Nassar, An approximate analytic method for solving dual-phase-lagging heat transfer equations, *International Journal of Heat and Mass Transfer* 45(2002) 1585-1593.
- [Dai 2004a] W. Dai, L. Shen and R. Nassar, A convergent three-level finite difference scheme for solving a dual-phase-lagging heat transport equation in spherical coordinates, *Numerical Methods for Partial Differential Equations* 20(2004) 60-71.
- [Dai 2004b] W. Dai, Q. Li, R. Nassar and L. Shen, An unconditionally stable three level finite difference scheme for solving parabolic two-step micro heat transport equations in a three-dimensional double-layered thin film, *International Journal of Numerical Methods Engineering* 59(2004) 493-509.
- [Dawson 2001] C. Dawson, and J. Proft, "Discontinuous/Continuous Galerkin Methods for Coupling the Primitive and Wave Continuity Equations of Shallow Water." Center for Subsurface Modelling. (2001).
- [DuChateau 2989] P. DuChateau, and D. Zachmann, *Applied Partial Differential Equations*. (Dover Publications, New York, 1989).
- [Duncan 1994] A. B. Duncan, and G. P. Peterson, Review of microscale heat transfer. *ASME Journal of Applied Mechanics Review* 47(1994) 397-428.

[Glass 1985] D. E. Glass, M. N. Özisik, and D. S. McRae, On the Numerical Solution of Hyperbolic Heat Conduction, *Numerical Heat Transfer* 8(1985) 497-504.

[Goockenbach 2002] M. S. Goockenbach, Partial Differential Equations – Analytical and Numerical Methods. (SIAM Publishing, 2002).

[Herwig 2000] H. Herwig, and K. Becjert, Fourier Versus Non-Fourier Heat Conduction in Materials with a Nonhomogeneous Inner Structure. *Journal of Heat Transfer* 22(2000) 363-365.

[Ho 1995] J. R. Ho, C. P. Grigoropolus and J. A. C. Humphrey, Computational study of heat transfer and gas dynamics in the pulsed laser evaporation of metals, *Journal of Applied Physics* 78(1995) 4696-4709.

[Ho 2003] J. R. Ho, C. P. Kuo and W. S. Jiamg, Study of heat transfer in multilayered structure within the framework of dual-phase-lag heat conduction model using lattice Boltzmann method, *International Journal of Heat and Mass Transfer* 46(2003) 55-69.

[Holman 1997] J. P. Holman, Heat Transfer, 8th ed (McGraw-Hill, New York, 1997).

[Joshi 1993] A. A. Joshi and A. Majumdar, Transient ballistic and diffusive phonon heat transport in thin films, *Journal of Applied Physics* 74(1993) 31-39.

[Kaganov 1957] M. I. Kaganov, I. M. Lifshitz, and M. V. Tanatarov, Relaxation between electrons and crystalline lattices, *Soviet Physics JETP* 4(1957) 173-178.

[Lees 1961] M. Lees, Alternating direction and semi-explicit difference methods for parabolic partial differential equations, *Numerical Mathematik* 3(1961) 398-412.

[Lin 1997] C. K. Lin, C. C. Hwang and Y. P. Chang, The unsteady solution of a unified heat conduction equation, *International Journal of Heat and Mass Transfer* 40(1997) 1716-1719.

[Özisik 1994] M. N. Özisik, and D. Y. Tzou, On the Wave Theory in Heat Conduction. *Journal of Heat Transfer* 116(1994) 526-535.

[Qui 1992] T. Q. Qui and C. L. Tien, Short-pulse laser heating on metals, *International Journal of Heat and Mass Transfer* 35(1992) 719-726.

[Qui 1993a] T. Q. Qui and C. L. Tien, Heat transfer mechanisms during short-pulse laser heating of metals, *ASME Journal of Heat Transfer* 115(1993) 835-841.

[Qui 1993b] T. Q. Qui and C. L. Tien, Size effects on nonequilibrium laser heating of metal films, *Journal of Heat Transfer* 115(1993)842-847.

- [Qui 1993c] T. Q. Qui, Energy dissipation and transport during high-power and short-pulse laser-metal interactions, Ph.D. Thesis, University of California, Berkely, CA 1993.
- [Qui 1994a] T. Q. Qui and C. L. Tien, Femtosecond laser heating of multilayer metals – I, *International Journal of Heat and Mass Transfer* 37(1994) 2789-2797.
- [Qui 1994b] T. Q. Qui, T. Juhasz, C. Suarez, W. E. Bron and C. L. Tien, Femtosecond laser heating of multi-layer metals II – experiments, *International Journal of Heat Transfer* 37(1994) 2799-2808.
- [Shen 2003] L. Shen, A Three-Level Finite Difference Scheme for Solving a Dual-Phase-Lagging Heat Transport Equation in Spherical Coordinates. Dissertation – Louisiana Tech University, (2003).
- [Smith 2004] A. N. Smith, and P. M. Norris, Heat Transfer Handbook (New York, Wiley and Sons Publishers, 2004).
- [Tang 1996] D.W. Tang and N. Araki, Non-Fourier Heat Conduction in a Finite Medium Under Periodic Surface Thermal Disturbance, *International Journal of Heat Transfer* 39(8)(1996) 1585-1590.
- [Tang 1999] D. W. Tang and N. Araki, Wavy, wavelike diffusive thermal responses of finite rigid slabs to high-speed heating of laser-pulses, *International Journal of Heat and Mass Transfer* 42(1999) 855-860.
- [Tsai 2003] C. S. Tsai and C. I. Hun, Thermal wave propagation in a bi-layered composite sphere due to a sudden temperature change on the outer surface, *International Journal of Heat and Mass Transfer* 46(2003) 5137-5144.
- [Tzou 1993] D. Y. Tzou, An Engineerin Assessment of the Relaxation Time in Thermal Wave Propagation, *International Journal of Heat Mass Transfer* 36(7)(1993) 1845-1851.
- [Tzou 1994] D. Y. Tzou, M. N. Özisik and R. J. Chiffelle, The lattice temperature in the microscopic two-step model, *Journal of Heat Transfer* 1994 (116) 1034-1038.
- [Tzou 1995a] D. Y. Tzou, A unified field approach for heat conduction from macro- to micro-scales, *Journal of Heat Transfer* 117(1995) 1837-11840.
- [Tzou 1995b] D. Y. Tzou, The generalized lagging response in small-scale and high-rate heating, *International Journal of Heat Mass Transfer* 38(1995) 3231-3240.
- [Tzou 1995c] D. Y. Tzou, Experimental support for the lagging behavior in heat propagation, *Journal of Thermophysics and Heat Transfer* 6(1995) 686-693.
- [Tzou 1995d] D. Y. Tzou and Y. S. Zhang, An analytic study on the fast-transient process in small scales, *International Journal of Engineering* 33(1995) 1449-1463.

- [Tzou 1996] D. Y. Tzou, Macro to Microscale Heat Transfer: The Lagging Behavior (Washington, DC, Taylor & Francis, 1996).
- [Tzou 1999] D. Y. Tzou, Ultrafast heat transport: the lagging behavior, 44th SPIE's Annual Meeting (1999) July 18-22, Denver, CO.
- [Tzou 2000a] D. Y. Tzou, Ultrafast transient behavior in microscale heat/mass transport, Advanced Photon Source, Millennium Lecture Series (2000), Argonne National Laboratories, Chicago, IL.
- [Tzou 2000b] D. Y. Tzou, Microscale heat transfer and fluid flow, 45th SPIE's Annual Meeting (2000) July 30 – August 4, San Diego, CA.
- [Tzou 2001] D. Y. Tzou and K. S. Chiu, Temperature-dependant thermal lagging in ultrafast laser heating, *International Journal of Heat and Mass Transfer* 44(2001) 1725-1734.
- [Tzou 2002] D. Y. Tzou, K. S. Chen and J. E. Beraun, Hot-electron blast induced by ultrashort-pulsed lasers in layered media, *International Journal of Heat and Mass Transfer* 45(2002) 3369-3382.
- [Van Ness 1969] H. C. Van Ness, Understanding Thermodynamics, (Dover Publications, 1969).
- [Wang 2000] L. Wang and X. Zhou, Dual-Phase-Lagging Heat Conduction, (Jinan, Shandong University Press, 2000).
- [Wang 2001a] L. Wang and X. Zhou, Dual-Phase-Lagging Heat Conduction: Problems and Solutions, (Jinan, Shandong University Press, 2001).
- [Wang 2001b] L. Wang, M. Xu and X. Zhou, Well-posedness and solution structure of dual-phase-lagging heat conduction, *International Journal of Heat and Mass Transfer* 44(2001)1659-1669.
- [Wang 2002] L. Wang and M. Xu, Well-posedness of dual-phase-lagging heat conduction equation: higher dimensions, *International Journal of Heat and Mass Transfer* 45(2002) 1165-1171.
- [Wolfram 1999] S. Wolfram The Mathematica Book 4th Ed. (Cambridge, Cambridge University Press, 1999).